Doctoral Dissertation

Study on Heat Transfer behavior of High-Prandtl number fluid and its feasibility to Passive Heat Transport System

Seok Bin Seo

Department of Nuclear Engineering

Graduate School of UNIST

2018. 07. 09

Study on Heat Transfer behavior of High-Prandtl number fluid and its feasibility to Passive Heat Transport System

A dissertation
submitted to the Graduate School of UNIST
in partial fulfillment of the
requirements for the degree of
Doctor of Philosophy

Seok Bin Seo

2018. 07. 09

Approved by

Bang, In Cheol

Advisor

Prof. In Cheol Bang

Study on Heat Transfer behavior of High-Prandtl number fluid and its feasibility to Passive Heat Transport System

Seok Bin Seo

This certifies that the dissertation of Seok Bin Seo is approved.

07. 09. 2018

signature

Bang, In Cheol

Advisor: In Cheol Bang

signature

Gwang Hyun Bang

signature

Ji Hyun Kim

signature

Ki Yong Choi

signature

Taesung Kim

Abstract

Molten salts are promising heat transfer media with high boiling temperature, which have advantages in single-phase heat transfer. Especially, the energy engineering systems operated in high temperature range like solar energy system or advanced nuclear system are strongly interested in using molten salts as heat transport or heat storage media. Therefore, there has been many researches to investigate the heat transfer behavior of molten salt system. However, still the fundamental knowledge on the single-phase heat transfer of molten salt is insufficient to assess its heat transfer performance. In addition, there are only few studies on the heat transport system using molten salt in both natural and forced circulation. Thus, this study focuses on the study on single-phase heat transfer behavior of molten salt, which is characterized by its high-Prandtl number, in both natural and forced circulation system with numerical and experimental approaches.

The first part of this paper includes the feasibility test on passive heat transport system using high-Prandtl number. The sensitivity analysis method is adopted to represent system reliability especially for high-Prandtl number fluid. The reliability assessment of the natural circulation system can give fundamental insight to the design of various passive safety systems for the advanced nuclear reactors. Especially for the passive system, the weak driving force requires accurate assessment of reliability and performance, or it can give large uncertainty during the operation of system. Here the reliability assessment employs one of efficient techniques referred as adjoint-based sensitivity method to test the heat transport system using high-Prandtl number fluid. The conservative governing equations in the natural circulation inside a closed rectangular loop were established, and its adjoint system were developed based on the Lagrangian approach. The developed adjoint system showed reasonable accuracy in the sensitivity analysis with more efficient computational effort as expected. Based on the developed adjoint sensitivity system, the reliability of natural circulation of molten salt simulant inside the closed loop is tested. The general sensitivity analyses are performed with different design parameters which were categorized into fluid property, geometric parameter, heater and cooler conditions, pressure drop parameters, and Nusselt correlation. Three different system conditions are imposed to investigate the effects of implementation of temperature-dependent fluid property, the orientations of heat exchanger, and operating temperature range, on the entire system reliability. It is found that the variation of fluid properties with respect to the temperature gives great effect on the reliability of heat transfer performance in the system. The further assessment on Nusselt correlation also verifies the importance of property variation with respect to the temperature in evaluating heat transfer performance. Thus, the reliable assessment on the heat transfer performance requires the consideration of property variation. Especially, the heat transport system using high-Prandtl number fluid should aware of property variation in estimating heat transfer performance, since the drastic temperature drop takes place near the heat

transfer surface due to thin thermal boundary layer.

The following parts describe the experimental study on heat transfer behaviors of high-Prandtl number fluid to give reliability to the assessment of high-Prandtl number fluid system. In specific, the second part includes the investigation of the convective heat transfer phenomena of high-Prandtl number oil and the third includes the experimental work using high-Prandtl number salt. In the previous studies of same research group, the distinct heat transfer behavior of high Prandtl number oil was reported in the natural circulation system. The present study extends the experimental work to the forced convective heat transfer and discusses the unique feature of heat transfer behavior of high-Prandtl number oil. Specifically, the convective heat transfer performance of high-Prandtl number oil in transition flow regime isn't fully understood with the previous correlations. It is suggested that the distinct heat transfer feature of high Prandtl number fluid is attributed to the existence of local natural convection in radial direction, which is induced by the weak thermal diffusivity and resulting large radial temperature difference of high Prandtl number fluid. The theoretical discussion on the local natural convection of high-Prandtl number oil verifies its existence in the heat transfer between fluid and heated wall. Based on the discussion, the newly developed correlation for high Prandtl number takes the local natural convection into consideration by adding Grashof number into the general convective heat transfer correlation. The proposed correlation well agrees with experimental data from the present work as well as the previous work, which demonstrates the effect of local natural convection on the convective heat transfer performance of high Prandtl number fluid. Finally, the experimental facility using heat transport salt is established and natural circulation test is performed giving opportunity to further discussion on distinct heat transfer behavior of high-Prandtl number fluid.

Contents

List of figures

List of table

Nomenclature

c_p	specific heat	$[Jkg^{-1}K^{-1}]$
D_h	hydraulic diameter	[m]
e	unit vector	
f	friction factor	
F	forward operator	
g	acceleration due to gravity	$[ms^{-2}]$
G	mass flux	$[kgm^{-2}s]$
Gr	Grashof number	
h	heat transfer coefficient	$[Wm^{-2}K^{-1}]$
k	thermal conductivity	$[Wm^{-1}K^{-1}]$
L	length	[m]
L	Lagrangian function	
Nu	Nusselt number	
Pr	Prandtl number	
p	pressure	$[kgm^{-1}s^{-2}]$
q"	heat flux	$[kWm^{-2}]$
Q	Heat	[W]
R	objective functional	
Ra	Rayleigh number	
Re	Reynolds number	
t	time	[s]
T	temperature	[K]
U	velocity	$[ms^{-1}]$

Greek symbols

α	thermal diffusivity	$[m^2s]$
β	thermal expansion coefficient	$[K^{-1}]$
λ	adjoint solution vector	
μ	dynamic viscosity	$[kgm^{-1}s^{-1}]$

ν	kinematic viscosity	$[m^2s^{-1}]$
ρ	density	$[kgm^{-3}]$

Subscripts

f	bulk fluid
i	inner
in	inlet
local	localized friction factor
m	mean
out	outlet
o	outer
ref	reference
s	flow direction
t	total length
w	wall
z	gravitational direction

Chapter 1. Introduction

1.1 Research Background and Motivation

Molten salts are promising heat transfer media with high boiling temperature, which have advantages in single-phase heat transfer. Especially, the energy engineering systems operated in high temperature range like solar energy system or advanced nuclear system are strongly interested in using molten salts as heat transport or heat storage media. The representative molten salt candidates for the heat transfer media are nitrate salt for solar energy system like HITEC (KNO_3-$NaNO_3$-$NaNO_2$) and fluoride salt for advanced nuclear energy system like FLiBe (LiF-BeF_2). The great potentials of molten salts as heat transfer and storage media are attributed to their high volumetric heat capacity without pressurization, which provides enhanced heat transfer, reduced pumping powers, and small heat exchanger volume. Naturally, many researches were dedicated to design the energy transport systems using molten salts and to test their performances. However, still the fundamental knowledge on the single-phase heat transfer of molten salt is insufficient to assess its heat transfer performance. For the energy transport systems using molten salts, both natural and forced circulation systems are adopted under different system objectives. The solar energy storage system adopts natural circulation of heat transfer salts, while the advanced nuclear reactor like molten salt reactor requires forced circulation of molten salts for the stable energy production. For various safety systems of advanced nuclear reactors, both natural and forced circulation systems of molten salts are recommended. That is, the reliable assessment of both natural and forced heat transfer behaviors of molten salt circulation system should be the prerequisite for the design molten salt systems. Unfortunately, due to the difficulties in experiment using molten salt, most of the studies on the heat transfer behavior of molten salt circulation are limited in numerical work or tested in limited experimental conditions. In addition, the previous experimental tests or even numerical tests on the heat transfer performance of molten salts rely on the classical correlations or qualitative comparison with other heat transport media. However, the classical and qualitative assessment for molten salt system would reduce the reliability of system design or performance especially in the aspect of thermal-hydraulics, since the classical correlations or performance assessment methods have not been verified for molten salt. Thus, the present study focuses on the quantitative assessment of the reliability of molten salt system and introducing fundamental insight in heat transfer of molten salt for high reliability. In specific, the present study defines the distinct feature of molten salt as high Prandtl number, so the entire works are interpreted in terms of high-Prandtl number fluid.

1.2 Review on Heat transport system using High-Pr fluid

The use of high-Prandtl number fluids as heat transport media has been widely considered in energy engineering systems such as Molten Salt Reactor (MSR) and Advanced High-Temperature Reactor (AHTR) in nuclear energy field or Concentrating Solar Power (CSP) plants in solar energy field. The representative fluid types with high Prandtl number are synthetic oils and molten salts.

In nuclear energy systems, various molten salts have been tested to use as liquid fuel and heat transport media for MSR since the first proposal by Oak Ridge National Laboratory (ORNL) in the middle of 20th century [1]. The first MSR utilized chloride-based salt, NaCl/KCl/$PuCl_3$ as liquid fuel and heat transport medium to operate as a breeder reactor in the fast neutron spectrum [2]. The chloride-based salts were also employed in the extended work by Taube et al. [3] as heat transport media for various designs of MSR systems like breeding reactor with plutonium, three zone reactor with a mixed fuel cycle, high flux burner reactor for transmutation, and internally cooled breeder with uranium-plutonium fuel. Ottewltte et al. [4,5] assessed the feasibility of molten chloride salt for fuel core salt with NaCl as the carrier salt, $ThCl_4$ for fertile material, and UCl_3 for fissile material, to provide a basis for the chloride-based MSR concept. Meanwhile, the fluoride-based salts were introduced as a liquid fuel and heat transport media for thermal- and fast- spectrum MSR. The first fluoride-based salt was LiF-BeF_2-AnF_4 for molten salt breeder in thermal spectrum, which was considered as liquid fuel carrier salt [6]. In Japan, MSR with thorium cycle employed LiF-AnF_4 salt as liquid fuel operating in fast spectrum [7]. In addition, fluoride-based salt was used for burner-type MSR like Actinides Molten Salt TransmutER (AMSTER) [8]. Recently, MSR concept was reviewed in the 21st century, since the advantages in neutronics and its liquid state of molten salt gave satisfaction to the world's principle toward Gen-IV nuclear energy systems which are enhanced safety and reliability, reduced waste generation, effective use of uranium or thorium ores, resistance to proliferation, and improved economic competitiveness. Under the EURATOM Framework Programs and MOST project, the potential of fluoride salts were emphasized for the liquid fuel of two representative fast spectrum MSRs: Molten Salt Fast Reactor (MSFR) for breeding with thorium fuel cycle [9,10] and MOlten Salt Actinide Recycler & Transmuter (MOSART) for spent fuel burner [11]. On the other hand, chloride-based salts were considered due to their expected potentials in fast neutron spectrum. Holcomb et al. [12] compared chloride-based salts with fluoride-based salts and evaluated the advantages of chloride-based salts in fast neutron spectrum providing possible reactor configurations, design features/options and performance considerations. Then, the development of actual molten chloride salt reactor was initiated by official supporting program with several institutions including TerraPower, ORNL, Electric Power Research Institute (EPRI), and Vaderbilt University [13]. Besides, Moltex Energy LLP initiated the development of MSR utilizing UCl_3-NaCl of fuel salt and NaF-KF- ZrF_4 of coolant salt [14].

Another representative heat transport system using molten salts in nuclear energy field is AHTR,

which utilizes high temperature fluoride salt to provides cooling of solid fuel. The distinct features of AHTR which are higher operating temperature and clean primary coolant circuit using molten salt without fuel require different candidate salts. The previous studies suggested that the requirements of candidate salts are thermal and chemical stability at high temperature (>800 ºC), proper melting temperature (~500 ºC), neutronic viability, and materials compatibility [15]. Then various molten salts for AHTR were reviewed and several salt compositions like ZrF_4-salts and BeF_2-salts were recommended as the best coolant in primary system of AHTR [16,17].

The commercial high-efficiency solar power facilities, especially parabolic trough CSPs utilizes both synthetic oil and molten salt as heat transfer fluids for their systems [18]. High-Pr thermal oils like Therminol® VP-1, Dowtherm® A, or Diphyl® are the most widely-used fluids in currently-operational CSPs [19–21]. The thermal oils have wide operating temperature range with high heat capacity which have advantages in heat transfer and heat storage systems. However, their problems like upper temperature limitation, degradation over time, high cost, and inflammability made themselves be replaced by heat transfer salts for CSPs. Then, nitrite-based salts have been highlighted as useful media for CSPs due to their economic efficiency and less corrosive characteristics. Solar Salt ($NaNO_3$-KNO_3) is the most commonly used salt for the commercial solar power systems like Solar Two central receiver systems and other solar plants [22,23]. HITEC is also widely used as a heat transfer fluid and thermal storage medium for its low melting point, good thermal stability, similar viscosity to water, and comparable thermal conductivity [24,25].

The ideal characteristics of heat transfer fluid for closed heat transport systems, especially for commercial facilities, include large operating temperature with low melting point, thermal stability, low vapor pressure, material compatibility, low viscosity, high thermal conductivity, high heat capacity, and economic efficiency [26,27]. In that sense, heat transfer characteristics of molten salts are not superior to other heat transfer fluids, since molten salts have comparable heat capacity but low thermal conductivity and high viscosity [28]. However, with large operating temperature range and economic efficiency, the molten salts become competitive media for the heat transport systems. And even, the detailed information of molten salt properties has not been studied yet. In the other words, heat transfer performance of molten salts in the heat transport system should be assessed mainly with respect to thermophysical properties such as heat capacity, thermal conductivity, and fluid viscosity.

1.3 Review on Heat Transfer behavior of High-Pr fluid

The dependency of mean Nusselt number (*Nu*) on the mean Prandtl number (*Pr*) has been widely accepted as a form of simple power law, especially for forced internal flow of broad Prandtl number range in a tube. Prandtl number is a dimensionless number that accounts for heat transfer mode of fluid, which is independent of external conditions. Then, Reynolds number (*Re*) or Grashof number (*Gr*) takes responsibility for the influence of external conditions on mean Nusselt number. Generally, forced convective heat transfer correlation is expressed as a function of Reynolds number and Prandtl number, while natural convective heat transfer correlations employ Grashof number, Prandtl number, and Rayleigh number.

$$\text{Reynolds number, } \mathrm{Re} = UL/\nu \tag{1.1}$$

$$\text{Grashof number, } \mathrm{Gr} = gL^3\beta\Delta T/\nu^2 \tag{1.2}$$

$$\text{Prandtl number, } \mathrm{Pr} = \nu/\alpha \tag{1.3}$$

$$\text{Rayleigh number, } Ra = Gr \cdot \mathrm{Pr} \tag{1.4}$$

where U is a velocity scale, L is a fluid characteristics length scale, ν is a kinematic viscosity, g is an acceleration of gravity, β is a thermal expansion coefficient, α is a thermal diffusivity, and ΔT is a temperature difference scale.

Table 1.1 summarizes previous Nusselt correlations for forced internal flow in a circular tube. In the first work done by Sieder-Tate et al. [29], the author proposed an exponent of 1/3 for the mean Prandtl number in laminar flow region. Similarly, Martinelli and Boelter developed Nusselt correlation in same form with different multiplication factor in laminar flow regime [30]. Beyond the laminar flow region, Hoffman and Cohen proposed the modified form of Hausen equation for transition region between laminar and turbulent flow [31]. Lastly, several Nusselt correlations were proposed in various forms for turbulent flow region. McAdams introduced well-known correlation referred as Dittus-Boelter equation for turbulent flow, while Sieder and Tate' equation and Hausen's equation modified it by considering wall viscosity effect [29,31,32]. On the other hand, Gnielinski proposed complex form of Nusselt correlation for turbulent flow region [33].

In the natural convection, previous studies proposed empirical Nusselt correlation as a function of Rayleigh number. In 1975, Morgan introduced simple form of Nusselt correlation with respect to Rayleigh number based on literature review [34]. The widely-accepted semi-empirical correlation

developed by Churchill and Chu also proposed the dependency of Nusselt number on Rayleigh number in complex form [35]. On the other hand, Fand [36] proposed additive form of Nusselt correlation with respect to Rayleigh number and Prandtl number. Table 1.2 summarizes Nusselt correlations for free convection, while the proposed correlations were only applicable to external flow on circular cylinders.

As shown in Table 1.1 and Table 1.2, the majority of Nusselt correlations are only applicable to turbulent flow region where Reynolds number is greater than 10,000. On the contrary, few heat transfer correlations exist in laminar and transition flow region. Especially, researches on the prediction of natural heat transfer inside the tube are rare. As mentioned in the previous section, the typical energy or heat transport system is closed circulation loop, mainly made by circular tube. In that aspect, there's always doubt on the feasibility of classical Nusselt correlations to the evaluation of heat transfer performance in practical heat transport system. Especially, for high-Prandtl number fluids like oils and salts, the reliability in employing the classical Nusselt correlations becomes weaken, since still the classical correlations don't take the distinct heat transfer feature of high Prandtl number fluid into consideration. Thus, the present study reports the distinct heat transfer feature of high Prandtl number fluid and proposes simple correlation which is specified to high Prandtl number fluids.

Table 1-1. Review on forced convective heat transfer correlations

Ref.	Nusselt correlation	Range Condition
Sieder-Tate [29]	$Nu = 1.86\,\mathrm{Re}^{1/3}\,\mathrm{Pr}^{1/3}\left(D/L\right)^{1/3}\left(\mu_b/\mu_w\right)^{0.14}$	$\mathrm{Re} \le 1000$
Martinelli and Boelter [30]	$Nu = 1.62\,\mathrm{Re}^{1/3}\,\mathrm{Pr}^{1/3}\left(D/L\right)^{1/3}$	$\mathrm{Re} \le 1000$
Hoffman [31]	$Nu = 0.116\left(\mathrm{Re}^{2/3}-125\right)\mathrm{Pr}^{1/3}\left(\mu_b/\mu_w\right)^{0.14}$	$2300 \le \mathrm{Re} \le 10^6$ $0.6 \le \mathrm{Pr} \le 1000$
Hausen [31]	$Nu = 0.037\left(\mathrm{Re}^{0.75}-180\right)\mathrm{Pr}^{0.42}\left[1+\left(d/l\right)^{2/3}\right]\left(\mu_b/\mu_w\right)^{0.14}$	$2300 \le \mathrm{Re} \le 10^6$ $0.6 \le \mathrm{Pr} \le 1000$
McAdams [32]	$Nu = 0.023\,\mathrm{Re}^{0.8}\,\mathrm{Pr}^{0.41}$	$10^4 \le \mathrm{Re}$ $0.6 \le \mathrm{Pr} \le 160$
Sieder-Tate [29]	$Nu = 0.027\,\mathrm{Re}^{0.8}\,\mathrm{Pr}^{1/3}\left(\mu_b/\mu_w\right)^{0.14}$	$10^4 \le \mathrm{Re}$ $0.7 \le \mathrm{Pr} \le 16700$
Gnielinski [33]	$Nu = 0.012\left(\mathrm{Re}^{0.8}-280\right)\mathrm{Pr}^{0.4}\left(1+\left(d/l\right)^{2/3}\right)\left(\mathrm{Pr}_b/\mathrm{Pr}_w\right)^{0.11}$	$10^4 \le \mathrm{Re}$ $0.7 \le \mathrm{Pr} \le 16700$
	$Nu = \left[\left(f/8\right)\mathrm{Re}\,\mathrm{Pr}\right]/\left[1+8.7\left(f/8\right)^{1/2}\left(\mathrm{Pr}^{2/3}-1\right)\right]$ $f = \left(1.82\log\mathrm{Re}-1.64\right)^{-2}$	$4\cdot10^3 \le \mathrm{Re} \le 10^5$ $0.5 \le \mathrm{Pr} \le 200$

Table 1-2. Review on free convective heat transfer correlations for external flow on circular cylinders

Ref.	Nusselt correlation	Range Condition
Morgan [34]	$Nu = C \cdot Ra^n$	$10^{-10} \le Ra \le 10^{12}$
Churchill and Chu [35]	$Nu = \left[0.6+0.387\left(Ra/\left(1+\left(0.599/\mathrm{Pr}\right)^{9/16}\right)^{16/9}\right)^{1/6}\right]^2$	$Ra < 10^{12}$
Fand [36]	$Nu = 0.4\,\mathrm{Pr}^{0.0432}\,Ra^{0.25}+0.503\,\mathrm{Pr}^{0.0334}\,Ra^{0.0816}+0.958Ge^{0.1222}/\left(\mathrm{Pr}^{0.06}\,Ra^{0.0511}\right)$	$10^{-8} \le Ra \le 10^8$

1.4 Research Objectives and Scope

The present study aims for the study on heat transfer behavior of high-Prandtl number fluid and its feasibility test to the passive heat transport system. The paper includes both numerical study using newly-developed sensitivity analysis method and experimental studies using high-Prandtl number oil and salt.

The research objectives are as follows:

1) Assessment of sensitivity of passive heat transport system using high-Prandtl number fluid
2) Development of effective sensitivity analysis method for direct assessment of heat transfer performance in high-Prandtl number fluid circulation system
3) Experimentally analysis of heat transfer performance of high-Prandtl number oil in natural and forced circulation
4) Establishment of experimental platform for high-Prandtl number salt in natural and forced circulation.
5) Study on the distinct heat transfer features of high-Prandtl number fluid in circulation systems

Chapter 1 reviews the various heat transport systems using high-Pr fluid and general heat transfer behaviors of high-Pr fluid to define the motivation, objectives, and originality of this paper.

Chapter 2 describes the numerical study on the feasibility test on passive heat transport system using high-Pr fluid.

Chapter 3 reports the experimental work on heat transfer behaviors of high-Pr oil in forced circulation system. The experiments using high-Pr oil in a closed rectangular loop were performed under forced circulation condition. The forced heat transfer performance of high-Pr oil was analyzed with respect to Reynolds number and Prandtl number. The distinct heat transfer feature of high-Pr fluid characterized by local natural convection was suggested based on the experimental data. Finally, new heat transfer correlation for high-Pr fluid was proposed taking the local natural convection into consideration.

Chapter 4 reports the establishment of experimental platform for high-Pr salt in natural and forced circulation. In a closed rectangular loop, natural circulation of high-Pr salt was tested in the aspect of heat transfer.

Chapter 5 concludes the paper with the conclusions and recommendations.

Chapter 2. FEASIBILITY TEST ON PASSIVE HEAT TRANSPORT SYSTEM USING HIGH-PRANDTL NUMBER FLUID

2.1 Introduction

Recently, the necessity of innovative passive heat removal systems has grown in the nuclear engineering field. The passive heat removal systems completely rely on the use of natural phenomena, which reduce the failure probability of active components and operational costs. Many Gen-IV reactors as well as existing nuclear reactors employ various heat removal systems to achieve these advantages from passive operations. Especially, a passive heat removal system is a representative passive system for Gen-IV reactor, thus various advanced nuclear reactors employ different types of passive decay heat removal system. Sodium-cooled fast reactors (SFRs) adopted natural circulation circuit using liquid metal such as sodium [37] and gallium [38] for its decay heat removal. Liquid metal-cooled fast reactors (LFRs) also utilize liquid metal like LBE [39,40] to the middle passive residual heat removal loop. In addition, the passive decay heat removal system is employed in the integrated-type of small-modular nuclear reactors (SMRs) like MASLWR [41] and SMART [42]. The unique feature of molten salt reactor (MSR) which employs liquid fuel system requires different kind of decay heat removal system called fuel salt drain system [43]. All these passive systems are designed to remove residual core heat only by single-phase natural circulation.

However, the driving forces for the passive systems are normally weak, which make themselves more sensitive to the small changes in design parameters. Thus, it is required to secure their reliability and performance, and numerous previous works assessed the reliability of the passive heat removal system for advanced nuclear reactor systems using various methods. The reliability of the sodium-cooled and gallium-cooled passive decay heat removal systems for SFR were assessed by transient analysis using thermal-hydraulic code [37,38] or by probabilistic approach [38,44]. Wu et al. [39] and Farmer et al. [40] analyzed the reliability of passive decay heat removal system for LFR in transient. The reliability of passive decay heat removal system for SMRs was also tested both in transient and probabilistic approaches [41,45,46]. However, there were few researches which tested the passive decay heat removal system using molten salt for MSR [43,47]. Instead, there has been several works on the natural circulation of fuel salt inside the primary loop of MSR or natural circulation of molten salt itself. Ruiz et al. [48] investigated the natural circulation of heat transport salt as well as internally-heated salt which represented fuel salt. The rectangular closed loop was developed using 1D numerical tool and its flow stability maps with respect to modified dimensionless numbers were computed under different loop configurations. Avigni et al. [49] also numerically tested the natural circulation of molten salt inside the Liquid Salt Test Loop for pebble bed advanced high temperature reactor. The simplified tool based on the point kinetics was developed using TRACE to evaluate the shutdown transients of molten salt fast reactor. They presented the

optimized input powers to maintain the certain fluid temperatures at the test section outlet and the heat exchanger outlet, respectively in the natural circulation loop. Kudariyawar et al. [50] performed both experimental and 3D computational works on the natural circulation behavior of molten salt inside the closed loop. The transient evolutions of temperature and mass flow rate were reported under different conditions such as flow initiation, power rising and power step back, power trip, and loss of heat sink. Similar work was done by Srivastava et al. [51] with same experimental facility and 1D numerical model. The loop performances in terms of mass flow rate and temperature were recorded under same transient conditions. Recently, Jiao et al. [52] analyzed the functional reliability of natural circulation system using molten salt. The authors employed best-estimate method to define the functional reliability of natural circulation system in terms of maximum and minimum temperatures of molten salt. However, still none of the previous works evaluated the reliability of natural circulation system in terms of both flow characteristics and heat transfer performance under different systematic conditions. Thus, this study investigated thermal-hydraulic reliability of natural circulation system using molten salt, with a typical configuration for the further extension to various applications.

The sensitivity analysis is one of effective techniques to assess the overall thermal-hydraulic reliability of certain system. However, the complexity of heat transport system requires large computational effort, especially in performing the sensitivity analysis with respect to various parameters. Then the adjoint-based approach has been paid attention to identify the importance of parameters as an effective method. The main principle of adjoint method is the formulation of second system of equations which is mathematically related to the forward system of equations, referred as an adjoint system. Then, only evaluating inner products for each sensitivity variable is required, after solving the forward and adjoint equations once. This feature of adjoint method leads to the independence from the number of design parameters, which reduces the computational effort rather than proportional to the number of design parameters. Therefore many classical research already adopted the adjoint method to solve engineering problems such as control theory [53–55], and design optimization [56–59].

In this study, this efficient sensitivity technique was employed to investigate the sensitivity of natural circulation system using molten salt, which represented the advanced passive heat removal system. From the previous studies [60,61], it was proven experimentally that the simulant fluid, DOWTHERM RP could represent the flow characteristics and heat transfer performance of molten salt. Based on the previous knowledge and experimental data, the present study initiated the establishment of sensitivity model from the validated 1D heat transport model. The adjoint-based sensitivity model was developed from the conservative governing equations in the natural circulation inside a closed rectangular loop. The verification and validation of adjoint-based sensitivity model was achieved. Finally, the adjoint-based sensitivity analysis the reliability of natural circulation of molten salt simulant inside the closed loop was tested with various design parameters, different cases, and different objectives of interest.

2.2 Development of adjoint sensitivity model

Based on the established pressurization strategies, the parameters will be controlled in the experiments were summarized to observe their influence. Fill ratio of the working fluid, initial amount of non-condensable gas (initial pressure), and heat loads were selected as controlled parameters. To confirm the feasibilities of the pressurization strategies and observe the effects of controlled parameters on the pressurization phenomena in the test sections, test matrix was established as presented in Table 2-1. In this section, the details on prepared test section for the experiments were described. Information on experimental facility, test procedure, and data processing which were utilized to measure the performances of the hybrid control rods according to parameters and pressure control strategies was demonstrated. Then, experimental uncertainties were analyzed to check the accuracy of the experimentally measured results.

2.2.1 Background of adjoint sensitivity model

In the process of reliability assessment, not only the fidelity of modelling the problems but also the computing power required to complete the calculations is challenge. As the number of parameters to be tested increases, the computing power issue becomes more important. The adjoint method is the most viable technique to reduce computational effort with maintaining the fidelity of calculations, especially in large and complex problems. The unique feature of adjoint method compared to other methods is to formulate the secondary problem called adjoint problem and relate it to the forward problem mathematically. Since the solution of secondary problem is independent of input parameters, solving desired objectives requires only a single calculation of secondary problem regardless of the number of input parameters. The only challenge in adjoint sensitivity approach is to formulate appropriate secondary problem and to get accurate adjoint solution. The distinguishing feature of adjoint sensitivity method in general mathematical form is described in the present section.

Let denote the arbitrary input parameter and dependent variable as α and $\mathbf{x}$, respectively. The set of forward problems is defined as $\mathbf{F}$, shown in Eq. (2.1).

$$\mathbf{F} = \begin{pmatrix} F_1 \\ F_2 \\ \vdots \\ F_N \end{pmatrix} = 0 \tag{2.1}$$

The objective function, r can be any function of α and $\mathbf{x}$. Then the sensitivity of objective function is

defined as follows:

$$\frac{d}{d\alpha}\left(r\left(\alpha,x\right)\right)=\frac{\partial r}{\partial \alpha}+\frac{\partial r}{\partial x}\cdot\frac{dx}{d\alpha} \tag{2.2}$$

With a finite difference approximation, the gradient of **x** with respect to α can be expressed as:

$$\frac{dx}{d\alpha}\approx\frac{x_1-x_0}{\alpha_1-\alpha_0} \tag{2.3}$$

where subscripts 0 and 1 are for the unperturbed problem and perturbed problem, respectively, which are expressed as Eqs. (2.4-2.5).

$$\mathbf{F}=\begin{pmatrix} F_1\left(\alpha_0,x_0\right) \\ F_2\left(\alpha_0,x_0\right) \\ \vdots \\ F_N\left(\alpha_0,x_0\right) \end{pmatrix}=0 \tag{2.4}$$

$$\mathbf{F}=\begin{pmatrix} F_1\left(\alpha_1,x_1\right) \\ F_2\left(\alpha_1,x_1\right) \\ \vdots \\ F_N\left(\alpha_1,x_1\right) \end{pmatrix}=0 \tag{2.5}$$

Then, the calculation of the gradient of **x** with respect to α requires additional solution of perturbed problem. That is, each addition of parameter to the sensitivity equation requires each additional calculation of forward problem, which burdens the computational tool with the increase of the number of iteration.

However, if the adjoint solution is defined to satisfy Eq. (2.6), adjoint sensitivity equation is evaluated as Eq. (2.8) from the substituting Eq. (2.7) into Eq. (2.2). Note that, Eq. (2.7) holds, as the forward equation **F** is always zero.

$$\left(\frac{\partial F}{\partial x}\right)^{\dagger}\lambda=\left(\frac{\partial r}{\partial x}\right)^{\dagger} \quad \text{or} \quad \lambda^{\dagger}=\left(\frac{\partial r}{\partial x}\right)\cdot\left(\frac{\partial F}{\partial x}\right)^{-1} \tag{2.6}$$

$$\frac{d\mathbf{F}}{d\alpha}=\frac{\partial\mathbf{F}}{\partial\alpha}+\frac{\partial\mathbf{F}}{\partial x}\cdot\frac{dx}{d\alpha}=0 \quad \text{or} \quad \frac{dx}{d\alpha}=-\left(\frac{\partial\mathbf{F}}{\partial x}\right)^{-1}\cdot\left(\frac{\partial\mathbf{F}}{\partial\alpha}\right) \tag{2.7}$$

$$\frac{dr}{d\alpha}=\frac{\partial r}{\partial\alpha}-\frac{\partial r}{\partial x}\cdot\left(\frac{\partial\mathbf{F}}{\partial x}\right)^{-1}\cdot\left(\frac{\partial\mathbf{F}}{\partial\alpha}\right)=\frac{\partial r}{\partial\alpha}-\left[\frac{\partial r}{\partial x}\cdot\left(\frac{\partial\mathbf{F}}{\partial x}\right)^{-1}\right]\cdot\left(\frac{\partial\mathbf{F}}{\partial\alpha}\right)=\frac{\partial r}{\partial\alpha}-\lambda^{\dagger}\left(\frac{\partial\mathbf{F}}{\partial\alpha}\right) \tag{2.8}$$

where $\lambda^{\dagger}$ is the adjoint solution vector.

Here, with the same objective function and forward equation, Eq. (2.6) holds for every α. Thus, the adjoint method requires solving a single forward equation and a single adjoint equation to complete the all the sensitivity computation, regardless of the number of parameters. Finally, the cost to produce sensitivity results using adjoint approach is nearly equals to the cost to solve two forward equations, which makes the adjoint method more efficient technique for the sensitivity analysis. The development of adjoint sensitivity equations for the practical engineering problem is presented in the following section.

2.2.2 Adjoint sensitivity model for passive heat transport system

In the present section, adjoint method for performing sensitivity analysis is described. For the sensitivity analysis, 1D heat transport system using molten salt inside the closed natural circulation loop was considered. The adjoint sensitivity equations were developed for the engineering problem with the objective functionals of mass flux and temperature.

2.2.2.1 General governing equations of 1D heat transport system

In the present work, the closed rectangular loop configuration was studied which benchmarked the experimental facility in UNIST. It composed of a single vertical heater and two water-cooled heat exchangers with a circular tube cross-section of constant diameter, as shown in Fig. 2.1. Then the system governing equations were developed with the following assumptions:

- The one-dimensional flow was considered with an incompressible fluid. The position inside the loop was denoted as curvilinear coordinate, “s” following the direction of fluid flow.
- The entrance of the cooler was set as the origin and the reference values were evaluated at the origin.
- The Boussinesq approximation was considered.

- The constant and uniform external heat flux was applied through the heater section as a heat source in the governing equations.
- The water-cooled heat exchangers were modeled as constant wall temperature coolers.
- The heat conduction and dissipative terms of the energy conservation equation were neglected.
- The friction factor for the distributed pressure drop, denoted as f, was assumed as Darcy friction factor in laminar flow regime. The localized friction factor was denoted as f_{local} and assumed as an arbitrary constant.

Then the governing equations with the above assumptions are:

$$\frac{\partial G}{\partial s} = 0 \tag{2.9}$$

$$\frac{\partial G}{\partial t} + \frac{\partial}{\partial s}\left(\frac{G^2}{\rho_{ref}}\right) = -\frac{\partial p}{\partial s} - \rho g \underline{e}_z \cdot \underline{e}_s - \left(f + f_{local}\right)\frac{1}{D_h}\frac{G^2}{2\rho_{ref}} \tag{2.10}$$

$$\frac{\partial\left(c_p T\right)}{\partial t} + \frac{1}{\rho_{ref}} G \frac{\partial\left(c_p T\right)}{\partial s} + \frac{4}{\rho_{ref} D_h} \cdot h\left(T\right) \cdot \left(T - T_w\right) - \frac{4}{\rho_{ref} D_h} \dot{q}'' = 0 \tag{2.11}$$

$$\rho\left(T\right) = \rho_{ref}\left[1 - \beta\left(T - T_{ref}\right)\right] \tag{2.12}$$

$$f = \frac{a}{\mathrm{Re}^b} = \frac{a\mu^b}{G^b D^b} \tag{2.13}$$

where G is the mass flux, ρ_{ref} is the reference density at the steady state, D_h is the hydraulic diameter of the loop, c_p is the fluid specific heat, h is the heat transfer coefficient of cooler, T_w is the cooler wall temperature, q'' is the external heat flux, β is the thermal expansion coefficient, μ is the fluid dynamic viscosity, a and b are the empirical constants in Darcy friction factor, $\mathbf{e_z}$ and $\mathbf{e_s}$ are the unit vectors of gravitation and flow, respectively.

Substituting Eqs. (2.12) and (2.13) into Eq. (2.10) and integrating over the entire loop produced:

$$\frac{\partial G}{\partial t}+\frac{a}{2D_h^{1+b}\rho_{ref}}\cdot\frac{\oint\mu(T)^b\,ds}{L_t}\cdot G^{2-b}+f_{local}\frac{1}{D_h}\frac{G^2}{2\rho_{ref}}-\frac{\rho_{ref}g\beta}{L_t}\cdot\oint T(s,t)\underline{e}_z\cdot\underline{e}_s(s)ds=0 \tag{2.14}$$

where L_t is the total length of entire loop.

The fundamental dependencies of properties on temperature were considered, thus the analytical forms of property variations were adopted in the temperature-dependent property model. Each property was evaluated as a product of reference value and temperature-dependent function, given by Eqs. (2.15-2.17) and plotted in Fig. 2.2. The analytical functions of fluid specific heat (kJ/kgK) and viscosity (Pa*s) with respect to the temperature (K) were derived from fitting using reference properties data of DOWTHERM RP oil with R^2=1.

$$c_p(T)=c_{p,ref}\cdot f_{c_p}(T)=0.0029T+0.748 \tag{2.15}$$

$$\mu(T)=\mu_{ref}\cdot f_\mu(T)=0.0002981+0.09146e^{\frac{272.8505-T}{17.03233}}+0.1256e^{\frac{272.8505-T}{7.00427}}+0.01064e^{\frac{272.8505-T}{64.36122}} \tag{2.16}$$

$$h(T)=h_{ref}\cdot f_h(T)=h_{ref}\cdot\frac{q_c''}{(T-T_w)} \tag{2.17}$$

Finally, the initial and boundary conditions were defined as follows:

$$T(s,t=0)=T_{ref} \tag{2.18}$$

$$G(t=0)=G_0 \tag{2.19}$$

$$T(s=0,t)=T_{ref} \tag{2.20}$$

$$T(s=0,t)=T(s=L_t,t) \tag{21}$$

Table 2.1 summarized the specifications and parameter values in this study. The values referred the specification of experimental facility in UNIST and properties of DOWTHERM RP oil used as a working fluid of previous experiments.

In the present section, adjoint method for performing sensitivity analysis is described. For the sensitivity analysis, 1D heat transport system using molten salt inside the closed natural circulation loop was considered. The adjoint sensitivity equations were developed for the engineering problem with the objective functionals of mass flux and temperature.

2.2.2.2 Formulation of adjoint sensitivity equations

The adjoint sensitivity system for the coupled set of equations was formulated by the Lagrangian approach, following the previous works [62–65]. Let the objective functional, R be defined as:

$$R = \int_{t_0}^{\tau} \langle r(x,\alpha) \rangle dt \tag{2.22}$$

Then, the Lagrangian was formed as follows:

$$\mathbf{L} = R - \int \langle \lambda^{\dagger}, \mathbf{F} \rangle dt \tag{2.23}$$

where $\mathbf{L}$ is the Lagrangian function, $\mathbf{F}$ is the forward operator in the coupled differential equations in this problem, the angular brackets denote integrals over all space. As $\mathbf{F}$ was defined to be zero in Eqs. (2.11) and (2.14), the objective functional is equivalent to the Lagrangian. Thus, the sensitivity of objective functional was derived from the derivative of the Lagrangian with respect to the design parameter, α, as follows:

$$\frac{dR}{d\alpha} = \frac{d\mathbf{L}}{d\alpha} = \int_{t_0}^{\tau} \langle r_{\alpha} + r_x \mathbf{x}_{\alpha} \rangle dt - \int \left\langle \lambda^{\dagger}, \frac{d\mathbf{F}}{d\alpha} \right\rangle dt \tag{2.24}$$

where $\mathbf{x}=(G\ T)^{\mathrm{T}}$ in this problem, and subscripts on functions are used to denote partial derivatives with respect to α,s, and t. The last term of RHS in Eq. (2.24) could be rewritten using integration by parts as:

$$\begin{aligned} \int \left\langle \lambda^{\dagger}, \frac{d\mathbf{F}}{d\alpha} \right\rangle dt &= \int \left\langle \lambda^{\dagger} \cdot \left(\mathbf{F}_{\alpha} + \mathbf{F}_x \mathbf{x}_{\alpha} + \mathbf{F}_{x_s} \mathbf{x}_{s,\alpha} + \mathbf{F}_{x_t} \mathbf{x}_{t,\alpha} \right) \right\rangle dt \\ &= \int \langle \lambda^{\dagger} \cdot \mathbf{F}_{\alpha} \rangle dt + \int \lambda^{\dagger} \cdot \mathbf{F}_{x_s} \mathbf{x}_{\alpha} \Big|_{s_0}^{L} dt + \langle \lambda^{\dagger} \cdot \mathbf{F}_{x_t} \mathbf{x}_{\alpha} \rangle \Big|_{t_0}^{\tau} + \int \left\langle \left(\lambda^{\dagger} \cdot \mathbf{F}_x - \frac{\partial \left(\lambda^{\dagger} \cdot \mathbf{F}_{x_s} \right)}{\partial s} - \frac{\partial \left(\lambda^{\dagger} \cdot \mathbf{F}_{x_t} \right)}{\partial t} \right) \mathbf{x}_{\alpha} \right\rangle dt \end{aligned} \tag{2.25}$$

Thus, Eq. (2.24) became:

$$\frac{dR}{d\alpha}=\frac{d\mathbf{L}}{d\alpha}=\int_{t_0}^{\tau}\left\langle r_\alpha-\lambda^\dagger\cdot\mathbf{F}_\alpha\right\rangle dt-\int\lambda^\dagger\cdot\mathbf{F}_{x_s}\mathbf{x}_\alpha\Big|_{s_0}^{L}dt-\left\langle\lambda^\dagger\cdot\mathbf{F}_{x_t}\mathbf{x}_\alpha\right\rangle\Big|_{t_0}^{\tau}$$
$$-\int\left\langle\left(-r_x+\lambda^\dagger\cdot\mathbf{F}_x-\frac{\partial\left(\lambda^\dagger\cdot\mathbf{F}_{x_s}\right)}{\partial s}-\frac{\partial\left(\lambda^\dagger\cdot\mathbf{F}_{x_t}\right)}{\partial t}\right)\mathbf{x}_\alpha\right\rangle dt \tag{2.26}$$

Finally, the adjoint equations were defined to eliminate the last integral term in Eq. (2.26), as follows:

$$-r_x+\lambda^\dagger\mathbf{F}_x-\frac{\partial\left(\lambda^\dagger\cdot\mathbf{F}_{x_s}\right)}{\partial s}-\frac{\partial\left(\lambda^\dagger\cdot\mathbf{F}_{x_t}\right)}{\partial t}=0 \tag{2.27}$$

,and the sensitivity of the objective functional was expressed as:

$$\frac{dR}{d\alpha}=-\left\langle\lambda^\dagger\cdot\mathbf{F}_{x_t}\mathbf{x}_\alpha\right\rangle\Big|_{t_0}^{\tau}-\int\lambda^\dagger\cdot\mathbf{F}_{x_s}\cdot\mathbf{x}_\alpha\Big|_{s_0}^{L}dt+\int_{t_0}^{\tau}\left\langle r_\alpha-\lambda^\dagger\cdot\mathbf{F}_\alpha\right\rangle dt \tag{2.28}$$

where the first and second terms became zero by imposing the initial and boundary conditions of adjoint sensitivity equations, respectively.

In addition, the normalized sensitivity, N_α, defined as Eq. (2.29) was employed to present the importance of each parameter for each variable.

$$N_\alpha=\frac{\alpha}{R}\frac{dR}{d\alpha} \tag{2.29}$$

2.2.3 Validation of adjoint sensitivity model for passive heat transport system

2.2.3.1 Mass flux and temperature

Let R be the general objective functional expressed as:

$$R = \int_{t_0}^{\tau} \left\langle G(s,t) + T(s,t) \right\rangle dt = \int_{t_0}^{\tau} \left\langle r(G,T,\alpha) \right\rangle dt \tag{2.30}$$

From Eqs. (2.11) and (2.14), forward operator **F** was defined as:

$$\mathbf{F} = \begin{pmatrix} F_1 \\ F_2 \end{pmatrix} = \begin{pmatrix} \dfrac{\partial G}{\partial t} \cdot \dfrac{1}{L_t} + f(G,T) \\ \dfrac{\partial (c_p T)}{\partial t} + \dfrac{G}{\rho_{ref}} \dfrac{\partial (c_p T)}{\partial s} + g(G,T) \end{pmatrix} = 0 \tag{2.31}$$

with

$$f(G,T) = \frac{a\mu^b}{2D_h^{1+b}\rho_{ref}L_t} \cdot G^{2-b} + f_{local}\frac{1}{D_h}\frac{G^2}{2\rho_{ref}} \cdot \frac{1}{L_t} - \frac{\rho_{ref} g\beta}{L_t} \cdot T(s,t)\underline{e}_z \cdot \underline{e}_s(s)$$

$$g(G,T) = \frac{4}{\rho_{ref} D_h} \cdot h(T) \cdot (T - T_w) - \frac{4}{\rho_{ref} D_h}\dot{q}''$$

Substituting Eqs. (2.30) and (2.31) into Eq. (2.28) and splitting into its constituent components produced the adjoint equations as:

$$-\frac{\partial G^\dagger}{\partial t} \cdot \frac{1}{L_t} + \left[\frac{a(2-b)\mu^b}{2D_h^{1+b}\rho_{ref}L_t} \cdot G^{1-b} + 2 \cdot f_{local}\frac{1}{D_h}\frac{G}{2\rho_{ref}L_t} \right] G^? + \frac{1}{\rho_{ref}}\frac{\partial (c_p T)}{\partial s} \cdot T^\dagger = 1 \tag{2.32}$$

$$\begin{aligned} &-\frac{\partial (c_p T)}{\partial T} \cdot \frac{\partial T^\dagger}{\partial t} - \frac{G}{\rho_{ref}}\frac{\partial (c_p T)}{\partial T} \cdot \frac{\partial T^\dagger}{\partial s} + \left[\frac{ab\mu^{b-1}G^{2-b}}{2D_h^{1+b}\rho_{ref}L_t} \cdot \frac{\partial \mu}{\partial T} - \frac{\rho_{ref} g\beta}{L_t}\underline{e}_z \cdot \underline{e}_s(s) \right] G^\dagger \\ &+ \left[\left(2\frac{\partial c_p}{\partial T} + T\frac{\partial}{\partial T}\left(\frac{\partial c_p}{\partial T} \right) \right) \cdot \left(\frac{\partial T}{\partial t} + \frac{1}{\rho^*} G \frac{\partial T}{\partial s} \right) + \frac{4(T - T_w)}{\rho_{ref} D_h} \cdot \frac{\partial h}{\partial T} + \frac{4h}{\rho_{ref} D_h} \right] T^\dagger = 1 \end{aligned} \tag{2.33}$$

where $\lambda \equiv (G^\dagger \; T^\dagger)^{\mathrm{T}}$ is the adjoint solution vector.

The numerical scheme for the sensitivity analysis employed implicit Euler discretization, which could preserve the properties of the adjoint equations [62]. The relative L-2 norm of the solutions for the convergence was set to 10^{-9} between iterations. Figs. 2.3 and 2.4 show the general solutions of forward equations and adjoint equations. Note that the adjoint equations required the appropriate terminal

conditions to be specified, while the forward equations imposed the initial conditions. The sensitivity of objective functional computed by adjoint method was compared with that computed by direct recalculation method. Here, direct recalculation referred the method that evaluated the sensitivity from dividing the change in objective functional by the change in the perturbed parameter. The parameters for the sensitivity analysis were categorized into four types. The first type was the reference fluid property including density (ρ_{ref}), viscosity (μ_{ref}), thermal expansion (β), and specific heat capacity ($c_{p,ref}$). The second was the geometric parameter including the diameter (D_h). The third was the heater and cooler conditions including reference heat transfer coefficient (h_{ref}), cooler wall temperature (T_w), and external input heat flux (q''). The last was the pressure drop parameters including Darcy friction factor constants (a, b) and localized friction factor (f_{local}). Table 2.2 summarized the comparison results between sensitivity of functional computed by direct recalculation method and adjoint method. The functional was evaluated through the entire loop in space and integrated from initial time to startup time where the mass flux became steady-state. The reference temperature was set to 423.15 K. The last column of Table 2.2 showed the error between results from direct method and adjoint method. Both methods gave the same order of sensitivity with the difference less than 6 %. Thus, it was confirmed that the adjoint sensitivity equations were established well.

Fig. 2.5 shows the computational efforts of direct and adjoint methods with the increase of the number of parameters, represented as computational time. The computation time increased almost linearly to the increase of number of parameters for direct method, since the direct method required to solve additional coupled forward equations with perturbed parameter for each sensitivity. On the contrary, the adjoint method solved only single parameter equation for each sensitivity, which led itself to be advantageous in saving time, especially for multiple parameters.

2.2.3.2 Specific objective of interest

In this study, the system performance of natural circulation loop was represented by three different objectives of interest: mass flux, temperature distribution, Nusselt number. Each variable was defined as the form of objective functional, as follows:

$$R_1 = \int_{t_0}^{\tau} \left\langle r\left(G,T,\alpha\right)\right\rangle dt = \int_{t_0}^{\tau}\int_{0}^{L} G\, dsdt \tag{2.34}$$

$$R_2 = \int_{t_0}^{\tau} \left\langle r\left(G,T,\alpha\right)\right\rangle dt = \int_{t_0}^{\tau}\int_{0}^{L} T\, dsdt \tag{2.35}$$

$$R_3 = \int_{t_0}^{\tau} \left\langle r\left(G,T,\alpha\right)\right\rangle dt = \int_{t_0}^{\tau}\int_{0}^{L} Nu\left(G,T,\alpha\right) dsdt = \int_{t_0}^{\tau}\int_{0}^{L} \frac{h\left(T,\alpha\right)D_h\left(\alpha\right)}{k_f} dsdt \tag{2.36}$$

where k_f is the constant fluid thermal conductivity.

With same forward operator **F**, each set of adjoint equations was defined as:

$$-\frac{\partial G_1^{\dagger}}{\partial t}\cdot\frac{1}{L_t} + \left[\frac{a\left(2-b\right)\mu^b}{2D_h^{1+b}\rho_{ref}L_t}\cdot G^{1-b} + 2\cdot f_{local}\frac{1}{D_h}\frac{G}{2\rho_{ref}L_t}\right]G_1^{?} + \frac{1}{\rho_{ref}}\frac{\partial\left(c_pT\right)}{\partial s}\cdot T^{\dagger} = 1 \tag{2.37a}$$

$$\begin{aligned} &-\frac{\partial\left(c_pT\right)}{\partial T}\cdot\frac{\partial T_1^{\dagger}}{\partial t} - \frac{G}{\rho_{ref}}\frac{\partial\left(c_pT\right)}{\partial T}\cdot\frac{\partial T_1^{\dagger}}{\partial s} + \left[\frac{ab\mu^{b-1}G^{2-b}}{2D_h^{1+b}\rho_{ref}L_t}\cdot\frac{\partial\mu}{\partial T} - \frac{\rho_{ref}g\beta}{L_t}\underline{e}_z\cdot\underline{e}_s\left(s\right)\right]G_1^{\dagger} \\ &+\left[\left(2\frac{\partial c_p}{\partial T} + T\frac{\partial}{\partial T}\left(\frac{\partial c_p}{\partial T}\right)\right)\cdot\left(\frac{\partial T}{\partial t} + \frac{1}{\rho^*}G\frac{\partial T}{\partial s}\right) + \frac{4\left(T-T_w\right)}{\rho_{ref}D_h}\cdot\frac{\partial h}{\partial T} + \frac{4h}{\rho_{ref}D_h}\right]T_1^{\dagger} = 0 \end{aligned} \tag{2.37b}$$

$$-\frac{\partial G_2^{\dagger}}{\partial t}\cdot\frac{1}{L_t} + \left[\frac{a\left(2-b\right)\mu^b}{2D_h^{1+b}\rho_{ref}L_t}\cdot G^{1-b} + 2\cdot f_{local}\frac{1}{D_h}\frac{G}{2\rho_{ref}L_t}\right]G_2^{?} + \frac{1}{\rho_{ref}}\frac{\partial\left(c_pT\right)}{\partial s}\cdot T_2^{\dagger} = 0 \tag{2.38a}$$

$$\begin{aligned} &-\frac{\partial\left(c_pT\right)}{\partial T}\cdot\frac{\partial T_2^{\dagger}}{\partial t} - \frac{G}{\rho_{ref}}\frac{\partial\left(c_pT\right)}{\partial T}\cdot\frac{\partial T_2^{\dagger}}{\partial s} + \left[\frac{ab\mu^{b-1}G^{2-b}}{2D_h^{1+b}\rho_{ref}L_t}\cdot\frac{\partial\mu}{\partial T} - \frac{\rho_{ref}g\beta}{L_t}\underline{e}_z\cdot\underline{e}_s\left(s\right)\right]G_2^{\dagger} \\ &+\left[\left(2\frac{\partial c_p}{\partial T} + T\frac{\partial}{\partial T}\left(\frac{\partial c_p}{\partial T}\right)\right)\cdot\left(\frac{\partial T}{\partial t} + \frac{1}{\rho^*}G\frac{\partial T}{\partial s}\right) + \frac{4\left(T-T_w\right)}{\rho_{ref}D_h}\cdot\frac{\partial h}{\partial T} + \frac{4h}{\rho_{ref}D_h}\right]T_2^{\dagger} = 1 \end{aligned} \tag{2.38b}$$

$$-\frac{\partial G_3^{\dagger}}{\partial t}\cdot\frac{1}{L_t} + \left[\frac{a\left(2-b\right)\mu^b}{2D_h^{1+b}\rho_{ref}L_t}\cdot G^{1-b} + 2\cdot f_{local}\frac{1}{D_h}\frac{G}{2\rho_{ref}L_t}\right]G_3^{?} + \frac{1}{\rho_{ref}}\frac{\partial\left(c_pT\right)}{\partial s}\cdot T_3^{\dagger} = 0 \tag{2.39a}$$

$$\begin{aligned} &-\frac{\partial\left(c_pT\right)}{\partial T}\cdot\frac{\partial T_3^{\dagger}}{\partial t} - \frac{G}{\rho_{ref}}\frac{\partial\left(c_pT\right)}{\partial T}\cdot\frac{\partial T_3^{\dagger}}{\partial s} + \left[\frac{ab\mu^{b-1}G^{2-b}}{2D_h^{1+b}\rho_{ref}L_t}\cdot\frac{\partial\mu}{\partial T} - \frac{\rho_{ref}g\beta}{L_t}\underline{e}_z\cdot\underline{e}_s\left(s\right)\right]G_3^{\dagger} \\ &+\left[\left(2\frac{\partial c_p}{\partial T} + T\frac{\partial}{\partial T}\left(\frac{\partial c_p}{\partial T}\right)\right)\cdot\left(\frac{\partial T}{\partial t} + \frac{1}{\rho^*}G\frac{\partial T}{\partial s}\right) + \frac{4\left(T-T_w\right)}{\rho_{ref}D_h}\cdot\frac{\partial h}{\partial T} + \frac{4h}{\rho_{ref}D_h}\right]T_3^{\dagger} = \frac{D_h}{k_f}\cdot\frac{\partial h}{\partial T} \end{aligned} \tag{2.39b}$$

Finally, each sensitivity of variable was expressed as:

$$\frac{dR_1}{d\alpha} = \int_{t_0}^{\tau} \left\langle r_{1,\alpha} - \lambda_1^{\dagger} \cdot \mathbf{F}_{\alpha} \right\rangle dt = \int_{t_0}^{\tau} \int_{0}^{L} \left[-\lambda_1^{\dagger} \cdot \mathbf{F}_{\boldsymbol{\alpha}} \right] ds dt \tag{2.40}$$

$$\frac{dR_2}{d\alpha} = \int_{t_0}^{\tau} \left\langle r_{2,\alpha} - \lambda_2^{\dagger} \cdot \mathbf{F}_{\alpha} \right\rangle dt = \int_{t_0}^{\tau} \int_{0}^{L} \left[-\lambda_2^{\dagger} \cdot \mathbf{F}_{\boldsymbol{\alpha}} \right] ds dt \tag{2.41}$$

$$\frac{dR_3}{d\alpha} = \int_{t_0}^{\tau} \left\langle r_{3,\alpha} - \lambda_3^{\dagger} \cdot \mathbf{F}_{\alpha} \right\rangle dt = \int_{t_0}^{\tau} \int_{0}^{L} \left[\frac{\partial D_h}{\partial \alpha} \cdot \frac{h}{k_f} + \frac{\partial h_{ref}}{\partial \alpha} \cdot \frac{D_h}{k_f} \cdot \frac{h}{h_{ref}} - \lambda_3^{\dagger} \cdot \mathbf{F}_{\boldsymbol{\alpha}} \right] ds dt \tag{2.42}$$

where $\lambda_1^{\dagger}$, $\lambda_2^{\dagger}$, $\lambda_3^{\dagger}$ are adjoint solution vectors of each variable, respectively.

The same numerical scheme was employed for the sensitivity analysis of each variable. Fig. 2.6 shows the adjoint mass flux and temperature of adjoint equations for Nusselt number. The sensitivities of variable computed by direct method and adjoint method were summarized in Table 2.3, 2.4, and 2.5. Both methods gave the same order of sensitivity for all objective functionals of interest, which gave the reliability in using adjoint sensitivity method.

Table 2.1. Specifications and parameter values for sensitivity analysis

Specifications	Value
L_{c1}	0.3 (m)
L_{c2}	0.74 (m)
L_3	1.2415 (m)
L_4	0.6 (m)
L_5	0.0315 (m)
L_h	0.19 (m)
L_6	1.76 (m)
L_7	0.3 (m)
D_h	0.023 (m)
T_w	293.15 (K)
q''	72.84 (kW/m^2)
T_{ref}	423.15 (K)
ρ_{ref}	1004.52 (kg/m^3)
μ_{ref}	0.0013 (Pa s)
β	0.0006987 (1/K)
c_p	1974.7 (J/kgK)
k_f	0.12 (W/(m K))
a	64
b	1
f_{local}	0.001

Table 2.2. Direct and adjoint sensitivities of general objective functionals

Parameter	Direct method	Adjoint method	Error(%)
ρ_{ref}	135.3529	134.5889	0.57
μ_{ref}	-4.7285E+07	-4.7203E+07	0.17
β	9.6049E+07	9.6682E+07	0.65
$c_{p,ref}$	-36.8470	-38.1620	3.45
D_h	2.4602E+06	2.3359E+06	5.32
$\boldsymbol{h_{ref}}$	-125.6408	-122.7629	2.34
$\boldsymbol{T_w}$	103.1026	100.1299	2.97
$\boldsymbol{q''}$	17.2930	17.6390	1.96
a	-991.0419	-989.3198	0.17
b	4.9544E+05	4.9259E+05	0.58
$\boldsymbol{f_{local}}$	-2.4948E+06	-2.3888E+06	4.44

Table 2.3. Direct and adjoint sensitivities of mass flux

Parameter	Direct method	Adjoint method	Error(%)
ρ_{ref}	2.7922	2.3673	17.95
μ_{ref}	-8.6507E+05	-8.1356E+05	6.33
β	1.6763E+06	1.5480E+06	8.29
$c_{p,ref}$	0.8351	0.7764	7.56
D_h	1.7458E+05	1.6343E+05	6.83
$\boldsymbol{h_{ref}}$	-56.9178	-55.6700	2.24
$\boldsymbol{T_w}$	46.0503	45.0297	2.27
$\boldsymbol{q''}$	1.4961	1.4771	1.28
a	-18.1308	-17.0513	6.33
b	9.0757E+03	8.4626E+03	7.25
$\boldsymbol{f_{local}}$	-4.5923E+04	-3.9629E+04	15.88

Table 2.4. Direct and adjoint sensitivities of temperature

Parameter	Direct method	Adjoint method	Error(%)
ρ_{ref}	132.5607	132.2149	0.26
μ_{ref}	-4.6420E+07	-4.6385E+07	0.08
β	9.4373E+07	9.5135E+07	0.80
$c_{p,ref}$	-37.6821	-38.9385	3.23
D_h	2.2856E+06	2.1719E+06	5.24
$\boldsymbol{h_{ref}}$	-68.7229	-67.0910	2.43
$\boldsymbol{T_w}$	57.0523	55.0987	3.55
$\boldsymbol{q''}$	15.7969	16.1618	2.26
a	-972.9110	-972.1684	0.08
b	4.8637E+05	4.8407E+05	0.47
$\boldsymbol{f_{local}}$	-2.4489E+06	-2.3488E+06	4.26

Table 2.5. Direct and adjoint sensitivities of Nusselt number

Parameter	**Direct method**	**Adjoint method**	**Error(%)**
ρ_{ref}	-0.1016	-0.1148	11.48
μ_{ref}	3.5527E+04	3.6951E+04	3.85
β	-7.2717E+04	-8.2795E+04	12.17
$c_{p,ref}$	-0.0289	-0.0284	1.55
D_h	1.7174E+05	1.7184E+05	0.06
$\boldsymbol{h_{ref}}$	41.2663	41.3305	0.16
$\boldsymbol{T_w}$	-0.9420	-0.9524	1.09
$\boldsymbol{q''}$	-0.0207	-0.0214	3.22
a	0.7446	0.7745	3.85
b	-3.7053E+02	-3.8585E+02	3.97
$\boldsymbol{f_{local}}$	1.8177E+03	1.8775E+03	3.18

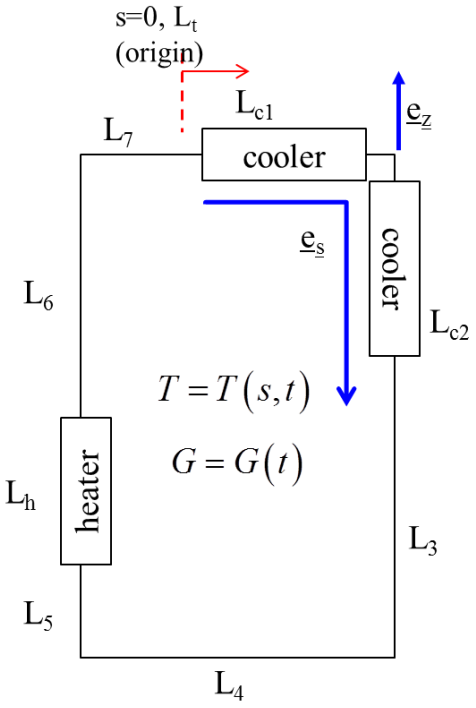

Fig. 2.1. The schematic configuration of experimental facility in UNIST

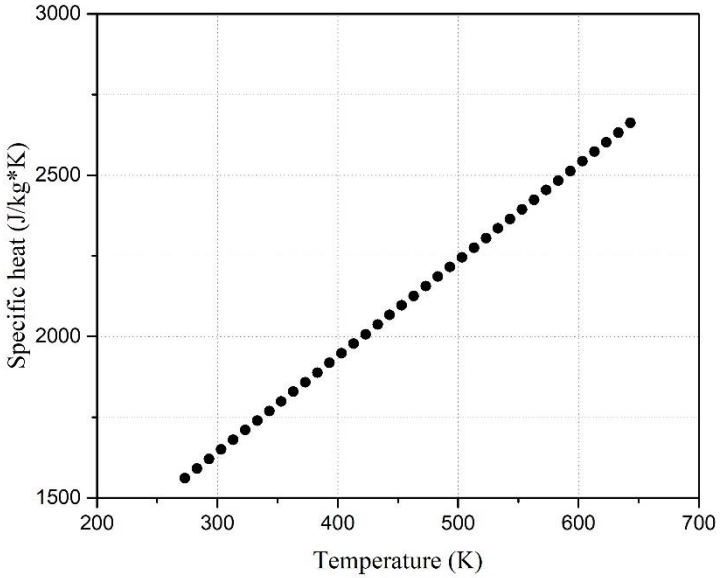

(a)

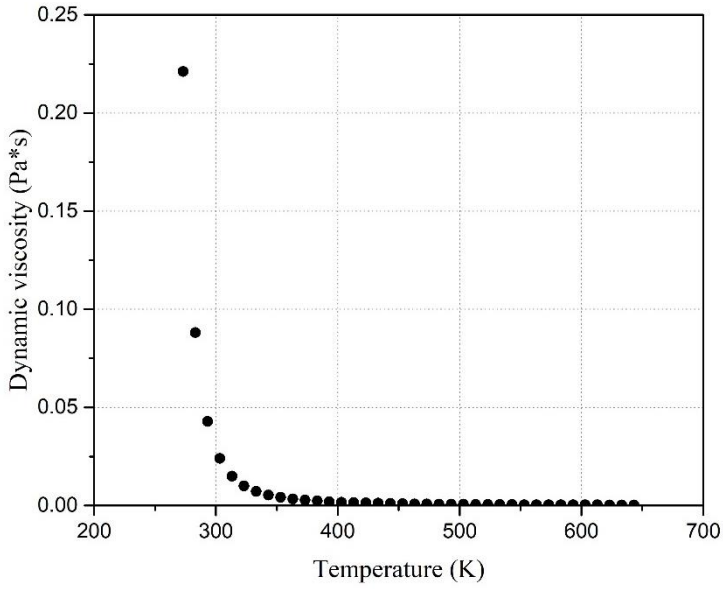

(b)

Fig. 2.2. Temperature-dependent function for fluid property of DOWTHERM RP: (a) Specific heat (b) Dynamic viscosity

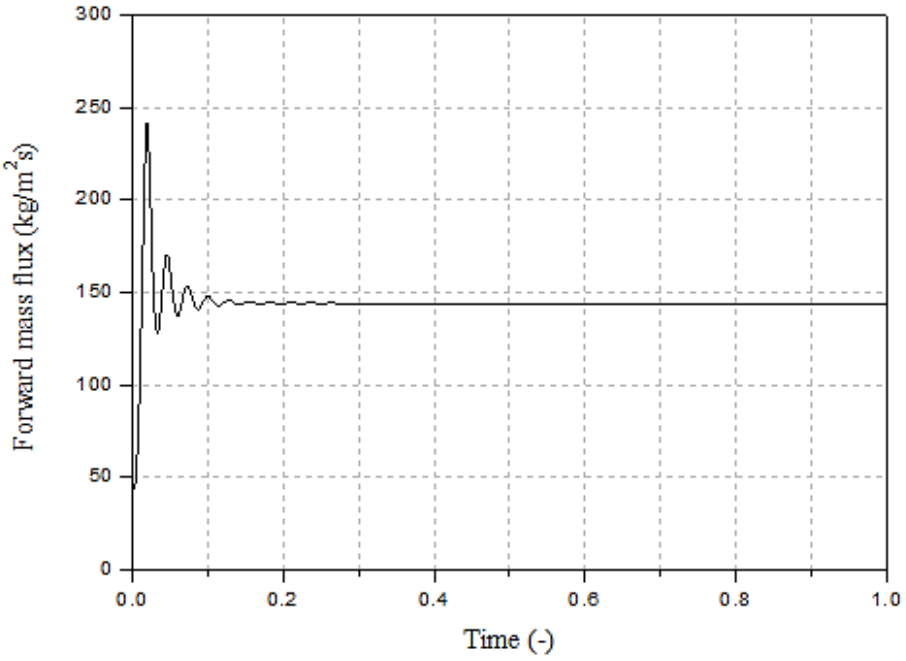

(a)

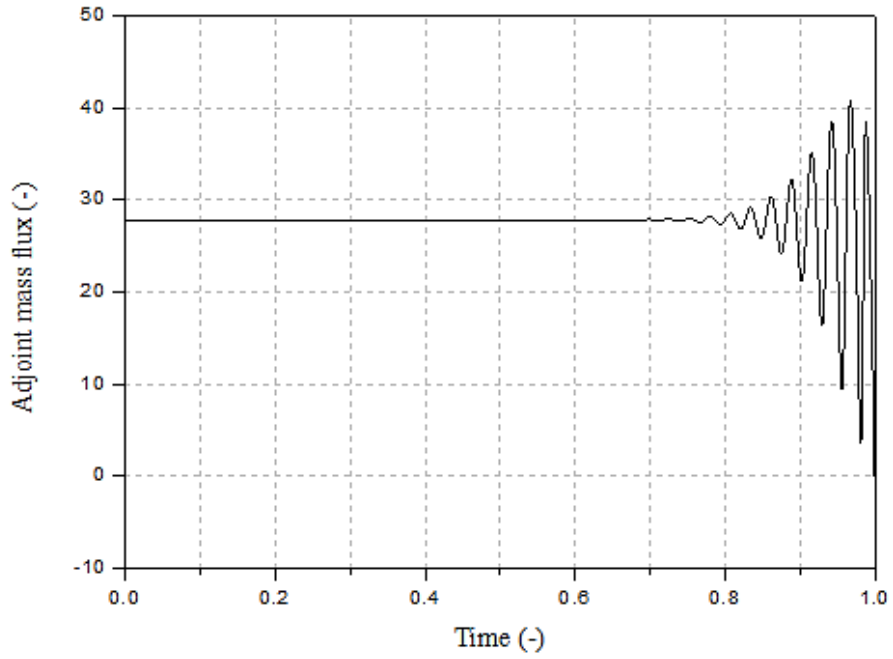

(b)

Fig. 2.3. (a) Time evolution of the forward mass flux (b) Time evolution of the adjoint mass flux

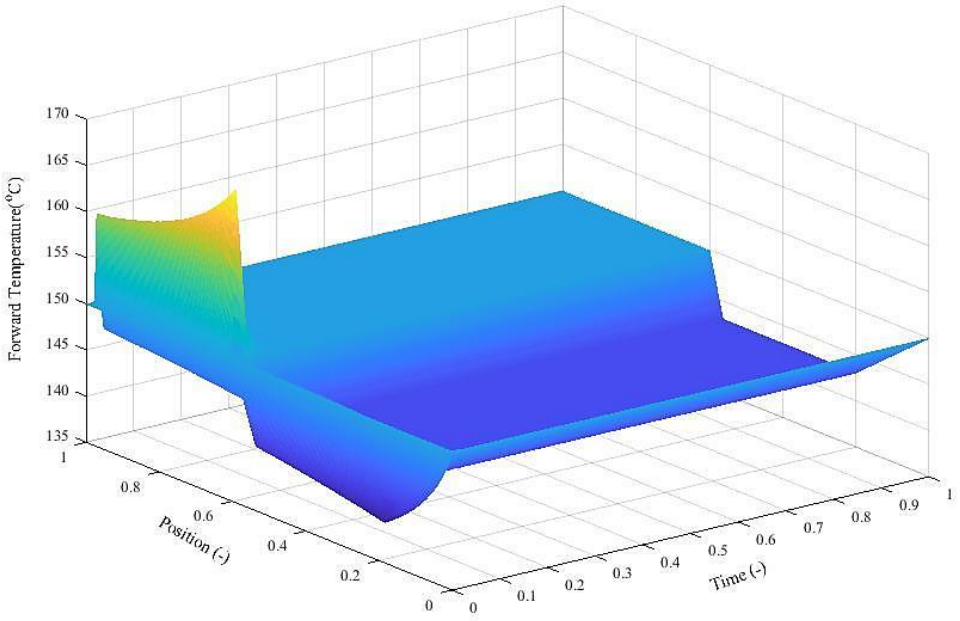

(a)

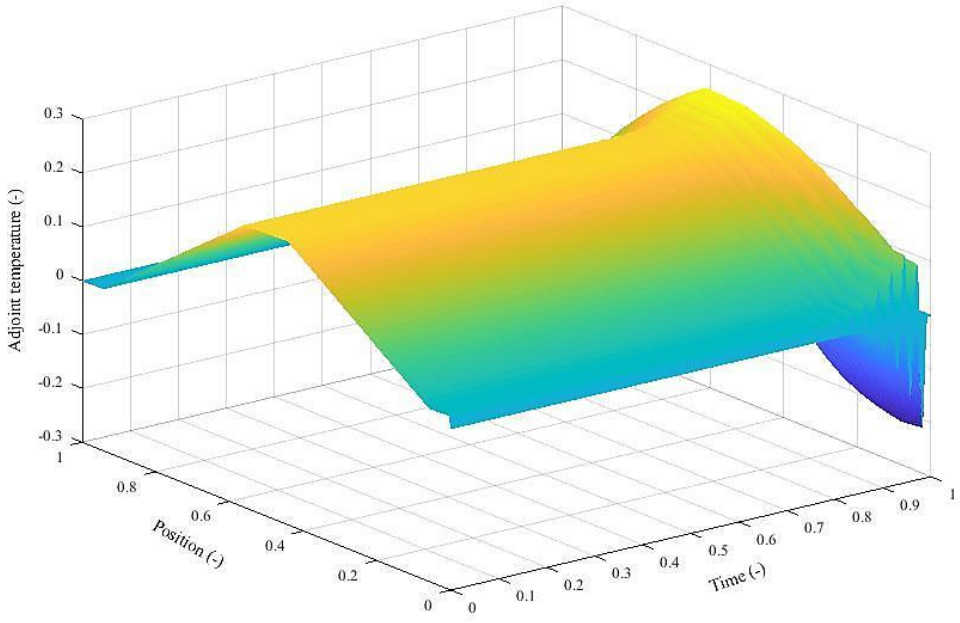

(b)

Fig. 2.4. (a) 3D surface of the forward temperature (b) 3D surface of the adjoint temperature

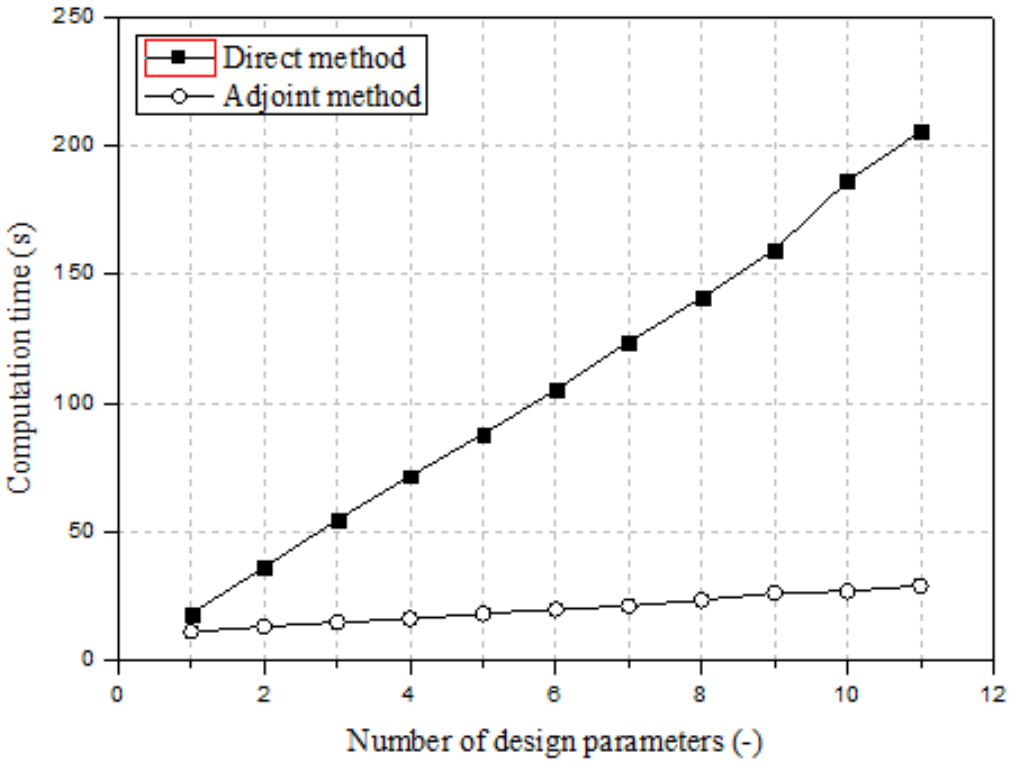

Fig. 2.5. The computation time of direct and adjoint methods with the number of design parameters

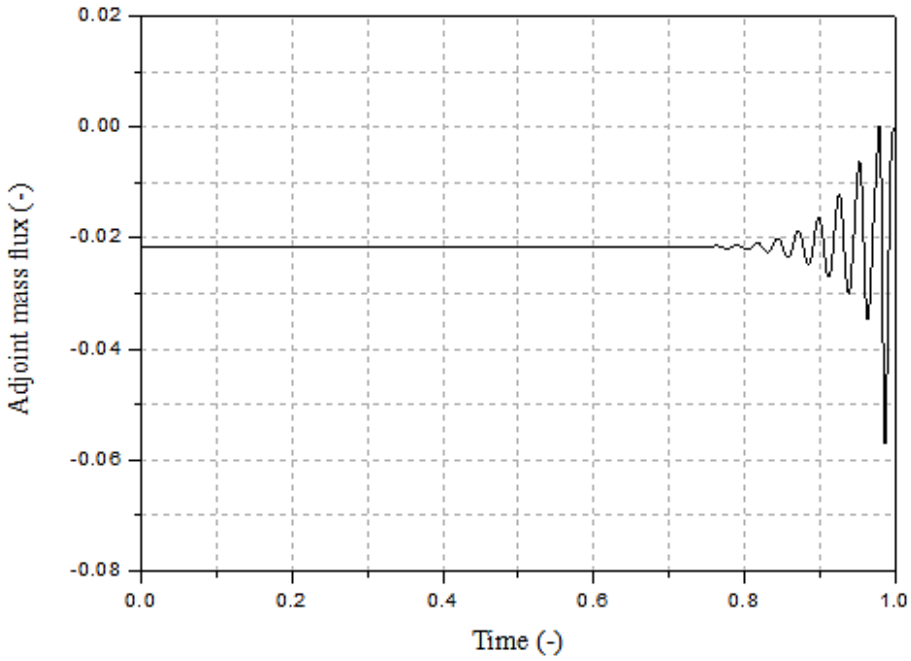

(a)

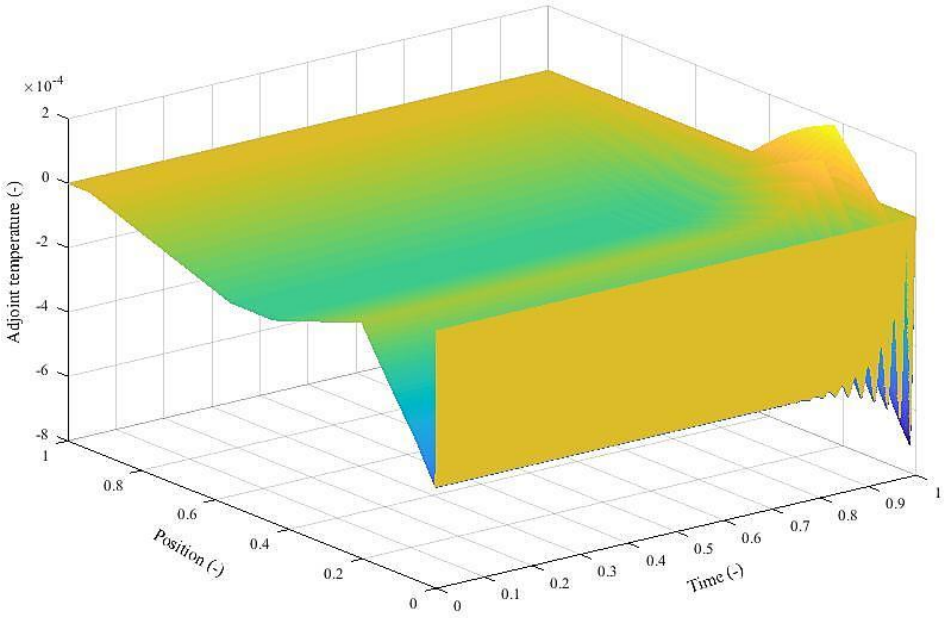

(b)

Fig. 2.6. (a) Time evolution of the adjoint mass flux from Eq. (32) (b) 3D surface of the adjoint temperature from Eq. (2.33)

2.3 Assessment results of system feasibility using high-Prandtl number fluid

2.3.1 Sensitivity test on passive heat transport system using high-Pr fluid

2.3.1.1 Effect of working fluid property

In the natural circulation system, the variation of fluid property gives significant effect on the heat transfer performance. Especially, the fluid dynamic viscosity directly affects the pressure drop over the system, and the specific heat determines the thermal inertia of fluid. Thus, it is important to implement appropriate fluid property function into the sensitivity model. To clarify the effect of fluid property variation, the sensitivities computed by adjoint method with constant fluid property were compared to those with temperature-dependent fluid viscosity and specific heat. Table 2.6 and Figs. 2.7-2.9 show the normalized sensitivities of three objective functionals computed by constant property model and temperature-dependent property model. Note that the normalized sensitivities in Figs. 2.7-2.9 are scaled in logarithm and red-colored bar indicates negative sensitivity. The positive sensitivity implies that the increase of parameter enhances the objective functional, while the negative sensitivity implies that the increase of parameter deteriorates the objective functional.

The implementation of temperature-dependent fluid property model led to the increase of magnitude of sensitivities, while the sign of sensitivity maintained. For the sensitivities of temperature and Nusselt number, the sequence of parameter importance remained even after the implementation of temperature-dependent property model. The input external heat flux gave the most significant effect on the temperature in positive way, while the reference heat transfer coefficient gave the most in negative way. For the sensitivity of Nusselt number, the hydraulic diameter and the reference heat transfer coefficient gave the most positive effect, while the external heat flux was the most negative parameter. However, for the sensitivity of mass flux, the importance of the reference heat transfer coefficient and cooler wall temperature extremely increased after the implementation of temperature-dependent property model. That is, if the property variation is considered, the effect of the reference heat transfer coefficient and cooler wall temperature on the natural mass flux cannot be negligible any longer. In other word, since these two parameters are highly associated with the heat exchanger, the optimized design of heat exchanger for the reliable natural circulation should be aware of property variation of working fluid.

For the further study on the fluid properties, various temperature-dependent functions for the fluid viscosity were considered. Compared to the reference function shown in Eq. (2.16), two different forms of analytic functions were employed: one is a polynomial form and the other is a power form. Two analytic functions shown in Eqs. (2.43) and (2.44) were derived from same reference viscosity data of DOWTHERM RP with R^2=0.99998 and R^2=0.99467, respectively. The comparison of analytic functions with the reference viscosity data is shown in Fig. 2.10. Note that the values of fluid viscosity

itself from different analytic functions are almost same in the given temperature range.

$$\mu(T) = \mu_{ref} \cdot f_{\mu}(T) = 2.69726 - 0.03041 \times T + 1.3817 \cdot 10^{-4} \times T^2 - 3.1560 \cdot 10^{-7} \times T^3 + 3.6200 \cdot 10^{-10} \times T^4 - 1.6667 \cdot 10^{-13} \times T^5 \quad (2.43)$$

$$\mu(T) = \mu_{ref} \cdot f_{\mu}(T) = 5.6083 \cdot 10^{11} \times T^{-5.56674} \quad (2.44)$$

The sensitivities of mass flux, temperature, and Nusselt number are plotted in Figs. 2.11-2.13 and summarized in Table 2.7-2.9. In general, the sensitivities computed by model employing polynomial viscosity function largely increased compared to those by reference model. The maximum increase in sensitivity lay on the temperature sensitivity with respect to thermal expansion coefficient and constant a from Darcy friction factor, up to 200 % from reference model. In addition, the sensitivities of mass flux with respect to parameters coupled with the temperature, like h_{ref} and T_w, showed the largest increase up to 130 % among all parameters. The sensitivities of Nusselt number also showed considerable increase with respect to all the parameters except for f_{local} which had no direct relation with temperature. In other words, it was clearly inferred that the changes in sensitivities were dominated by the change in sensitivity of temperature and the temperature was largely influenced by the fluid viscosity function.

However, power form of viscosity function gave less effect on the sensitivities of the system than polynomial function. The change in sensitivities with power form of viscosity function lay on the range of 20~30 %, and the maximum increase of sensitivity was only 50 % which was only a quarter of that with polynomial function. Since the viscosity values themselves from different functions were almost same, the large difference in sensitivities between employed property functions came from other contribution. Fig. 2.14 shows the viscosity gradients with respect to the temperature of different analytic functions. In the operating temperature range from 400-440 K, the viscosity gradient with respect to temperature of polynomial function was higher than that of reference case, while the viscosity gradient of power function showed insignificant difference from that of reference. That is, it was inferred that not only the viscosity function itself but also the gradient of viscosity function with respect to the temperature played a crucial role in evaluating the sensitivity of system. It was also confirmed by Eq. (2.33) which the gradient of viscosity with respect to temperature was included in.

2.3.1.2 Effect of heat exchanger orientation

In this section, the effect of geometric condition of heat exchanger was tested by changing the location of heat exchangers. The reference case employed a short horizontal heat exchanger and a long

vertical heat exchanger for the sensitivity analysis, as shown in Fig. 2.15(a). The test case 1 employed a long horizontal heat exchanger and a short vertical heat exchanger. On the contrary, a single vertical heat exchanger on the top of right side was modeled for the test case 2. The simplified configurations of test cases 1 and 2 are presented in Fig. 2.15(b) and (c), respectively. The total length of heat exchangers from each test case was set to be equal to total length of two heat exchangers from the reference case. The location of heater was kept with maintaining width and height of the loop.

Table 2.10-2.12 summarize the normalized sensitivities of objectives for each case and Figs. 2.16-2.18 show them as a column bar. In general, absolute normalized sensitivities of objectives for the reference case showed the smallest values, which implied the most reliable system configuration. Regardless of the orientation of heat exchanger, the sensitivities of mass flux and temperature were the most sensitive to the variation of external heat flux and constant b from Darcy friction factor. Both parameters gave positive sensitivities to the mass flux, since they directly enhanced the driving buoyancy force and reduced pressure drop, respectively. Both parameters also gave large effects on the Nusselt number, however the diameter and the reference heat transfer coefficient gave the most.

The comparison between cases showed that the absolute sensitivity of mass flux with respect to the performance parameters of heat exchanger such as heat transfer coefficient and wall temperature significantly increased for the test case 2. The increase of absolute sensitivity leads to the deterioration of system reliability. That is, the orientation of heat exchanger determined directly heat transfer performance, which could reduce the reliability of stable natural circulation. On the contrary, the sensitivities of temperature and Nusselt number slightly increased in the test cases compared to those in the reference case, which implied that the orientation of heat exchangers rarely affected the sensitivities of temperature and Nusselt number. Finally, the shorter horizontal heat exchanger and longer vertical exchanger showed the most reliable natural circulation system among the tested configurations. In addition, if the orientation of heat exchanger has to be changed, one should firstly test the sensitivity of mass flux with respect to the performance parameters of heat exchangers.

2.3.1.3 Effect of operating temperature

The reference temperature, defined as the temperature at the entrance of cooler in this study, represented the controlled heater outlet temperature or the maximum temperature in practical system. Thus, it is important to investigate the effect of reference temperature on the sensitivities of objective in order to secure the reliability of natural circulation system. The sensitivities of mass flux, temperature and Nusselt number were tested at three different reference temperatures: 333.15 K, 423.15 K, and 523.15 K.

Table 2.13-2.15 summarize the normalized sensitivities of objectives for each case. 6 and Figs. 2.19-2.21 show the normalized sensitivities of three objective functionals at three different reference

temperatures. The importance of parameters for sensitivities of each objective was remained at all the reference temperatures. That is, the reference temperature gave insignificant effect on the priority of parameters for mass flux temperature, and Nusselt number. However, the magnitude of sensitivities largely differed from case by case, especially at the reference temperature of 333.15 K. For the objective of mass flux, the sensitivity with respect to cooler wall temperature increased up to 20 times at the reference temperature of 333.15 K compared to that at the reference temperature of 423.15 K, while the sensitivity with respect to fluid viscosity and localized friction factor became half. In other words, as the maximum temperature through the system decreased, the effect of heat transfer-related parameters overwhelmed that of pressure drop-related parameters for natural mass flux. The sensitivities of temperature were also varied at low reference temperature, with respect to most of parameters. Unlikely to the change in mass flux sensitivities, temperature sensitivities with respect to fluid properties and major friction factors also showed considerable changes. The changes in sensitivities became the most for Nusselt number, which stated that the reliability of heat transfer performance was significantly reduced. Note that, the change in sensitivities at the reference temperature of 523.15 K was much smaller than that at the reference temperature of 333.15 K. Interestingly, as shown in Fig. 2.2, the fluid dynamic viscosity of DOWTHERM RP is rapidly increased as the temperature becomes below 353.15 K. Thus, it was inferred that the rapid variation of fluid properties below certain temperature amplified the propagation of sensitivity, eventually leading to the large increase of sensitivities. Since molten salt fluid has similar property function, the operation temperature range of molten salt heat transport system should be properly set in the range where the property variation is not stiff.

2.3.2 Feasibility test on high-Pr fluid in passive heat transport system

To test the feasibility of high-Pr fluid and clarify the advantages in using high-Pr fluid for passive heat transport system, especially for passive safety system, the further analyses using different fluids were performed in different operating temperature conditions. 4 different fluids were considered including DOWTHERM RP depending on its Prandtl number. Liquid sodium was chosen to represent low Prandtl number fluid, while liquid water represented medium Prandtl number fluid. For high Prandtl number fluid, both oil and salt were considered : DOWTHERM RP, and HITEC. The Boussinesq approximation was applied, and only the fluid viscosity and specific heat were set as temperature-dependent property. Eqs. (2.45-2.50) shows the property function of each fluid evaluated from the previous studies [25,66–68].

Sodium

$$\ln \mu = -6.4406 - 0.3958 \cdot \ln T(K) + \frac{556.835}{T(K)} \quad (Pa \cdot s) \tag{2.45}$$

$$c_p = 1.6582 - 8.479\times10^{-4}\cdot T(K) + 4.4541\times10^{-7}\cdot T^2(K) - \frac{2992.6}{T^2(K)} \quad (kJ/kg\cdot K) \tag{2.46}$$

Water

$$\log_{10}\left(\frac{\mu}{1.002}\right) = \frac{1.1709\left(20 - T(°C)\right) - 0.001827\left(T(°C) - 20\right)^2}{T(°C) + 89.93} \quad \left(\times10^{-3}\, Pa\cdot s\right) \tag{2.47}$$

$$c_p = 4189.7 \quad (J/kg\cdot K) \tag{2.48}$$

HITEC

$$\mu = \frac{e^{5.9(T(K)-9.638)/990.362} + e^{-5.9(T(K)-9.638)/990.362}}{e^{5.9(T(K)-9.638)/990.362} - e^{-5.9(T(K)-9.638)/990.362}} - 0.999 \quad (Pa\cdot s) \tag{2.49}$$

$$c_p = 1560 - \left(T(K) - 273.15\right) \quad (J/kg\cdot K) \tag{2.50}$$

Figs. 2.22(a)-(d) show the sensitivities of Nusselt number with respect to fluid properties as the maximum operating temperature changes, for 4 different fluids. The temperature-dependent function of fluid viscosity is presented together with the sensitivity result for each fluid. For all the analyzed cases of fluids, the sensitivities of Nusselt number with respect to fluid properties were slightly increased at high operating temperature. At the corresponding temperature range, the fluid viscosity also slightly increased as the temperature decreased. However, the sensitivities of Nusselt number exponentially increased at certain temperature where the gradient of viscosity with respect to temperature rapidly changed: ~500 K for liquid sodium, ~340 K for water, ~370 K for DOWTHERM RP, ~560 K for HITEC. Thus, as described earlier, it was confirmed that the rapid variation of fluid properties, especially temperature-dependent viscosity, was attributed to the increase of sensitivity. In addition, the larger the gradient of properties with respect to temperature was, the larger the increase of sensitivities was, in general. Finally, it was verified that the rapid variation of fluid properties reduced the reliability of heat transfer performance inside the closed circulation system.

Then, to understand the advantages in using high-Pr fluids for passive heat transport system, the sensitivities of Nusselt number were compared with different fluids. Fig. 2.23 presents normalized sensitivity of Nusselt number with respect to all the parameters for different fluids. For clear understanding, the sensitivity for water was set as the reference value. Except for the sensitivities with

respect to tube diameter and heat transfer coefficient, overall sensitivities were largely reduced when the fluids were replaced with high-Pr fluids. Although the kind of fluid gave no effect on the importance of parameters, the reduction of sensitivity values itself implied less uncertainties in heat transfer performance of system. That is, the passive heat transport system using high-Pr fluids worked more stable and reliable in the aspect of heat transfer performance.

2.3.3 Reliability assessment of Nusselt correlation for high-Pr fluid

With the consideration of the rapid properties variation effect on the heat transfer performance, the present section presents the direct reliability assessment of heat transfer correlation including the properties variation effect. The classical Nusselt correlations for the natural circulation inside the closed loop include dimensionless Grashof number and Prandtl number of fluid, which is usually presented together as Rayleigh number (*Ra=Gr*Pr*). However, the validity of the classical Nusselt number with Rayleigh number is limited by Prandtl number of fluid, generally less than 1. In the same manner, the classical Nusselt correlations for the forced convective heat transfer inside the closed loop employed Peclet number (*Pe=Re*Pr*), but for middle to high Prandtl number fluid, the effect of Reynolds number and Prandtl number is separated by imposing different exponential constants. In addition, the ratio between Prandtl numbers evaluated from the fluid state near the wall and fluid state at the core, was introduced for high Prandtl number range. Here, for the assessment of Nusselt correlation reliability, the general form of correlation was tested as shown in Eq. (2.51).

$$Nu = \frac{D_h}{k_f} \cdot h(T) = A \cdot Gr^{a_2} \cdot \mathrm{Pr}^{b_2} \cdot \left(\frac{\mathrm{Pr}_f}{\mathrm{Pr}_w} \right)^{c_2} \tag{2.51}$$

where, A, a_2, b_2, c_2 are arbitrary constants which are generally evaluated from experimental data.

The parameters for the sensitivity analysis were re-defined, since the reference heat transfer coefficient and wall temperature were no longer fixed. Instead, the empirical constants in Eq. (2.51) denoted as A, a_2, b_2, and c_2 were included. As a result, the newly-defined set of parameters included reference fluid density (ρ_{ref}), fluid viscosity (μ_{ref}), fluid thermal expansion (β), fluid specific heat capacity ($c_{p,ref}$), diameter (D_h), external input heat flux (q''), Darcy friction factor constants (a, b), localized friction factor (f_{local}), and empirical constants (A, a_2, b_2, c_2) in classical Nusselt correlation. To specify the analyses, only the sensitivities with respect to empirical constants in classical Nusselt correlation were presented in this section.

The sensitivity analysis of Nusselt correlation was also performed using adjoint method. Eqs. (2.52-2.55) present the development of adjoint sensitivity equations employing Nusselt correlation. The

Nusselt number was set as the response objective expressed as follows:

$$R_3 = \int_{t_0}^{\tau} \left\langle r\left(G,T,\alpha\right)\right\rangle dt = \int_{t_0}^{\tau}\int_{0}^{L} Nu\left(G,T,\alpha\right) dsdt = \int_{t_0}^{\tau}\int_{0}^{L} \left[A\cdot Gr^{a_2}\,\mathrm{Pr}^{b_2}\left(\frac{\mathrm{Pr}_f}{\mathrm{Pr}_w}\right)^{c_2}\right] dsdt \tag{2.52}$$

With same forward operator **F** from Eq. (2.31), corresponding adjoint equations were defined as:

$$-\frac{\partial G_4^{\dagger}}{\partial t}\cdot\frac{1}{L_t} + \left[\frac{a\left(2-b\right)\mu^b}{2D_h^{1+b}\rho_{ref}L_t}\cdot G^{1-b} + 2\cdot f_{local}\frac{1}{D_h}\frac{G}{2\rho_{ref}L_t}\right] G_4^{?} + \frac{1}{\rho_{ref}}\frac{\partial\left(c_pT\right)}{\partial s}\cdot T_4^{\dagger} = 0 \tag{2.53a}$$

$$\begin{aligned} &-\frac{\partial\left(c_pT\right)}{\partial T}\cdot\frac{\partial T_4^{\dagger}}{\partial t} - \frac{G}{\rho_{ref}}\frac{\partial\left(c_pT\right)}{\partial T}\cdot\frac{\partial T_4^{\dagger}}{\partial s} + \left[\frac{ab\mu^{b-1}G^{2-b}}{2D_h^{1+b}\rho_{ref}L_t}\cdot\frac{\partial\mu}{\partial T} - \frac{\rho_{ref}g\beta}{L_t}\underline{e}_z\cdot\underline{e}_s\left(s\right)\right] G_4^{\dagger} \\ &+\left[\left(2\frac{\partial c_p}{\partial T} + T\frac{\partial}{\partial T}\left(\frac{\partial c_p}{\partial T}\right)\right)\cdot\left(\frac{\partial T}{\partial t} + \frac{1}{\rho^*}G\frac{\partial T}{\partial s}\right) + \frac{4\left(T-T_w\right)}{\rho_{ref}D_h}\cdot\frac{\partial h}{\partial T} - \frac{4h}{\rho_{ref}D_h}\cdot\frac{\partial T_w}{\partial T} + \frac{4h}{\rho_{ref}D_h}\right] T_4^{\dagger} \\ &=\frac{\partial Nu}{\partial T} = Nu\cdot\left[1+\frac{a}{\left(T-T_w\right)}\frac{q''}{h}\right]^{-1}\left[\frac{\left(-2a+b+c\right)}{\mu\left(T\right)}\cdot\frac{\partial\mu}{\partial T} + \frac{\left(b+c\right)}{c_p\left(T\right)}\cdot\frac{\partial c_p}{\partial T}\right] \end{aligned} \tag{2.53b}$$

where,

$$\frac{\partial h}{\partial T} = h\cdot\left[1+\frac{a}{\left(T-T_w\right)}\frac{q''}{h}\right]^{-1}\left[\frac{\left(-2a+b+c\right)}{\mu\left(T\right)}\cdot\frac{\partial\mu}{\partial T} + \frac{\left(b+c\right)}{c_p\left(T\right)}\cdot\frac{\partial c_p}{\partial T}\right]$$

$$\frac{\partial T_w}{\partial T} = 1+\frac{q''}{h^2}\frac{\partial h}{\partial T}$$

Finally, each sensitivity of variable was expressed as:

$$\frac{dR_4}{d\alpha} = \int_{t_0}^{\tau}\left\langle r_{4,\alpha} - \lambda_4^{\dagger}\cdot\mathbf{F}_{\alpha}\right\rangle dt = \int_{t_0}^{\tau}\int_{0}^{L} r_{4,\alpha}\,dsdt - \int_{t_0}^{\tau}\int_{0}^{L}\left(\lambda_4^{\dagger}\cdot\mathbf{F}_{\boldsymbol{\alpha}}\right) dsdt \tag{2.54}$$

where $r_{4,\alpha}$ is expressed as follow:

$$r_{4,\alpha} = \frac{\partial A}{\partial \alpha}\cdot\frac{Nu}{A} + \frac{\partial \rho}{\partial \alpha}\cdot 2a_2\frac{Nu}{\rho} + \frac{\partial \beta}{\partial \alpha}\cdot a_2\frac{Nu}{\beta} + \frac{\partial D_h}{\partial \alpha}\cdot 3a_2\frac{Nu}{D_h}$$
$$\frac{\partial k_f}{\partial \alpha}\cdot\left(-b_2\right)\frac{Nu}{k_f} + \frac{\partial c_{p,ref}}{\partial \alpha}\cdot b_2\frac{Nu}{c_{p,ref}} + \frac{\partial \mu_{ref}}{\partial \alpha}\cdot\left(-2a_2+b_2\right)\frac{Nu}{\mu_{ref}}$$
$$\frac{\partial a_2}{\partial \alpha}\cdot\ln Gr\cdot Nu + \frac{\partial b_2}{\partial \alpha}\cdot\ln \mathrm{Pr}\cdot Nu + \frac{\partial c_2}{\partial \alpha}\cdot\ln\left(\mathrm{Pr}_f/\mathrm{Pr}_w\right)\cdot Nu \quad (2.55)$$

Fig. 2.24 presents normalized sensitivity of Nusselt number with respect to empirical constants in correlation for different fluids. Here also the sensitivity for water was set as the reference value. Unlikely to the sensitivity results of Nusselt number in the previous section, the sensitivity of Nusselt number in this section implied the uncertainties in the prediction of heat transfer performance using existing correlations. Then, the larger sensitivities for high-Pr fluids, especially with respect to constants associated with the Pr term, increased the uncertainties in the prediction of Nusselt number using existing correlations. It was clear that the sensitivities of Nusselt number with respect to exponent constants associated with Prandtl number depended on the fluids. For example, the lowest Pr fluid, liquid sodium showed the largest sensitivity with respect to exponent constant, b_2, while it had the smallest sensitivity with respect to exponent constant, c_2. However, the sensitivities of high-Pr fluids were the largest with respect to c_2 and the second largest with respect to b_2. In other word, the use of high-Pr fluid to the passive heat transport system made it difficult to predict reliable Nusselt number if the existing correlation was applied. Considering the reduction in system sensitivities of high-Pr fluid as shown in Fig. 2.23, the larger uncertainties in heat transfer performance of system were attributed to the failure of prediction with existing correlation. That is, it was inferred that there could be distinct heat transfer feature of high-Pr fluid that the previous correlations didn't take account of.

Finally, the feasibility of high-Pr fluid to the passive heat transport system was successfully tested showing the most reliable heat transfer performance, while the reliable prediction of heat transfer performance required to clarify the distinct heat transfer behavior of high-Pr fluid that the existing correlations couldn't expect. The following section includes the experimental study on the distinct heat transfer behavior of high-Pr fluids.

Table 2.6. Summary of normalized sensitivities of objectives with different fluid property model

	N_R (G)		N_R (T)		N_R (Nu)	
	Constant property	*Variable property*	*Constant property*	*Variable property*	*Constant property*	*Variable property*
ρ_{ref}	0.8923	1.0996	0.0157	0.0220	-0.0308	-0.0385
μ_{ref}	-0.4098	-0.5151	-0.0070	-0.0101	0.0127	0.0165
β	0.4483	0.5503	0.0069	0.0100	-0.0155	-0.0193
$c_{p,ref}$	-0.5241	-0.6366	0.0108	0.0142	-0.0147	-0.0187
D_h	0.3137	0.4136	0.0251	0.0347	0.9610	1.3178
h_{ref}	-0.0078	-0.0569	-0.0393	-0.0526	1.0325	1.4107
T_w	0.0013	0.0091	0.0062	0.0083	-0.0048	-0.0064
q''	7.1344	9.7465	0.7403	0.9935	-0.3832	-0.5188
a	-0.4098	-0.5151	-0.0070	-0.0101	0.0127	0.0165
b	3.2559	4.0077	0.0556	0.0781	-0.1012	-0.1287
f_{local}	-0.0183	-0.0194	-0.0003	-0.0004	0.0006	0.0006

Table 2.7. Normalized sensitivities of mass flux with analytic viscosity functions

	N_R (G)		
	Ref.	*Polynomial*	*Power*
ρ_{ref}	0.9014	1.5321	1.0910
μ_{ref}	-0.4223	-0.4705	-0.5137
β	0.4512	0.7644	0.5456
$c_{p,ref}$	-0.5219	-0.8817	-0.6289
D_h	0.3390	0.6343	0.4189
h_{ref}	-0.0466	-0.1084	-0.0708
T_w	0.0075	0.0175	0.0114
q''	7.9901	14.1765	9.9765
a	-0.4223	-0.7504	-0.5140
b	3.2855	5.3348	3.9963
f_{local}	-0.0159	-0.0144	-0.0193

Table 2.8. Normalized sensitivities of temperature with analytic viscosity functions

	N_R (T)		
	Ref.	*Case 1*	*Case 2*
ρ_{ref}	0.0160	0.0466	0.0204
μ_{ref}	-0.0073	-0.0140	-0.0095
β	0.0073	0.0223	0.0095
$c_{p,ref}$	0.0103	0.0268	0.0127
D_h	0.0253	0.0720	0.0320
h_{ref}	-0.0384	-0.1030	-0.0478
T_w	0.0061	0.0164	0.0076
q''	0.7245	1.9546	0.9049
a	-0.0073	-0.0223	-0.0095
b	0.0570	0.1585	0.0734
f_{local}	-0.000267	-0.000421	-0.000344

Table 2.9. Normalized sensitivities of Nusselt number with analytic viscosity functions

	N_R (Nu)		
	Ref.	*Case 1*	*Case 2*
ρ_{ref}	-0.0281	-0.0699	-0.0336
μ_{ref}	0.0121	0.0204	0.0147
β	-0.0141	-0.0348	-0.0168
$c_{p,ref}$	-0.0137	-0.0346	-0.0165
D_h	0.9630	1.9688	1.1643
h_{ref}	1.0308	2.1462	1.2470
T_w	-0.0046	-0.0121	-0.0057
q''	-0.3791	-1.0073	-0.4688
a	0.0121	0.0326	0.0147
b	-0.0940	-0.2313	-0.1146
f_{local}	0.000457	0.000622	0.000554

Table 2.10. Normalized sensitivities of mass flux with geometric conditions of heat exchanger

	N_R (Nu)		
	Ref.	*Case 1*	*Case 2*
ρ_{ref}	0.9014	1.7915	1.2512
μ_{ref}	-0.4223	-0.7930	-0.5454
β	0.4512	0.9715	0.6720
$c_{p,ref}$	-0.5219	-1.1156	-0.6691
D_h	0.3390	0.4995	0.4412
h_{ref}	-0.0466	-0.0404	-0.2158
T_w	0.0075	0.0064	0.0345
q''	7.9901	16.5184	12.7590
a	-0.4223	-0.7930	-0.5454
b	3.2855	6.1294	4.1965
f_{local}	-0.0159	-0.0284	-0.0189

Table 2.11. Normalized sensitivities of temperature with geometric conditions of heat exchanger

	N_R (Nu)		
	Ref.	*Case 1*	*Case 2*
ρ_{ref}	0.0160	0.0414	0.0254
μ_{ref}	-0.0073	-0.0186	-0.0107
β	0.0073	0.0215	0.0129
$c_{p,ref}$	0.0103	0.0231	0.0143
D_h	0.0253	0.0611	0.0361
h_{ref}	-0.0384	-0.0836	-0.0638
T_w	0.0061	0.0132	0.0101
q''	0.7245	1.6574	1.1708
a	-0.0073	-0.0186	-0.0107
b	0.0570	0.1441	0.0820
f_{local}	-0.000267	-0.000661	-0.000357

Table 2.12. Normalized sensitivities of Nusselt number with geometric conditions of heat exchanger

	N_R (Nu)		
	Ref.	*Case 1*	*Case 2*
ρ_{ref}	-0.0281	-0.0605	-0.0440
μ_{ref}	0.0121	0.0245	0.0184
β	-0.0141	-0.0328	-0.0235
$c_{p,ref}$	-0.0137	-0.0260	-0.0210
D_h	0.9630	1.9568	1.3500
h_{ref}	1.0308	2.0937	1.4586
T_w	-0.0046	-0.0096	-0.0079
q''	-0.3791	-0.8328	-0.6612
a	0.0121	0.0245	0.0184
b	-0.0940	-0.1891	-0.1413
f_{local}	0.000457	0.000871	0.000636

Table 2.13. Normalized sensitivities of mass flux at different reference temperatures

	N_R (G)		
	T_{ref}=333.15 K	T_{ref}=423.15 K	T_{ref}=523.15 K
ρ_{ref}	0.7822	0.9014	0.9783
μ_{ref}	-0.0712	-0.4223	-1.0810
β	0.3801	0.4512	0.4935
$c_{p,ref}$	-0.2858	-0.5219	-0.6564
D_h	0.5120	0.3390	0.1300
h_{ref}	-0.0654	-0.0466	-0.0924
T_w	0.1515	0.0075	0.0046
q''	8.1886	7.9901	11.2424
a	-0.3790	-0.4223	-0.4158
b	1.8820	3.2855	3.7265
f_{local}	-0.0009	-0.0159	-0.0510

Table 2.14. Normalized sensitivities of temperature at different reference temperatures

	N_R (G)		
	T_{ref}=333.15 K	T_{ref}=423.15 K	T_{ref}=523.15 K
ρ_{ref}	0.0783	0.0160	0.0097
μ_{ref}	-0.0065	-0.0073	-0.0109
β	0.0344	0.0073	0.0044
$c_{p,ref}$	0.0532	0.0103	0.0063
D_h	0.1156	0.0253	0.0161
h_{ref}	-0.0470	-0.0384	-0.0510
T_w	0.1039	0.0061	0.0025
q''	2.8322	0.7245	0.5517
a	-0.0346	-0.0073	-0.0042
b	0.1690	0.0570	0.0375
f_{local}	-0.000074	-0.000267	-0.000506

Table 2.15. Normalized sensitivities of Nusselt number at different reference temperatures

	N_R (G)		
	T_{ref}=333.15 K	T_{ref}=423.15 K	T_{ref}=523.15 K
ρ_{ref}	-2.7712	-0.0281	-0.0055
μ_{ref}	0.2499	0.0121	0.0053
β	-1.3441	-0.0141	-0.0028
$c_{p,ref}$	-1.6576	-0.0137	-0.0024
D_h	1.7390	0.9630	0.6075
h_{ref}	2.7196	1.0308	1.0992
T_w	-1.9359	-0.0046	-0.0006
q''	-40.0188	-0.3791	-0.0899
a	1.3309	0.0121	0.0021
b	-6.5939	-0.0940	-0.0184
f_{local}	0.003122	0.000457	0.000253

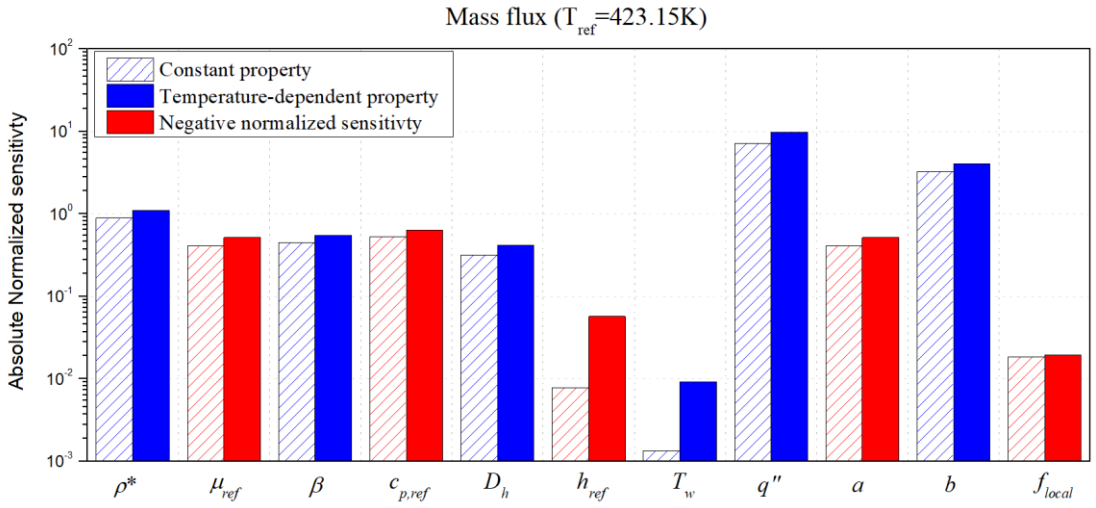

Fig. 2.7. The absolute normalized sensitivity of mass flux with constant and temperature-dependent properties (*Red bar indicates negative value)

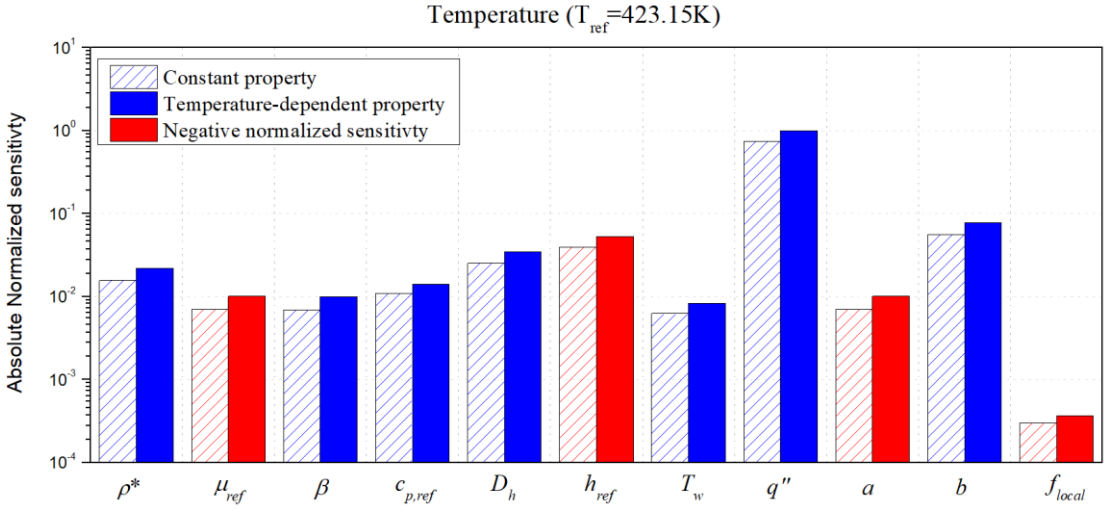

Fig. 2.8. The absolute normalized sensitivity of temperature with constant and temperature-dependent properties (*Red bar indicates negative value)

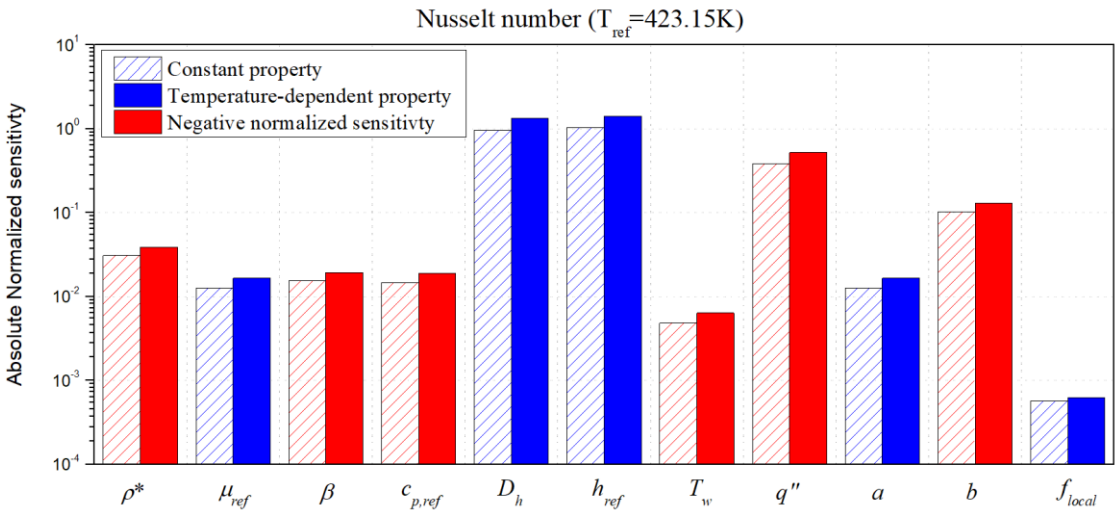

Fig. 2.9. The absolute normalized sensitivity of Nusselt number with constant and temperature-dependent properties (*Red bar indicates negative value)

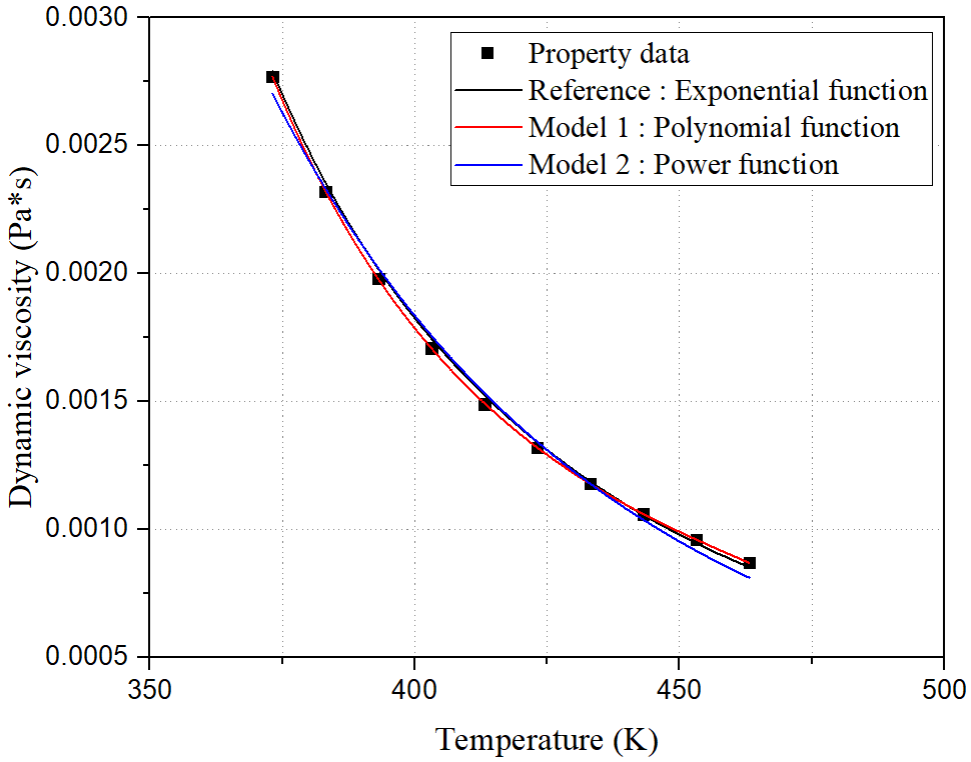

Fig. 2.10. Dynamic viscosity data of DOWTHERM RP and different analytic functions

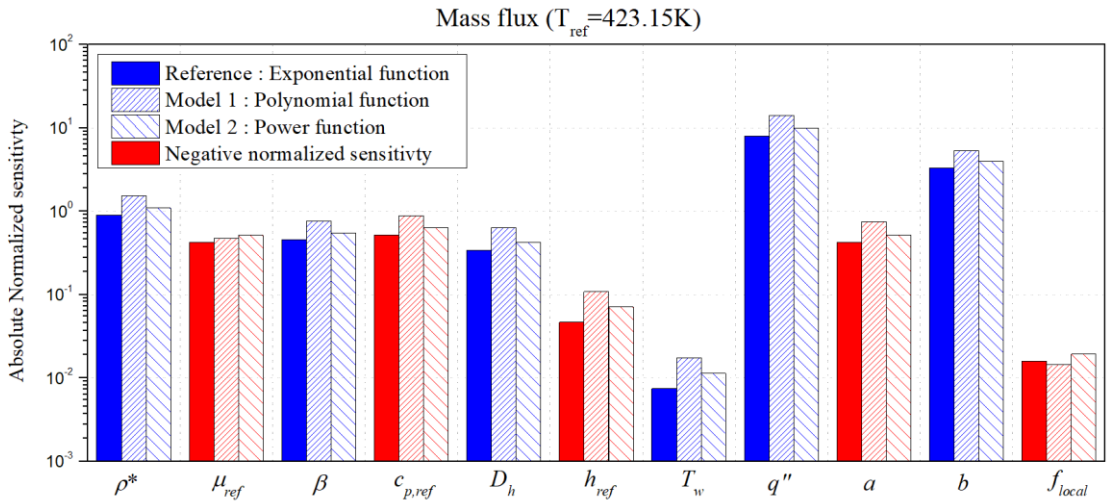

Fig. 2.11. The absolute normalized sensitivity of mass flux with different property functions (*Red bar indicates negative value)

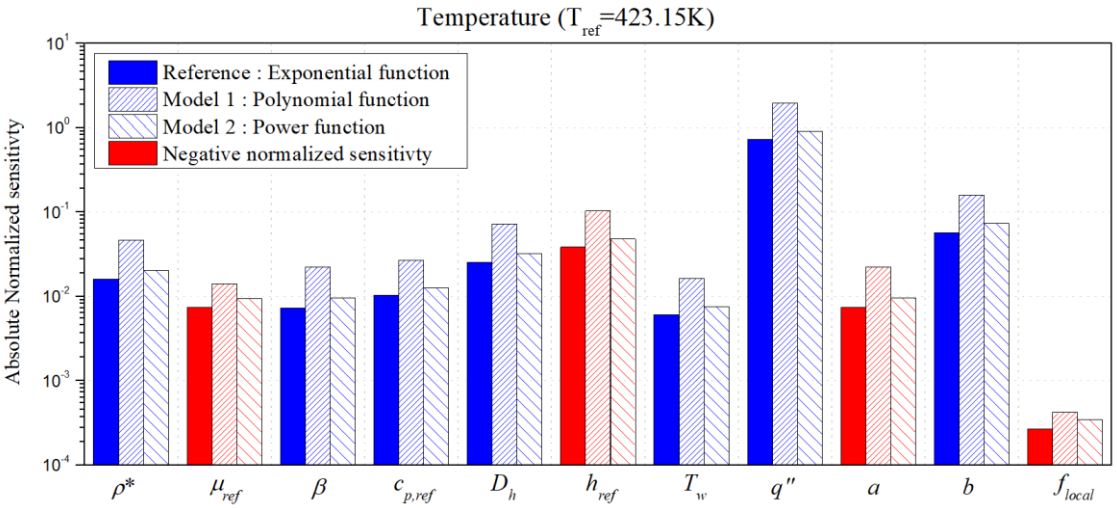

Fig. 2.12. The absolute normalized sensitivity of temperature with different property functions (*Red bar indicates negative value)

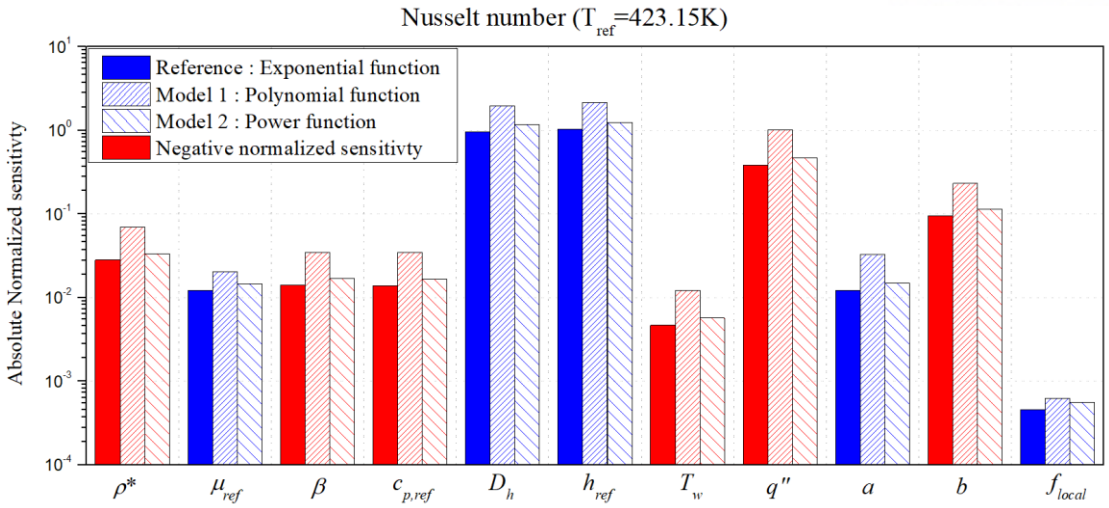

Fig. 2.13. The absolute normalized sensitivity of Nusselt number with different property functions (*Red bar indicates negative value)

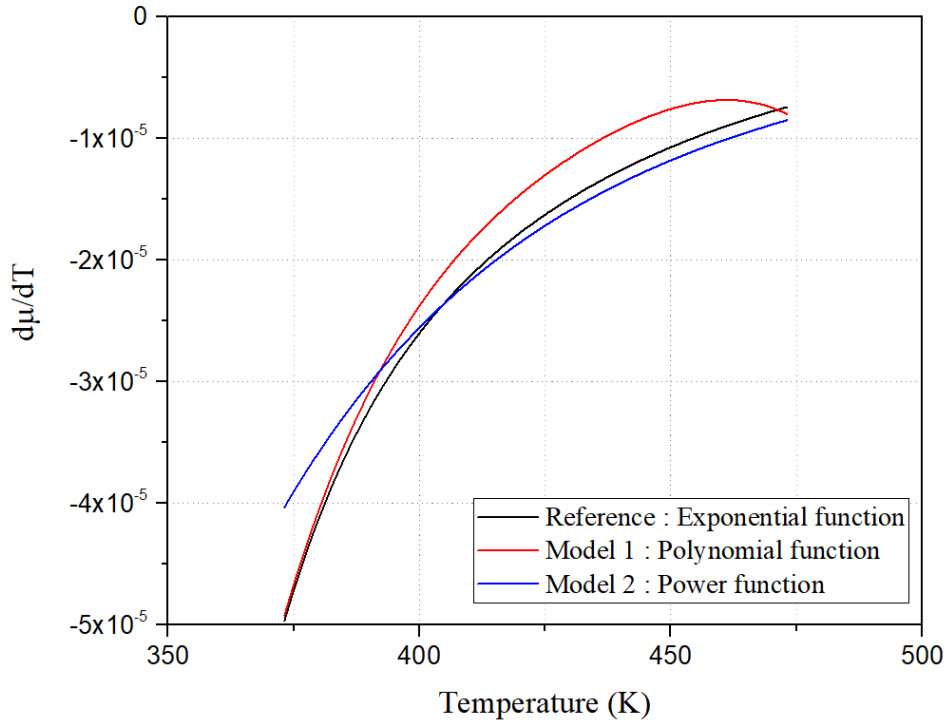

Fig. 2.14. Gradient of dynamic viscosity with respect to temperature for different analytic functions

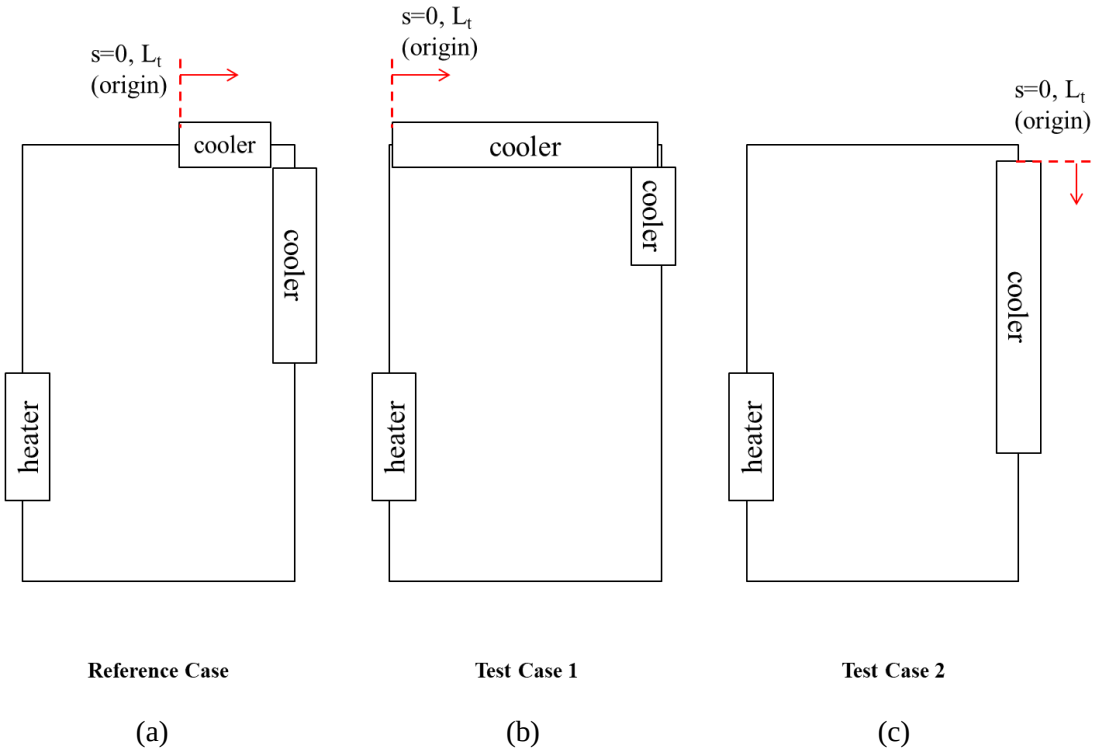

Fig. 2.15. Simplified loop configurations : (a) Reference case (b) Test case 1 (c) Test case 2

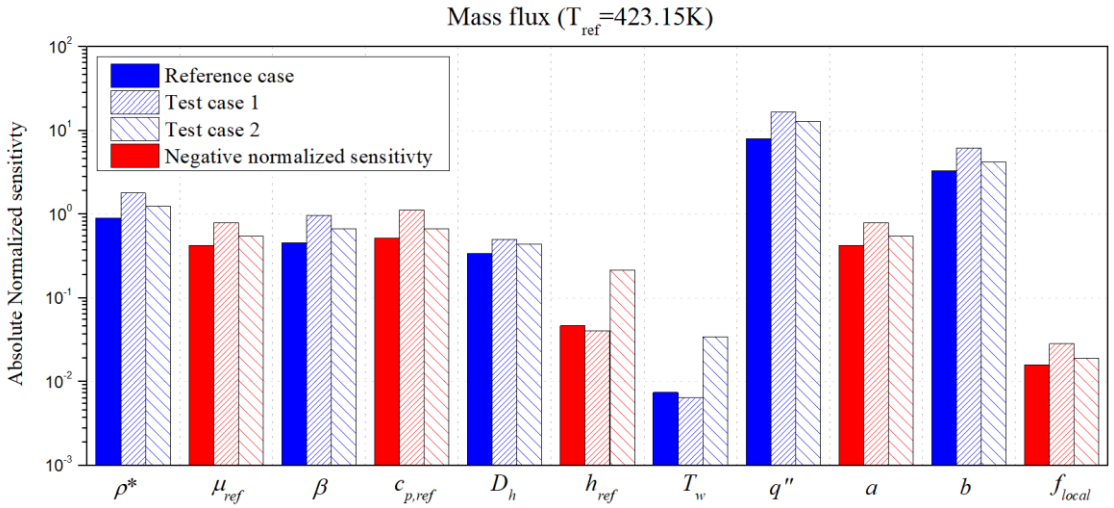

Fig. 2.16. The absolute normalized sensitivity of mass flux for different geometric conditions of heat exchanger (*Red bar indicates negative value)

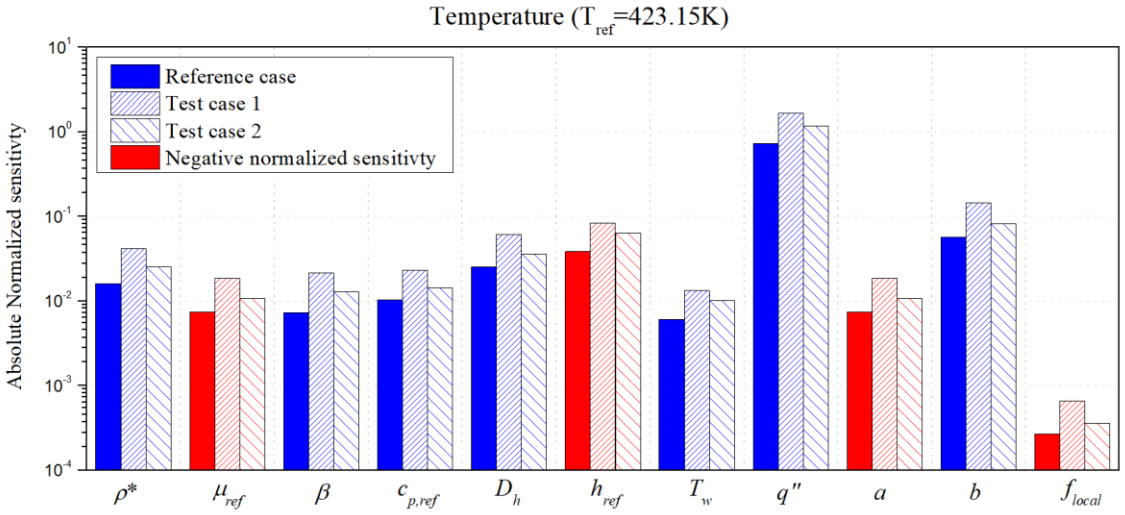

Fig. 2.17. The absolute normalized sensitivity of temperature for different geometric conditions of heat exchanger (*Red bar indicates negative value)

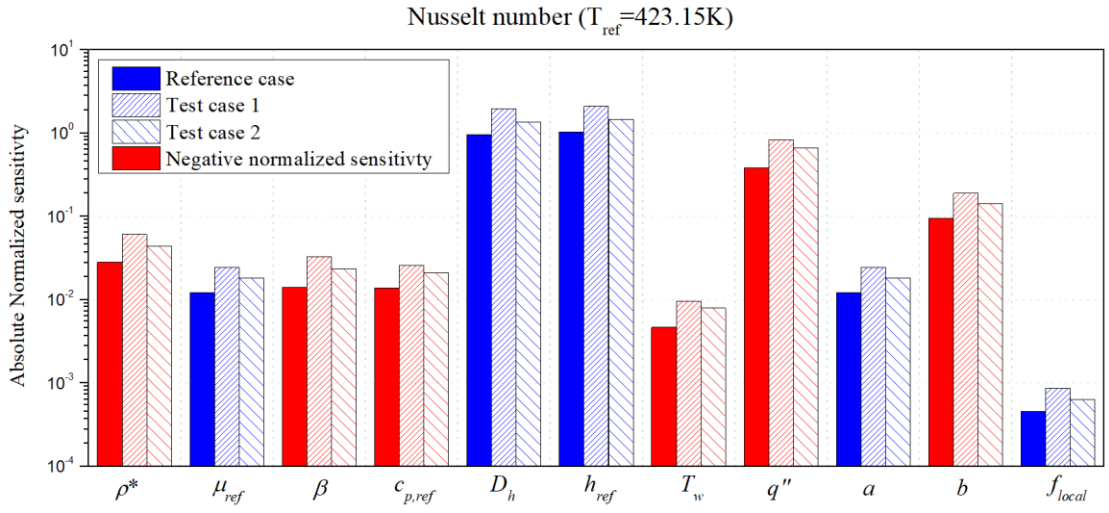

Fig. 2.18. The absolute normalized sensitivity of Nusselt number for different geometric conditions of heat exchanger (*Red bar indicates negative value)

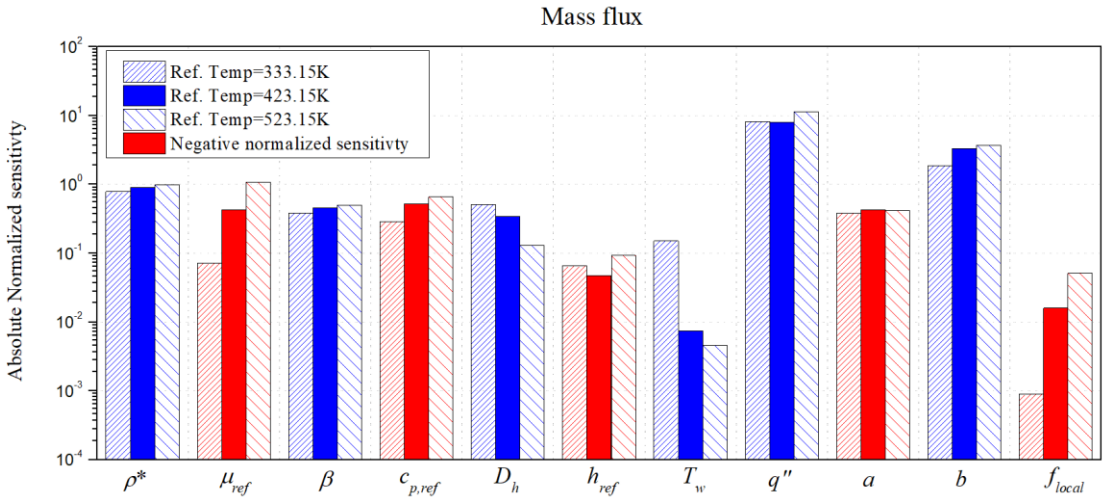

Fig. 2.19. The absolute normalized sensitivity of mass flux at different reference temperatures (*Red bar indicates negative value)

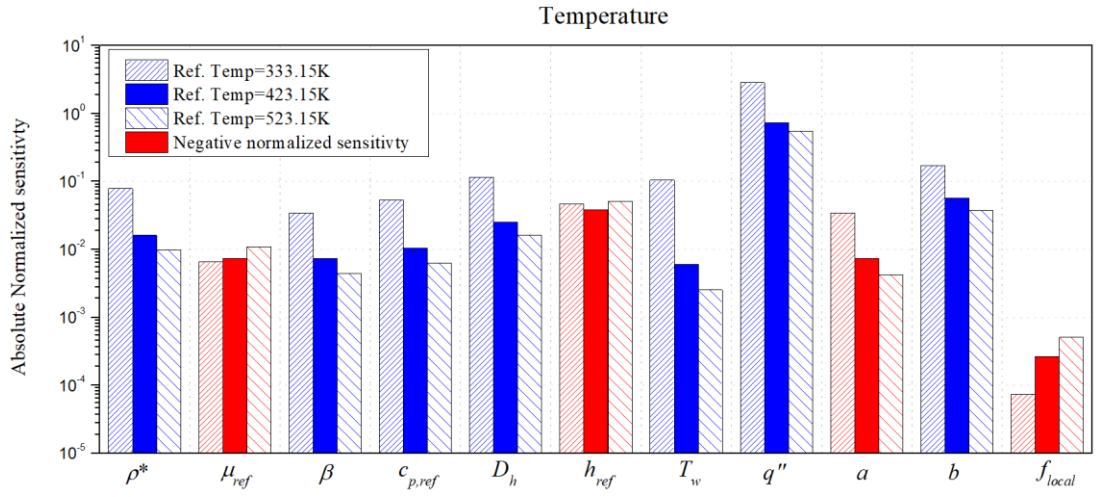

Fig. 2.20. The absolute normalized sensitivity of temperature at different reference temperatures (*Red bar indicates negative value)

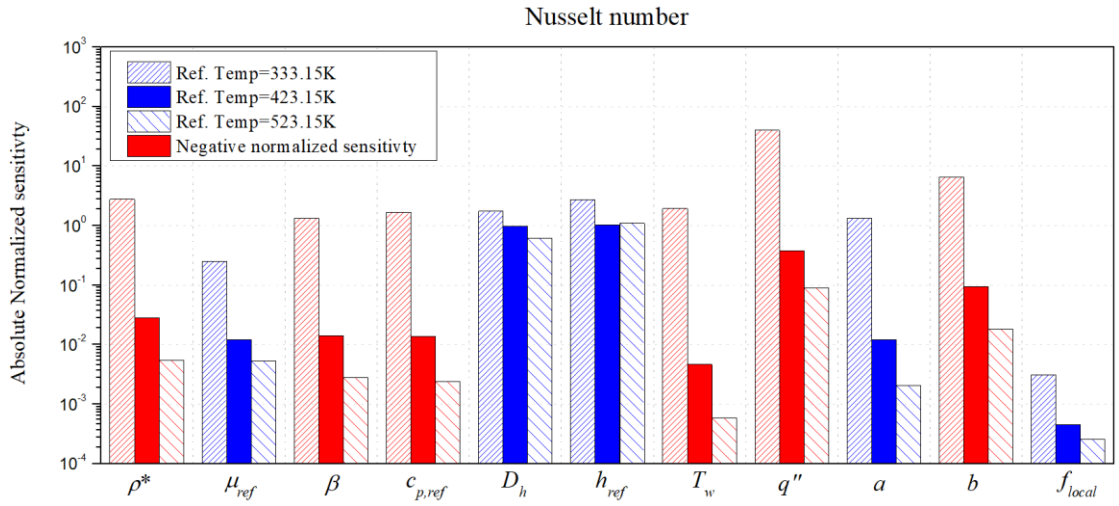

Fig. 2.21. The absolute normalized sensitivity of Nusselt number at different reference temperatures (*Red bar indicates negative value)

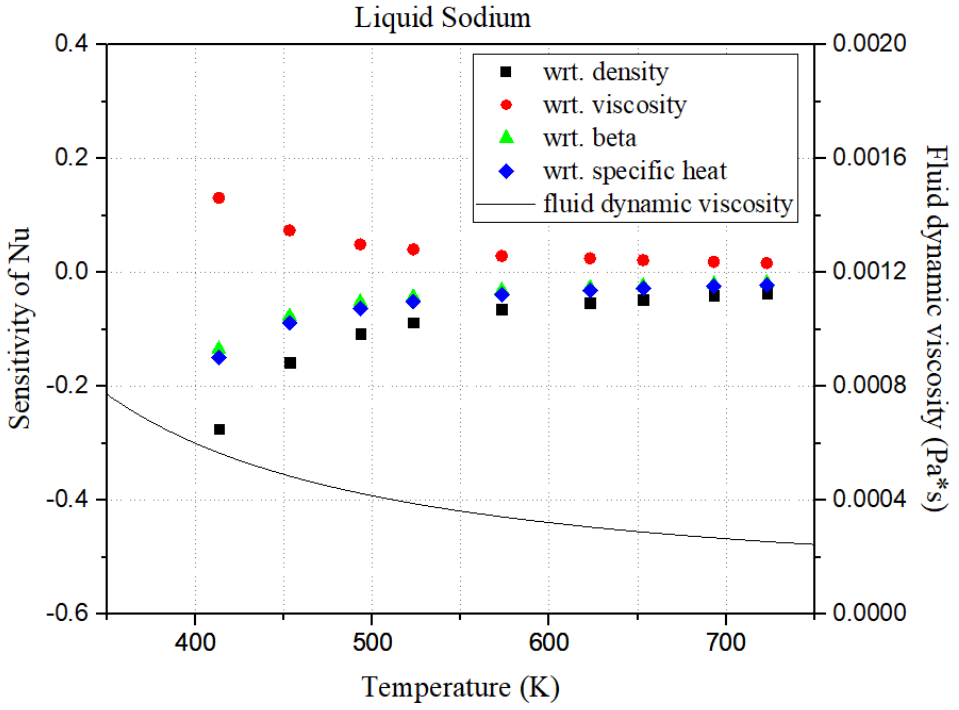

(a)

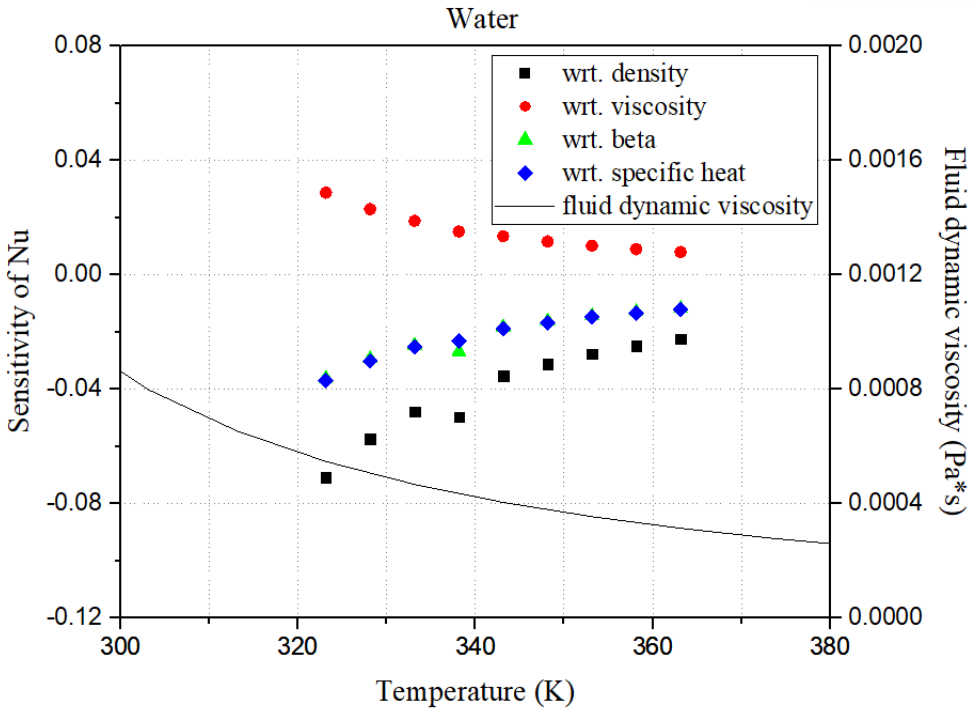

(b)

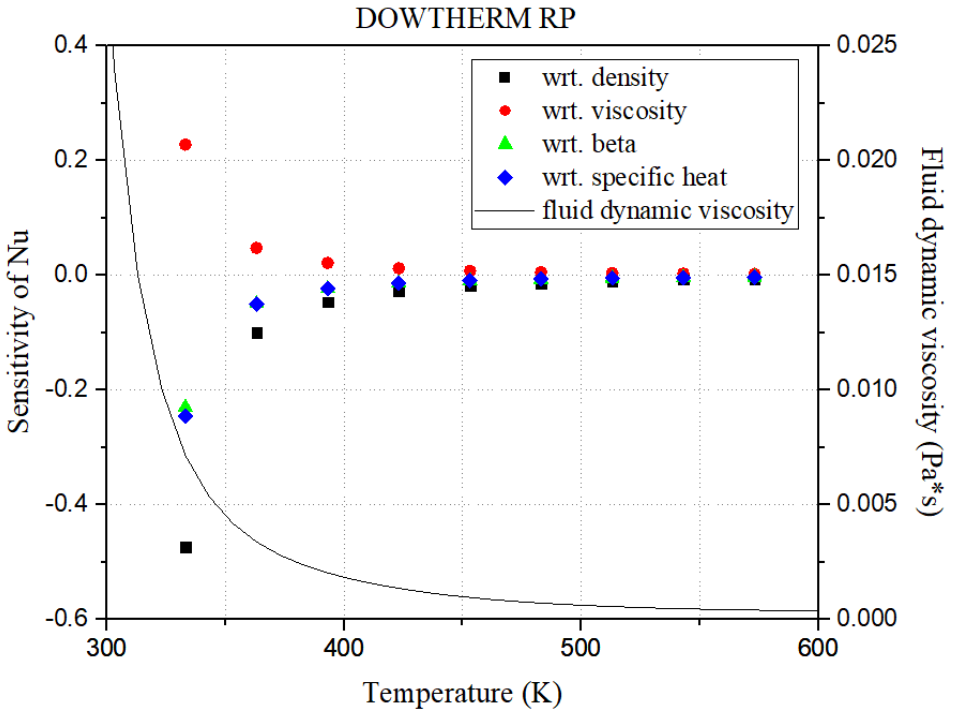

(c)

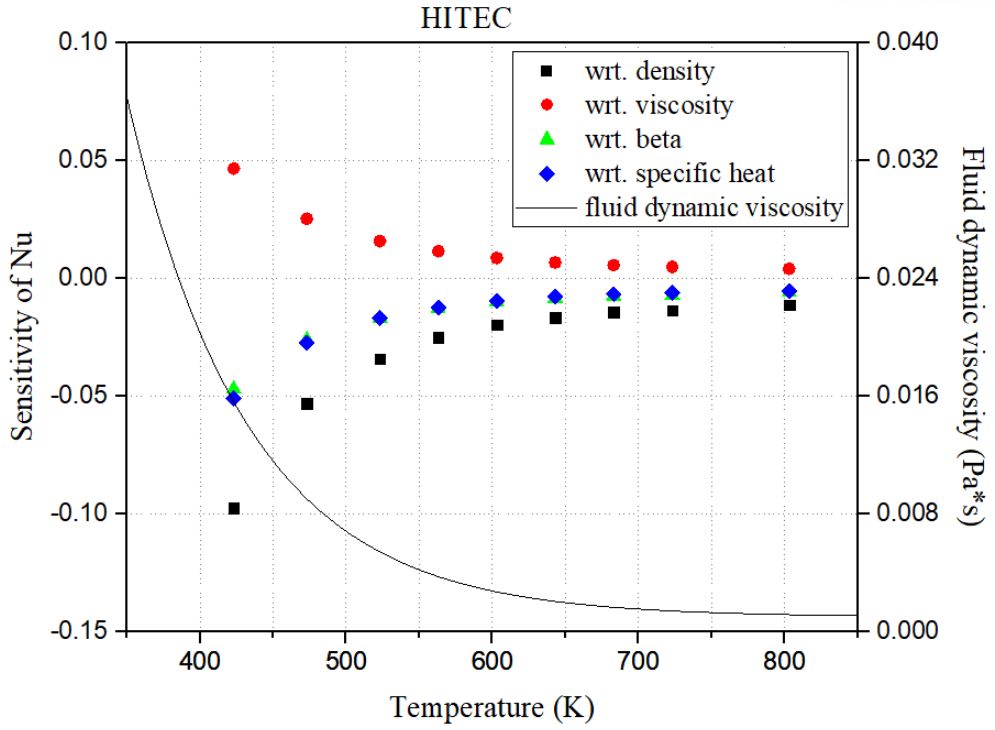

(d)

Fig. 2.22. Normalized sensitivity of Nusselt number with respect to the fluid properties as the increase of operating temperature for different fluids : (a) liquid sodium (b) water (c) DOWTHERM RP (d) HITEC

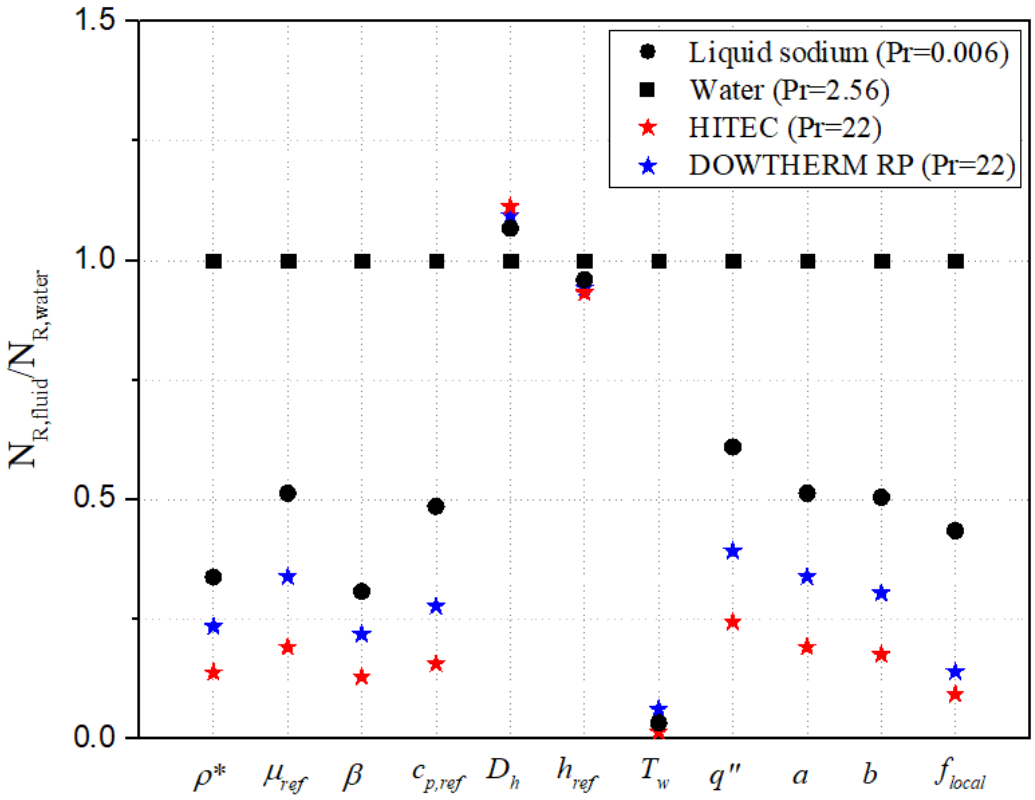

Fig. 2.23. Normalized sensitivity of Nusselt number of different fluids (Normalized sensitivity of water is set as Ref.)

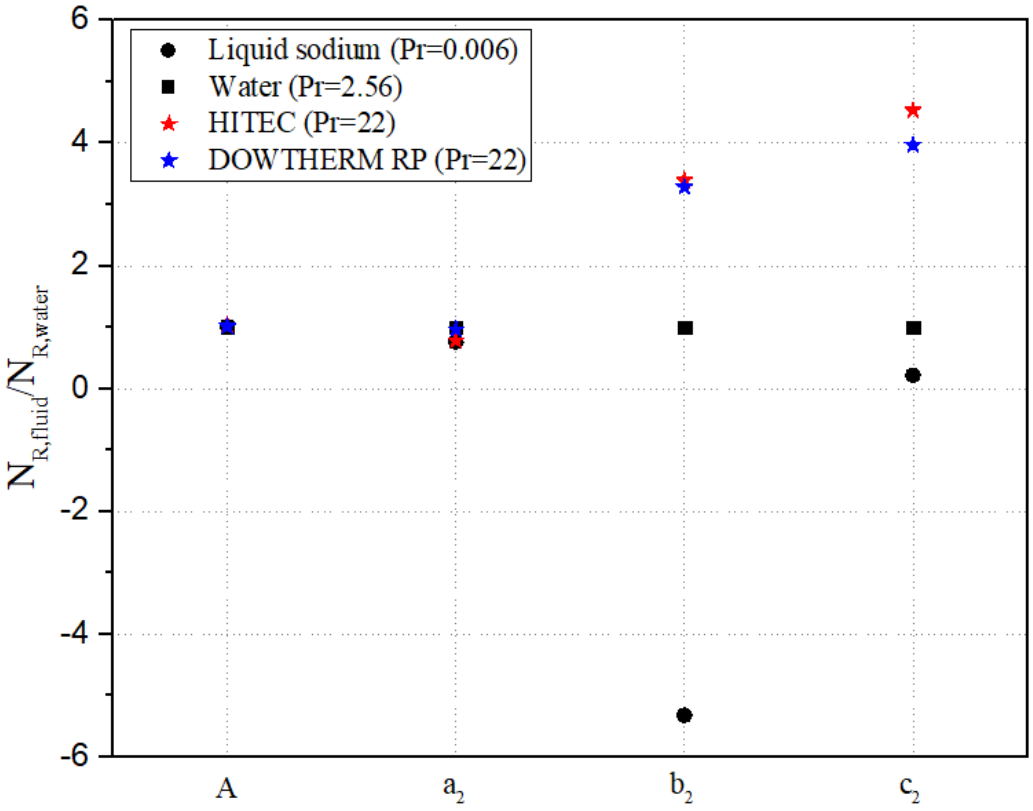

Fig. 2.24. Normalized sensitivity of Nusselt number with respect to empirical constants in typical Nusselt correlation (Normalized sensitivity of water is set as Ref.)

Chapter 3. HEAT TRANSFER BEHAVIOR OF HIGH-PRANDTL NUMBER FLUID : DOWTHERM RP OIL

3.1 Introduction

It can be easily inferred that fluids with similar dimensionless number (especially *Pr* in this study) give similar thermal characteristics, and this concept becomes the starting point of the development of similarity technique [69,70]. In engineering system, the similarity technique gives reasonable possibility to replace the difficult full-scale experiment with scaled experiments under simpler conditions, without any violation of predicting thermal characteristics of desired fluids. There are lots of experimental works to predict the thermal-hydraulic characteristics of engineering systems using similarity technique, such as natural convection [71], heat transfer in microchannels [72,73], heat and mass transport in fluidized beds [74,75], or heat transfer evaluation based on *Pr* of fluid [76,77], etc.

Especially, for high-Prandtl number fluid, Bardet and Peterson [78] suggested that oils and molten salts in similar *Pr* range gave potentials to approximate the single phase momentum and convective heat transfer behaviors. In addition, previous study in UNIST numerically tested the thermal-hydraulic characteristics of synthetic oil and molten salts in natural circulation system [60]. The previous studies pointed out the large temperature gradient between bulk fluid and wall, and the phenomenon was induced by larger momentum diffusivity of fluid compared to thermal diffusivity. In other words, high *Pr* is a key parameter holding the unique heat transfer feature representing the thermal-hydraulic characteristics of oil and heat transfer salts. Table 3.1 summarizes *Pr* range of various liquids including synthetic oils and major heat transfer salts.

The thermal-hydraulic characteristics of synthetic oil, DOWTHERM RP was already tested in natural circulation condition experimentally by same research group [60,79]. The present study extended it to the forced circulation condition using same fluid. Based on the experimental data, the forced convective heat transfer behavior of DOWTHERM RP oil was analyzed and discussed with respect to Prandtl number.

Table 3.1. Thermo-physical properties of key molten salts and synthetic oil

	T (K)	ρ (kg/m^3)	ν (m^2/s *10^6)	C_p (kJ/kg·K)	k (W/m·K)	Prandtl number
$LiF-ThF_4$ [80]	973	4125.4	2.460	1.594	1.010	16
	1023	4081.3	2.044	1.733	1.014	14
	1073	4037.2	1.727	1.872	1.018	13
$LiF-BeF_2-NaF$ [81]	873	2163.5	3.830	2.090	0.829	21
	930	2140.2	3.116	2.090	0.880	16
	988	2116.9	2.597	2.090	0.932	12
$LiF-BeF_2-ThF_4-UF_4$ [82]	839	3373.5	4.231	1.357	1.19	16
	909	3326.8	2.948	1.357	1.23	10
	979	3280.0	2.167	1.357	1.19	8
$2LiF-BeF_2$ (FLiBe) [83,84]	873	1986.7	4.309	2.385	1.1	19
	973	1937.8	2.839	2.385	1.1	12
	1073	1889.0	2.033	2.385	1.1	8
DOWTHERM RP [85]	423	937.3	1.408	2.007	0.115	23
	473	901.0	0.888	2.156	0.108	16
	623	768.1	0.398	2.602	0.089	9
HITEC [68]	473	1896.9	4.764	1.360	0.428	29
	573	1828.0	1.879	1.260	0.383	11
	673	1759.2	0.988	1.160	0.339	6

3.2 Experimental Setup and Procedures

3.2.1 Experimental facility

The experimental system for the heat transfer performance of high-Prandtl number fluid mainly consisted of a heated section, water-cooled heat exchanger, pump, expansion pipe, and acquisition system, as illustrated in Fig. 3.1. The whole experimental system was a rectangular closed loop with total height of 2.66m and width of 0.6m. The circular SS316L tube of system had inner diameter of 0.023m with the thickness of 0.0024m. The vertical heated section was wrapped by the electrical resistive coil wire generating heat source and the tube surface through the entire loop was insulated using fiberglass insulator to minimize heat loss. The maximum input power was restricted by 1kW to prevent the working fluid, DOWTHERM RP, from boiling. The uncertainty in input power was 0.5%. A tube-to-tube heat exchanger cooled by the water with constant temperature and mass flow rate was installed at the upper part of right-vertical side. The expansion pipe located at the highest elevation allowed for the thermal expansion of fluid. The turbine pump with the frequency converter, which was installed at the bottom section, enabled to perform the experiments within the range of Reynolds number from 2000 to 10000. The wall temperatures across the heater were measured by K-type thermocouples which were installed on the outer surface of tube. The bulk fluid temperatures across the heater and cooler were also measured by four K-type thermocouples of which tips were placed at the radially center position inside the tube. The volumetric flow rate of DOWTHERM RP fluid was measured by turbine flow meter at the downstream of cooling section. The uncertainties in the measurement were 0.1% and 3% for the temperature and flow rate, respectively.

3.2.2 Test procedure and experimental uncertainty

The thermophysical properties of DOWTHERM RP were evaluated at the averaged bulk temperature, which was calculated as:

$$T_f = \frac{T_{in} + T_{out}}{2} \tag{3.1}$$

where T_{in} and T_{out} were fluid temperatures at the inlet and outlet, respectively.

The applied heat flux along the heated section was calculated as:

$$q'' = \frac{Q_{in}}{\pi D_i L_h} \tag{3.2}$$

where Q_{in} was input power (W), D_i was the inner diameter of the tube, L_h was the length of heated section.

The wall temperature of outer surface, T_{wo} was directly calculated by averaging the measured outer surface temperatures, and then the wall temperature of inner surface T_w can be calculated as:

$$T_w = T_{wo} + q'' \frac{r_i}{k_w} \ln \frac{D_i}{D_o} \tag{3.3}$$

where r_i was the inner radius of tube, k_w was the thermal conductivity of tube, D_o was the outer diameter of the tube.

Then, the average heat transfer coefficient can be calculated as:

$$h = \frac{q''}{\Delta T_m} = \frac{q''}{T_w - T_f} \tag{3.4}$$

Finally, mean Reynolds number, Prandtl number, Grashof number, and Nusselt number of fluid were calculated as follows:

$$\mathrm{Re}_f = \frac{VD_i}{\nu} = \frac{4}{\pi} \frac{\dot{m}_f}{\mu_f D_i} \tag{3.5}$$

$$\mathrm{Pr}_f = \frac{\nu}{\alpha} = \frac{\mu_f c_p}{k_f} \tag{3.6}$$

$$\mathrm{Gr}_f = \frac{g \beta_f \Delta T_m D_i^3}{\left(\mu_f / \rho_f \right)^2} \tag{3.7}$$

$$\mathrm{Nu} = \frac{hD_i}{k_f} \tag{3.8}$$

where V was fluid velocity, ν was a kinetic viscosity of fluid, α was a thermal diffusivity of fluid, m_f was measured bulk mass flow rate of primary fluid, μ_f was the dynamic viscosity of fluid, c_p was the specific heat capacity of fluid, k_f was the thermal conductivity of fluid, β_f was the thermal expansion

coefficient of fluid, and ρ_f was the fluid density. Here, we defined the Grashof number of fluid using the radial temperature difference, ΔT_m to consider the radial natural convection by buoyancy effect. The detailed explanations are presented in Section 3.3.2.

The overall uncertainty of calculated parameters was deduced by root sum square of each variable uncertainty as follows [86]:

$$\sigma_f = \sqrt{\sum \left(\frac{\partial f\left(x_1,...,x_n\right)}{\partial x_i} \sigma_{x_i} \right)^2} \tag{3.9}$$

where x_i and σ_{xi} were independent parameter and its uncertainty of calculated parameter, $f(x_1,...,x_n)$, respectively.

According to the present experimental conditions, uncertainties in Reynolds number, Prandtl number, Grashof number, and Nusselt number were 3%, 0.17%, 0.33%, and 0.2%, respectively.

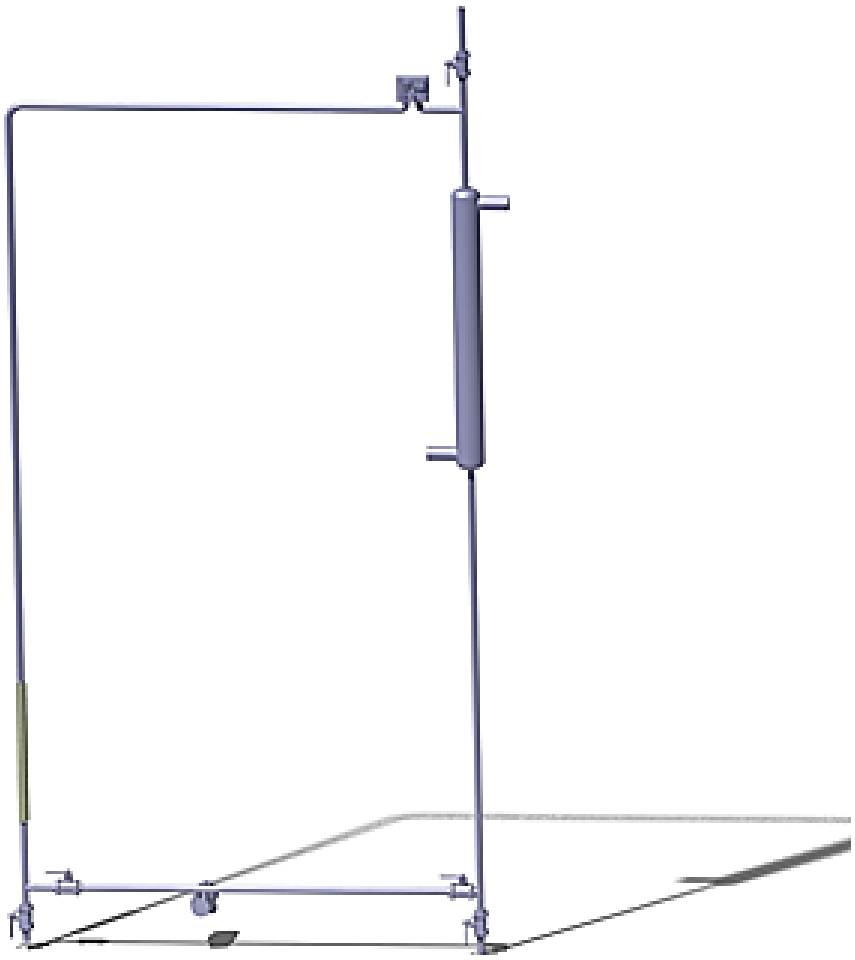

Fig. 3.1. Schematic drawing of experimental setup

Table 3.2. Specification of DOWTHERM RP circulation loop

Design parameter	**(m)**
Loop height	2.66
Loop width	0.6
Inner/Outer diameter	0.023/0.0254
Heating section length	0.195
Cooling section length	0.74
Thermal center elevation	1.3975

Table 3.3. Test matrix of DOWTHERM RP experiment

Volumetric flow rate	0.00017 – 0.0005 m^3/s
Reynolds number	2000 – 10000
Heat input	400 – 900 W
Operating temperature	30 – 150 ^oC
Prandtl number	30 - 70
2^{nd} temperature in H.X.	Water, 20 ^oC

3.3 Experimental results

The convective heat transfer performance of DOWTHERM RP was tested in sets of experiments with different heat inputs and mass flow rates. In each set of experiment, the heat input was varied from 400W to 900W by the voltage control, while the frequency of pump was adjusted to maintain the initial mass flow rate of fluid. The input power was increased step by step, after the measured temperature reached steady state in each step. The experimental results were analyzed with respect of heat input and mass flow rate, respectively: the heat input implied the temperature effect and the mass flow rate implied the inertia effect on the heat transfer performance. Based on the experimental data, the distinct heat transfer feature of high-*Pr* oil was discussed, and new specified *Nu* correlation for high-*Pr* fluid was developed to take the distinct heat transfer behavior into consideration.

3.3.1 Forced heat transfer behavior of high-Pr oil

With the fixed inlet fluid temperature of heater, the increasing input power led to the increase of fluid temperature, which gave significant effect on the heat transfer performance. Reynolds number increased as the input power increased due to the decreased dynamic viscosity of fluid at fixed mass flow rate, as shown in Fig. 3.2. The change in Reynolds number was larger at low mass flow rate where the larger change in dynamic viscosity occurred. Fig. 3.3 shows the change in Prandtl number with the increase of input power. The change in Prandtl number was dominated by the change of the input power, since Prandtl number is defined only by the fluid properties. In addition, the change in Prandtl number at high mass flow rate became smaller, as the input power increased, which implied the smaller average temperature change in the flow direction. Fig. 3.4 shows Nusselt number variation as the input power increased. At fixed mass flow rate, Nusselt number increased as the input power increased due to the dominant influence by increasing Reynolds number.

Figs. 3.5-3.6 show the Nusselt number with respect to Prandtl number and Reynolds number, respectively. At the same input power, it was obvious that Nusselt number increased as Prandtl number and Reynolds number increased, respectively. Especially, the increase ratio of Nusselt number with respect to Prandtl number became larger, as the input power increased. It was attributed to the radical change in Prandtl number at high fluid temperature induced by high input power.

The fluid velocity varied from 0.36 to 0.92 m/s with same input power, and the corresponding Reynolds number is plotted in Fig. 3.7. Due to the drastic decrease in dynamic viscosity of DOWTHERM RP, Reynolds number increased even at the same fluid velocity, as the input power increased.

Nusselt number with respect to fluid velocity is shown in Fig. 3.8. Obviously, Nusselt number increased as the fluid velocity increased. However, the effect of fluid velocity on Nusselt number was

overwhelmed by the effect of input power. In other words, the temperature of fluid had a crucial role in the evaluation of Nusselt number more than the fluid velocity. It implied the significant effect of fluid properties on the heat transfer performance, since the temperature variation induced by input power change directly affects the fluid properties while the fluid velocity is an independent parameter from the fluid properties. That is, especially for high Pr number fluid including DOWTHERM RP, the large variation of fluid properties should be seriously taken into consideration in the evaluation of heat transfer performance.

Many single-phase heat transfer correlations for wide range of Prandtl number included the variation of fluid properties as a ratio of dynamic viscosities, or Prandtl numbers between bulk fluid and wall, as shown in Eqs. (3.10) - (3.12) from Table 1.1.

$$Nu = 0.027\,\mathrm{Re}^{0.8}\,\mathrm{Pr}^{1/3}\left(\frac{\mu_b}{\mu_w}\right)^{0.14} \tag{3.10}$$

$$Nu = 0.012\left(\mathrm{Re}^{0.8} - 280\right)\mathrm{Pr}^{0.4}\left[1+\left(\frac{d}{l}\right)^{2/3}\right]\left(\frac{\mathrm{Pr}_b}{\mathrm{Pr}_w}\right)^{0.11} \tag{3.11}$$

$$Nu = 0.037\left(\mathrm{Re}^{0.75} - 180\right)\mathrm{Pr}^{0.42}\left[1+\left(\frac{d}{l}\right)^{2/3}\right]\left(\frac{\mu_b}{\mu_w}\right)^{0.14} \tag{3.12}$$

where, μ is dynamic viscosity, d is a hydraulic diameter of tube, l is a length of tube, and the subscripts b and w are bulk fluid and wall, respectively.

However, the previous correlations were still insufficient to explain the single-phase convective heat transfer of DOWTHERM RP, as shown in Figs. 3.9-3.11. Especially, under the region of Re = 5000, the deviation became larger. The flow regime of Re < 5000 is the transition flow between laminar flow and turbulent flow. Thus, it was inferred that the inertia of fluid is not sufficient to enable the forced convective heat transfer to dominate the overall heat transfer performance of fluid. Instead, the natural convective heat transfer has a considerable role in the heat transfer between the fluid and heated wall. Especially, high Pr number fluid induced large temperature gradient near the wall, which enhanced local natural convective heat transfer. Based on the concept, new convective heat transfer correlation for high-Pr fluid was proposed considering both forced and natural convective heat transfer in transition flow regime, as shown in Eq. (3.13).

$$Nu = C_1\left(\mathrm{Re}^{a_1} - A\right)\mathrm{Pr}^{b_1}\left(\frac{\mathrm{Pr}_b}{\mathrm{Pr}_w}\right)^c + C_2 Gr^{a_2}\,\mathrm{Pr}^{b_2} \tag{3.13}$$

where, C, a, b, c are empirical constants.

The second term in Eq. (3.13), which was independent from forced convective heat transfer, represented the natural convective heat transfer enhanced by high-*Pr* fluid. With proper empirical constants, newly proposed correlation in Eq. (3.14) well agreed with the present experimental data, as shown in Fig. 3.12.

$$Nu = 0.025\left(\mathrm{Re}^{0.815} - 210\right)\mathrm{Pr}^{0.33}\left(\frac{\mathrm{Pr}_b}{\mathrm{Pr}_w}\right)^{0.14} + 0.0014 Gr^{0.62}\,\mathrm{Pr}^{0.4} \tag{3.14}$$

For the validation of proposed correlation, the previous experimental data using high-*Pr* fluid like molten salts were compared in Fig. 3.13. The proposed correlation employed firstly simple additive terms of previous Nusselt-Grashof relationship in natural convection to represent enhanced local natural convective heat transfer in high-*Pr* fluid. Here, the main point is that the local natural convective heat transfer is enhanced in high-*Pr* fluid and is independent from bulk convective heat transfer. The proposed correlation was just the simplest form to understand the concepts, but even the simplest correlation well expected the previous experimental data using high-*Pr* fluid within the deviation of 20%. Thus, it is worthy to discuss the enhanced local natural convective heat transfer as a distinct heat transfer feature of high-Pr fluid. The detailed discussion was described in the following section.

3.3.2 Discussion on heat transfer behavior of high-Pr fluid

The exponents of Prandtl number in the previous correlation were suggested based on the theoretical boundary layer in two-dimensional flows. Starting from the typical formation of laminar boundary layer through the heat transfer wall surface, it might explain the mean heat transfer phenomena [87]. However, it couldn't prove its validity in predicting local convective heat transfer phenomena based on the physical and experimental insight, even though the modified versions of correlations employed the fluid-to-wall ratio of viscosity or Prandtl number. This issue becomes serious in the case of high-Prandtl number fluid flow, since the mean properties of fluid are largely different from local properties of fluid near heat transfer surface. Thus, the physical insight in the prediction of overall heat transfer including local phenomena is required for high-Prandtl number fluid flow, especially for internal flow through heated circular tube in this study.

There have been several precise experiments to measure accurate local heat transfer phenomena in external cross flow through various objects. Early in 20th century, several German researchers conducted independent experiments to measure the local heat transfer coefficients in external cross flow through different objects and reported that it was rather high compared to mean heat transfer coefficient [88]. In addition, the recent experimental data of air flow through square cylinders obtained by several researchers reported larger heat transfer coefficients than predicted mean heat transfer coefficients at the same conditions [89–91]. Even for the fluid flow with Prandtl number near unity like air, the local heat transfer phenomena were found to be different from mean convective heat transfer due to the influence of Prandtl number. In other words, the influence of high-Pr on the mean and local convective heat transfer is highly questionable. The issue is that only experiments can explain the local Prandtl number effect on the convective heat transfer, but there is no report on the experimental measurement of local heat transfer in high-Pr fluid flow so far.

Recently, same research group in UNIST conducted experiments using high-Pr oil in closed natural circulation loop and reported the experimental data with the distinct flow behavior [61,92]. Especially, the visualized PIV results pointed out that the local natural convection was generated enhancing radial flow velocity. The author introduced boundary layer theory computed from CFD simulation results to explain the effect of high-Prandtl number. It was found that the ratio of velocity boundary layer to thermal boundary layer computed by CFD simulation results was smaller than predicted ratio. Based on the previous data, the present discussion gave the detailed explanation. As the fluid velocity became larger, the radial thermal boundary layer became thinner compared to the velocity boundary layer. However, at the low fluid velocity or weak inertia condition, the radial thermal boundary layer became relatively thicker compared to the predicted value, which implied certain radial mixing phenomena to thicken the thermal boundary layer.

Still, it is insufficient to confirm the proposed flow feature from the present study. For the verification, the further experimental works using molten heat transfer salt was designed and prepared by construction of the experimental facility. The preliminary test on molten salt natural circulation using built experimental facility is presented in the following section.

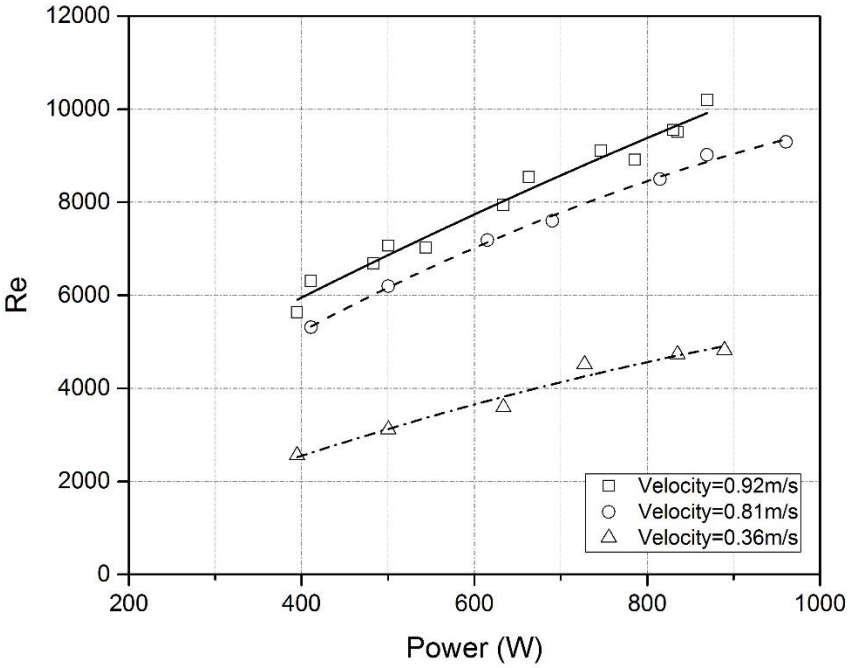

Fig. 3.2. Reynolds number plot with input power

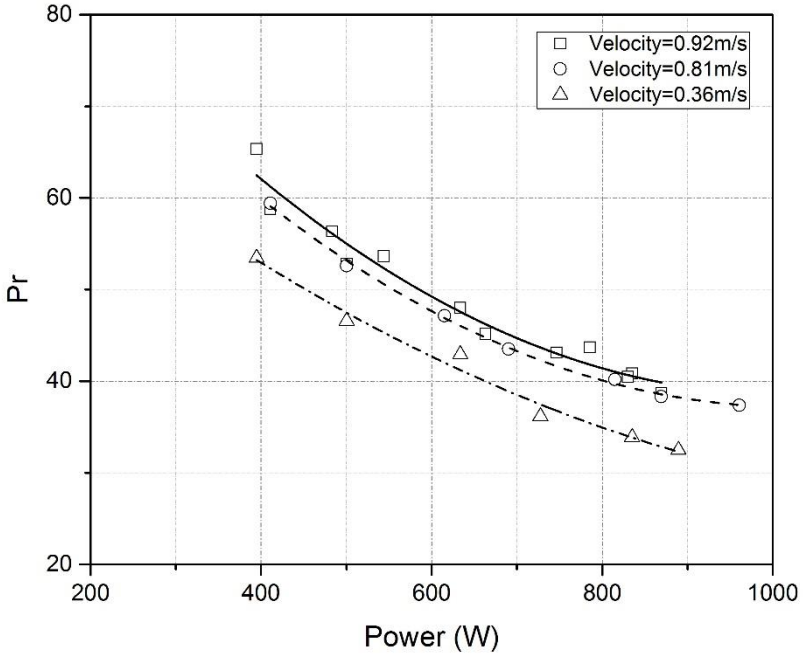

Fig. 3.3. Prandtl number plot with input power

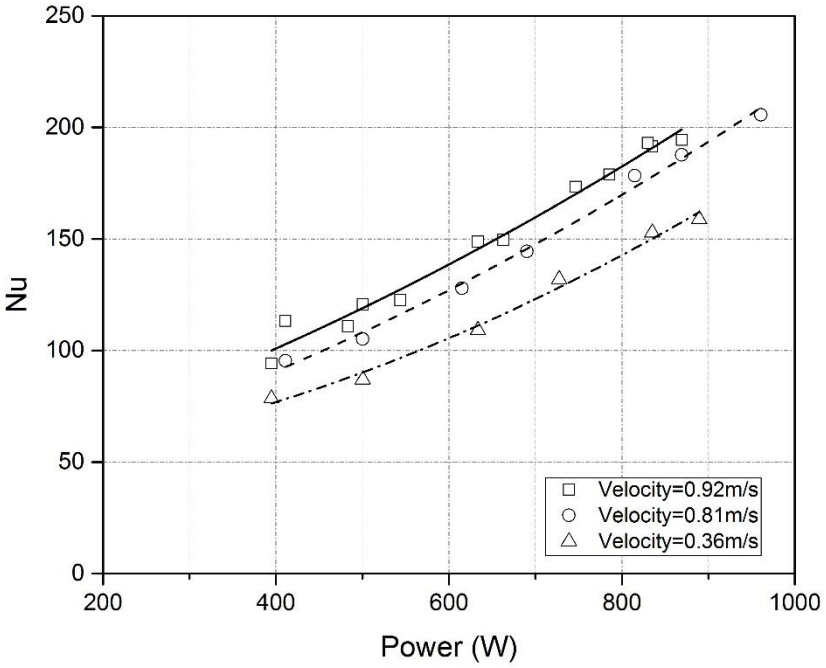

Fig. 3.4. Nusselt number plot with input power

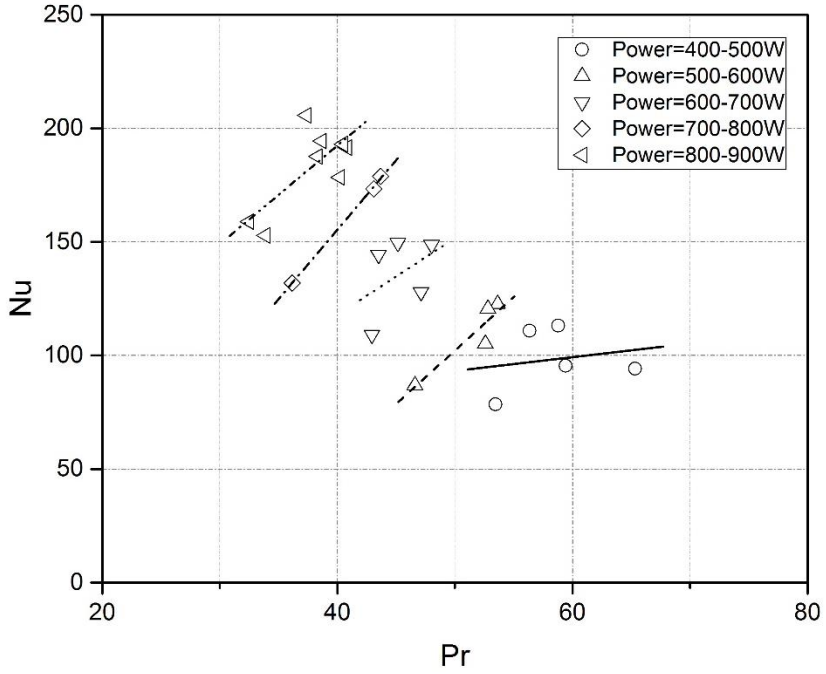

Fig. 3.5. Nusselt number plot with Prandtl number

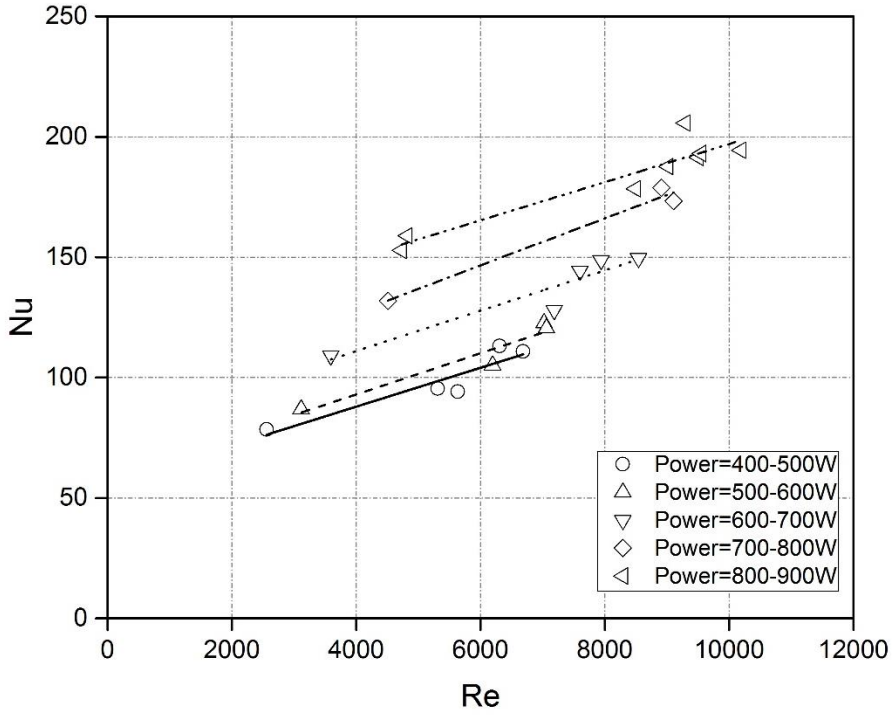

Fig. 3.6. Nusselt number plot with Reynolds number

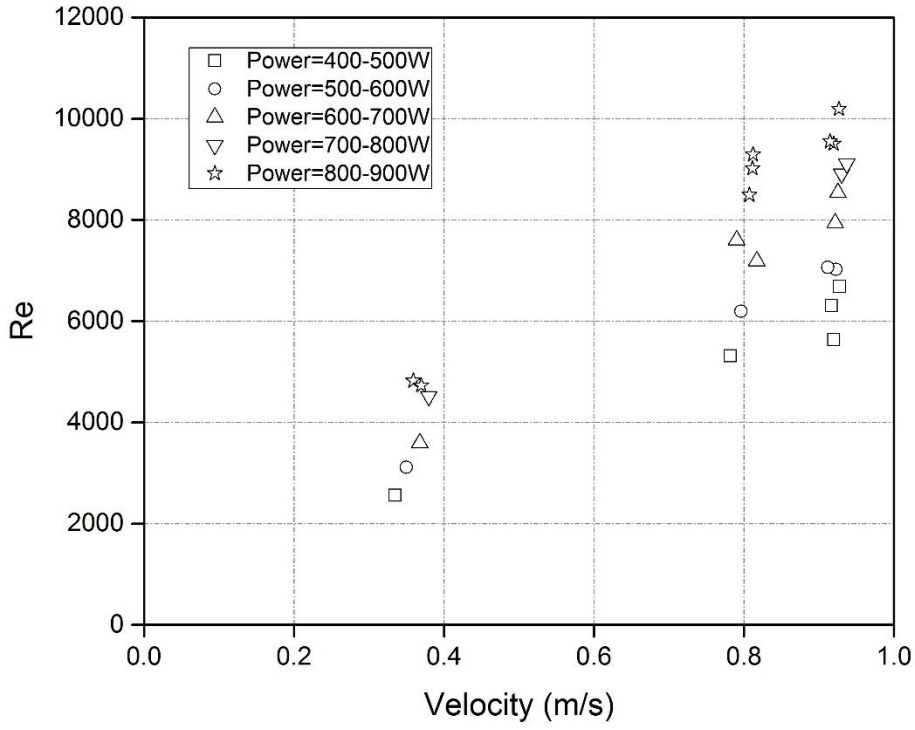

Fig. 3.7. Reynolds number plot with the corresponding fluid velocity

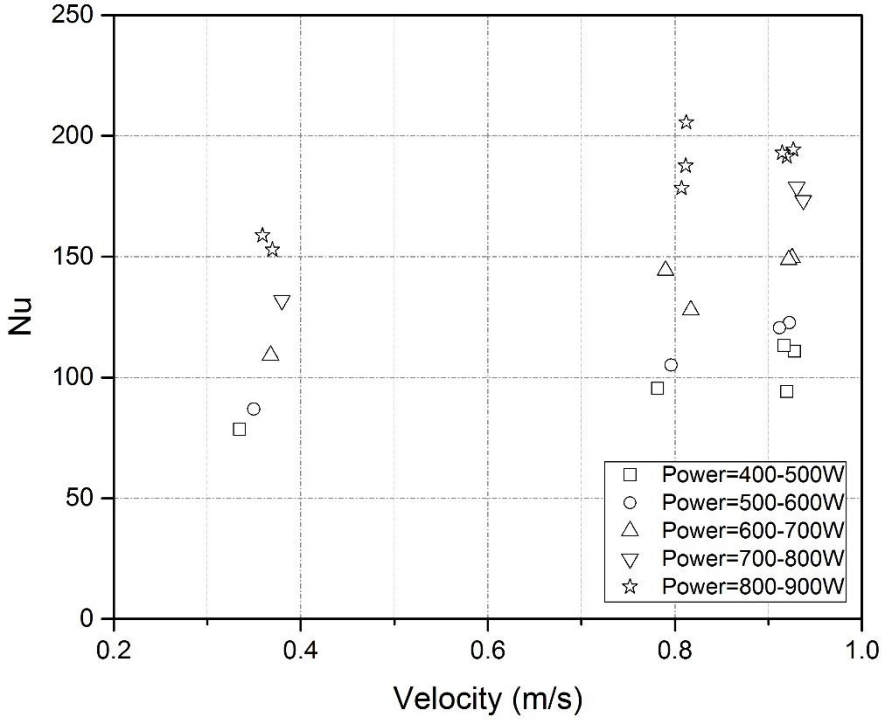

Fig. 3.8. Nusselt number plot with the fluid velocity

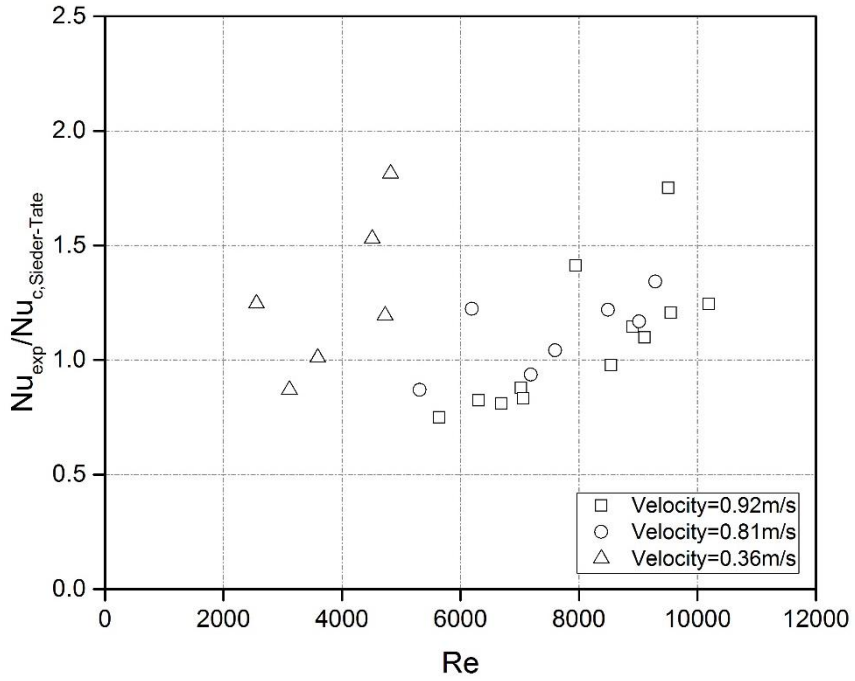

Fig. 3.9. Comparison of Nusselt numbers: vs. Sieder-Tate's

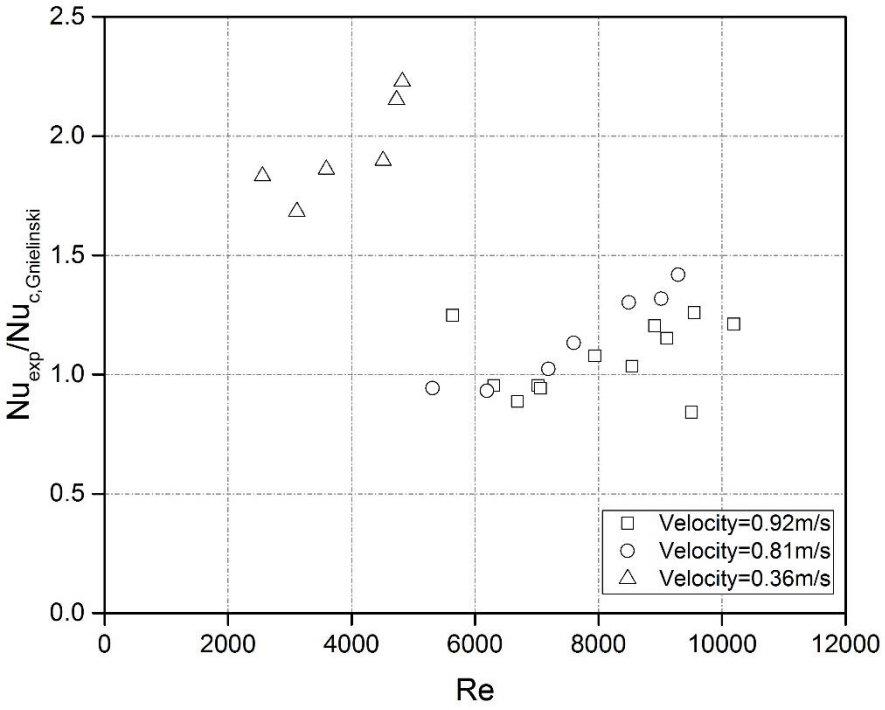

Fig. 3.10. Comparison of Nusselt numbers: vs. Gnielinski's

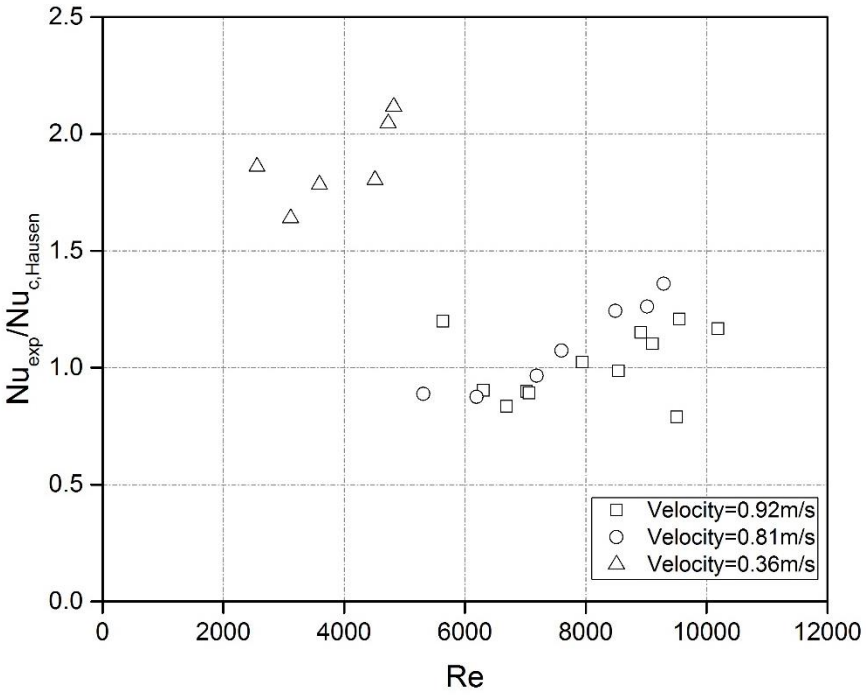

Fig. 3.11. Comparison of Nusselt numbers: vs. Hausen's

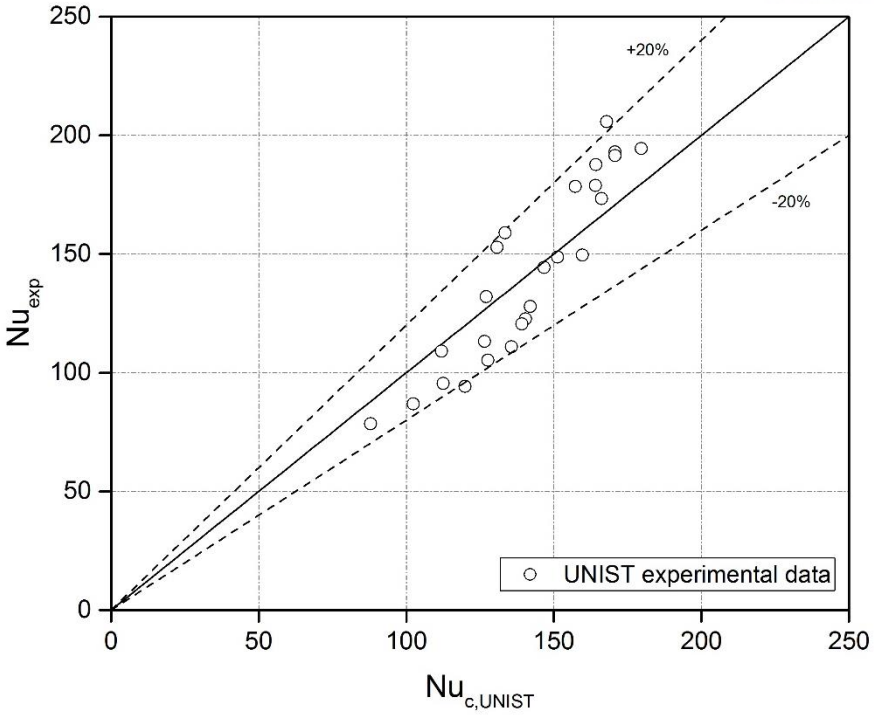

Fig. 3.12. Comparison of proposed correlation with the present experimental data

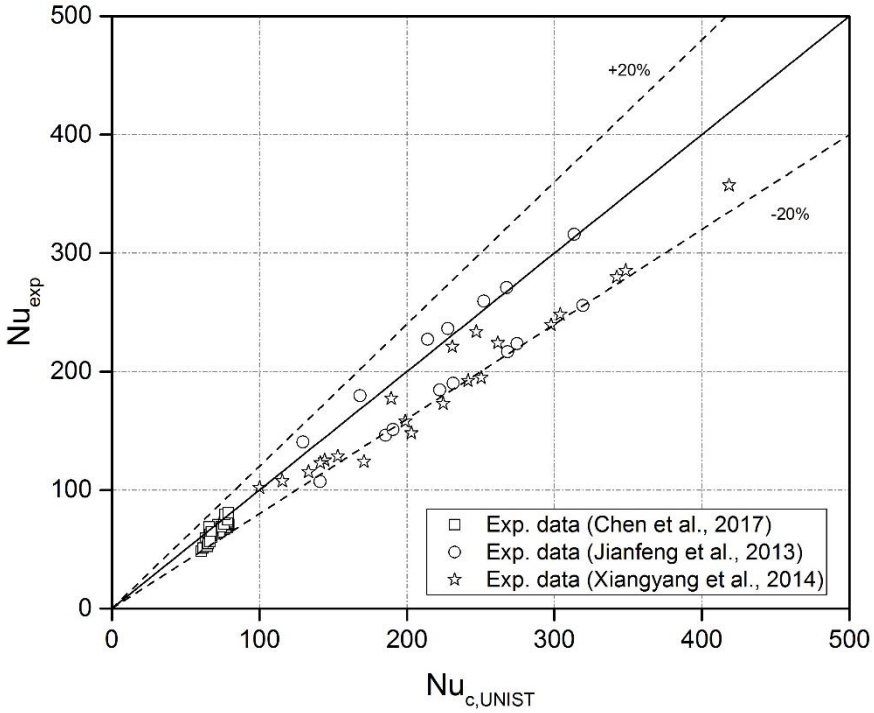

Fig. 3.13. Comparison of proposed correlation with the previous experimental data

Chapter 4. HEAT TRANSFER BEHAVIOR OF HIGH-PRANDTL NUMBER FLUID : HEAT TRANSFER SALT

4.1 Introduction

The first experimental investigation on heat transfer of molten salt was conducted at Oak Ridge National Laboratory in 1950s using fluoride salt [93] and nitrate salt [31]. The forced convective heat transfer of molten salts in circular tubes were investigated and associated correlations were proposed from the experimental studies. Then, further experiments using two more fluoride salts were also conducted in a forced convection loop at the same research group [94]. In 21st century, many researchers investigated the convective heat transfer of molten salt in various kinds of fluid path. Wu et al. [95,96] designed transversally corrugated tubes to study the heat transfer of molten salt, while Lu et al. [97,98] employed spirally grooved tube and transversely grooved tube to test the enhancement in heat transfer of molten salts. Shen et al. [99] conducted forced circulation experiments to investigate convective heat transfer of molten salt with nonuniform heat flux and proposed experimental correlation derived from general form. Recently, Xia et al. [100] investigated the mixed convective heat transfer of molten salt in horizontal square tubes and characterized the mixed convection by superposition of inertia-driven heat transfer and buoyancy-driven heat transfer. However, the horizontally installed test section made the buoyancy-driven heat transfer be confused with gravity-driven phenomena. In order to clarify buoyancy-driven heat transfer, the studies on the natural heat transfer behavior of molten salts are required, however there have been few experimental studies on natural circulation heat transfer of molten salts. Bhabha Atomic Research Centre (BARC) built molten salt natural circulation loop to experimentally investigate the thermal-hydraulic behaviors of molten nitrate salt. Kudariyawar et al. [50] carried out the experimental study on steady state and transient characteristics of the molten salt using built natural circulation loop. In the same manner, Srivastava et al. [51] also conducted steady state and transient experiments using nitrate salt in natural circulation loop. They analyzed the natural mass flow and temperature histories under various postulated transients of passive molten salt heat transport systems, while the further investigation of heat transfer behaviors of molten salt wasn't carried out. The experimental studies on the heat transfer of molten salt would give the concrete basis on the feasibility test results for practical heat transport system and verification of proposed heat transfer of high-Pr fluids. Thus, the present section gave experimental analysis of steady-state behavior of molten salt as well as the heat transfer performance to give fundamental insight on heat transfer behavior of molten salt.

4.2 Experimental Setup and Procedures

4.2.1 Experimental facility

New experimental facility was designed to conduct the natural and forced circulation experiments using heat transfer salt, referred as preliminary version of Nuclear-Highly Optimized Prandtl number Experimental facility (NuHOPE-pre) in UNIST. NuHOPE-pre mainly consisted of a vertical heater, vertical heat exchanger cooled by air, a thermal expansion tank, a filling tank, pump, and measurements and acquisition system, as shown in Fig. 4.1. NuHOPE-pre was a rectangular closed loop with total height of 2.6m and width of 0.6m and the whole system was made of circular SS304 tube with inner diameter of 0.023m. The tube surface through the entire loop was wrapped by the electric surface heater to maintain desired temperature above the melting temperature of HITEC, except for the vertical heated section which was wrapped by the electrical resistive coil wire generating heat source. The entire system was insulated using fiberglass insulator covered by aluminum insulator to minimize heat loss. The power capacity was 4kW with the uncertainty of 0.5%. A tube-to-tube heat exchanger cooled by the air with constant temperature and mass flow rate was installed at the upper part of right-vertical side. The temperature and mass flow rate of secondary air was maintained at desired value by external heater and injection valve, respectively. The expansion tank was located at the highest elevation for the suppression of expanded fluid. The turbine pump with the frequency converter, which was installed at the bottom section, enabled to perform further experiments in forced flow condition. The wall temperatures across the heater were measured by K-type thermocouples which were installed on the outer surface of tube. The bulk fluid temperatures across the heater and cooler were also measured by four K-type thermocouples of which tips were placed at the radially center position inside the tube. The volumetric flow rate of working fluid was measured by vortex flow meter at the downstream of cooling section. The uncertainties in the measurement were 0.1% and 1% for the temperature and flow rate, respectively.

4.2.2 Test procedure and experimental uncertainty

The natural heat transfer performance of HITEC was tested in sets of experiments with different heat inputs while the secondary flow condition of heat exchanger was fixed. The external heat was applied through the wrapped copper coil varied from 500W to 2200W by the voltage control. The input power was increased step by step, after the measured temperature reached steady state in each step. The experimental results were analyzed by using dimensionless numbers such as Grashof number and Rayleigh number.

The uncertainties during the experiments were evaluated by using same method in the previous section, so uncertainties in Grashof number, Rayleigh number, and Nusselt number were 0.3%, 0.3%, and 0.05%, respectively.

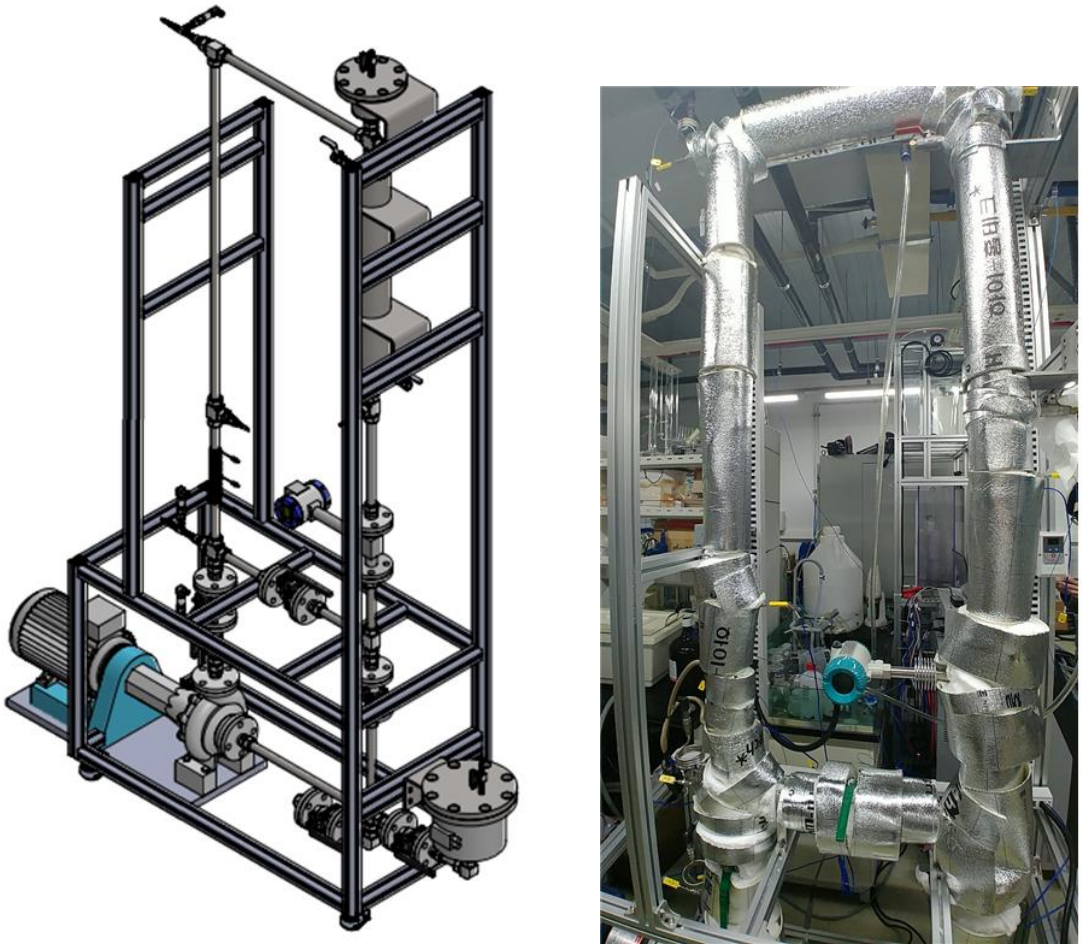

(a) (b)

Fig. 4.1. (a) 3D drawing of experimental setup for heat transfer salt (b) Construction of experimental setup for heat transfer salt

Table 4.1. Specification of HITEC circulation loop

Design parameter	**(m)**
Loop height	2.6
Loop width	0.6
Inner/Outer diameter	0.023/0.0254
Heating section length	0.193
Cooling section length	0.74
Thermal center elevation	1.4

Table 4.2. Test matrix of HITEC experiment

Controlled parameter	
Reynolds number	200 - 3000
Heat input	500 – 2200 W
Operating temperature	180 – 350 ^{o}C
Prandtl number	15 - 30
2nd temperature in H.X.	Air, 200 ^{o}C

4.3 Experimental results

4.3.1 Natural heat transfer behavior of heat transfer salt

The steady state natural heat transfer of HITEC was tested in sets of experiments with different heat inputs varied from 500W to 2200W. In the operating power range, the natural flow remains mostly in laminar regime, where Re < 2500. Before analyzing steady state natural heat transfer of molten salt, the steady state temperature histories were judged as shown in Figs. 4.2. Figs. 4.2(a)-(c) show the steady state temperature histories at three different powers of 500W, 1200W, and 1700W, respectively. It can be easily known that all the temperature histories were at steady state, while the patterns were different from each other. For all power inputs, temperatures histories showed periodic pulsation, while the period of pulsation became short as the power input increased. In addition, the magnitude of temperature pulsation became large with the increase of power input. That is, as the power input increased, the flow pulsation in the circulation loop was enhanced still maintaining the stable natural circulation. Due to the lack of experimental data, the present paper only dealt with the stable formation of natural circulation of molten salt inside the loop in order to test the feasibility of stable molten salt system. The further experimental works is needed to give fundamental investigation of natural flow stability of molten salt. Figs. 4.3-4.4 show the steady state temperature and mass flow rate of molten salt with respect to power inputs. The measured temperatures at different locations linearly increased as the power input increased. Since the secondary air temperature of heat exchanger was fixed at 200^{o}C, the fluid temperature should be increased to achieve heat balance through the entire loop from heater to heat exchanger. Then, to achieve heat balance across the heater, the natural mass flow rate increased as the power input increased. As a result, the stable formation of natural circulation and linear relationship between steady state flow with the power input ensured the feasibility of experimental work and further passive heat transport system using molten salt.

The heat transfer of HITEC was analyzed by employing classical Nu – Ra relationship. Fig. 4.5 shows the comparison of present experimental data in Nu – Ra relationship with previous experimental data of high-Pr fluids including oil and molten salts [101–103]. The previous literature employed closed circulation loop for natural heat transfer of high-Pr fluid mainly to design and test the passive heat transport system of advanced nuclear reactors like fluoride salt-cooled high temperature reactor. The present experimental data using HITEC well agreed with the previous data distribution, which verified again the experimental results. In other word, the present experimental works could be extended to the design and performance test of passive heat transport system using molten salts. In addition, it was proven that HITEC could reproduce the natural heat transfer of fluoride-based molten salts.

Since the feasibility of passive heat transport system using HITEC was tested, then the natural heat transfer of HITEC was predicted by previous well-known correlations, as shown in Eqs. (4.1) - (4.3)

from Table 1.2.

$$\text{(Morgan)} \qquad Nu = 0.3Ra^{0.28}\,\mathrm{Pr}^{-0.028} \tag{4.1}$$

$$\text{(Churchill and Chu)} \qquad Nu = \left[0.6 + 0.387\left(Ra / \left(1 + \left(0.599/\mathrm{Pr}\right)^{9/16}\right)^{16/9}\right)^{1/6}\right]^2 \tag{4.2}$$

$$\text{(Fand)} \qquad Nu = 0.4\,\mathrm{Pr}^{0.0432}\,Ra^{0.25} + 0.503\,\mathrm{Pr}^{0.0334}\,Ra^{0.0816} + 0.958Ge^{0.1222} / \left(\mathrm{Pr}^{0.06}\,Ra^{0.0511}\right) \tag{4.3}$$

$$\text{(UNIST)} \qquad Nu_{NC} = 0.0014Gr^{0.62}\,\mathrm{Pr}^{0.4} \qquad \text{for natural heat transfer} \tag{4.4}$$

Fig. 4.6 shows the comparison of measured Nusselt number with predicted Nusselt number. It was found that the previous correlations overestimated the heat transfer of HITEC. On the contrary, Nu-Gr correlation in Eq. (4.4) proposed by UNIST well predicted the heat transfer of HITEC in validated range, as shown in Fig. 4.6. While previous correlations weighted on the constant rather than Rayleigh number and Prandtl number, UNIST correlation reduced the importance of constant and enhanced the importance of Grashof number to take account of local natural convection effect in high-Pr fluid flow. In addition, the listed correlations were basically applicable to the heat transfer of external flow. That is, specific correlation which is applicable to the internal flow through closed circulation loop was needed to predict the accurate natural heat transfer performance of high-Pr fluid system. Unfortunately, the insufficient experimental data couldn't give the validation of proposed correlation in the broad range. However, it was applicable to at least laminar flow regime where the local natural convection gave considerable effect on the convective heat transfer. In addition, the fundamental insight on the distinct heat transfer behavior of high-Pr fluid was introduced and roughly tested. The further experimental campaign will be the extension of proposed concept and prediction of heat transfer performance to the broad range of flow regime and optimization of high-Pr fluid system based on the prediction.

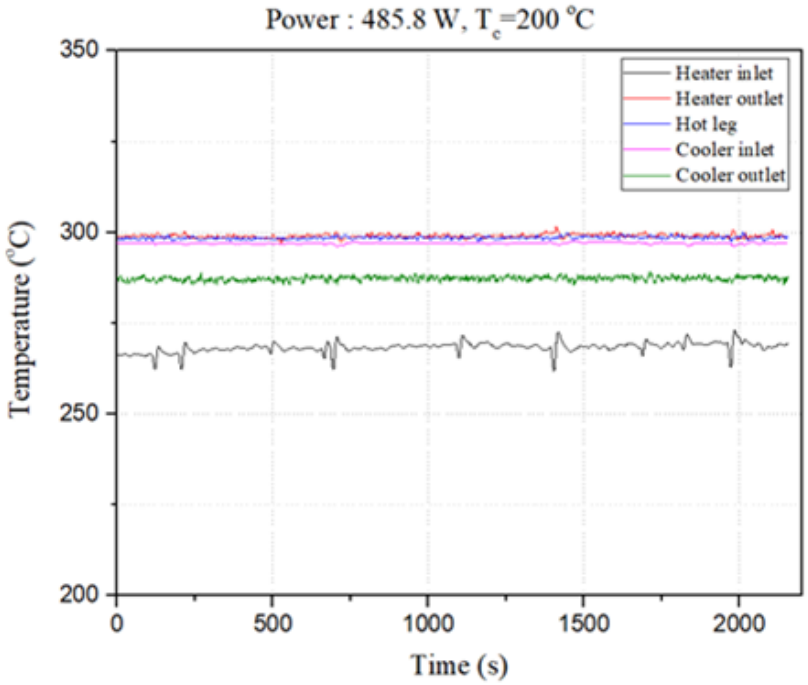

(a)

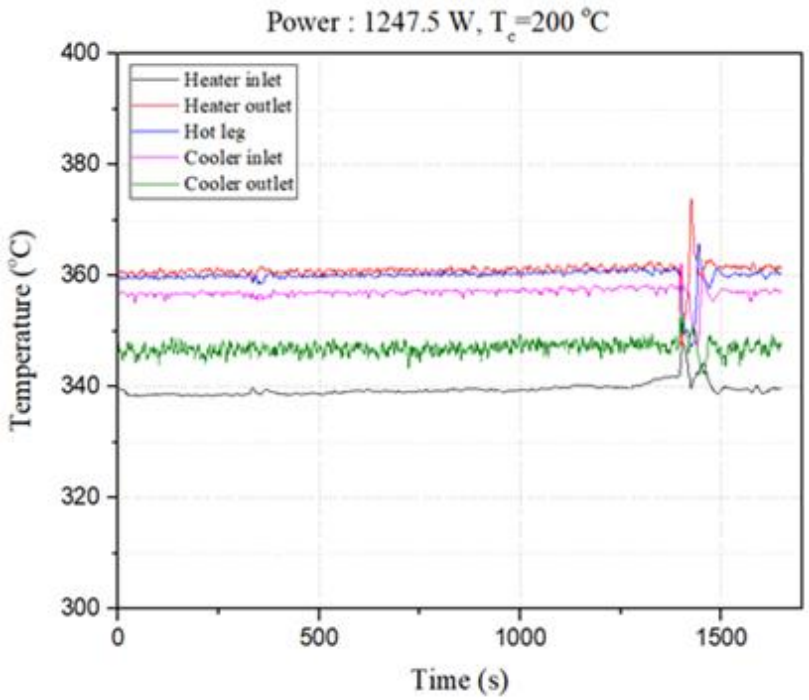

(b)

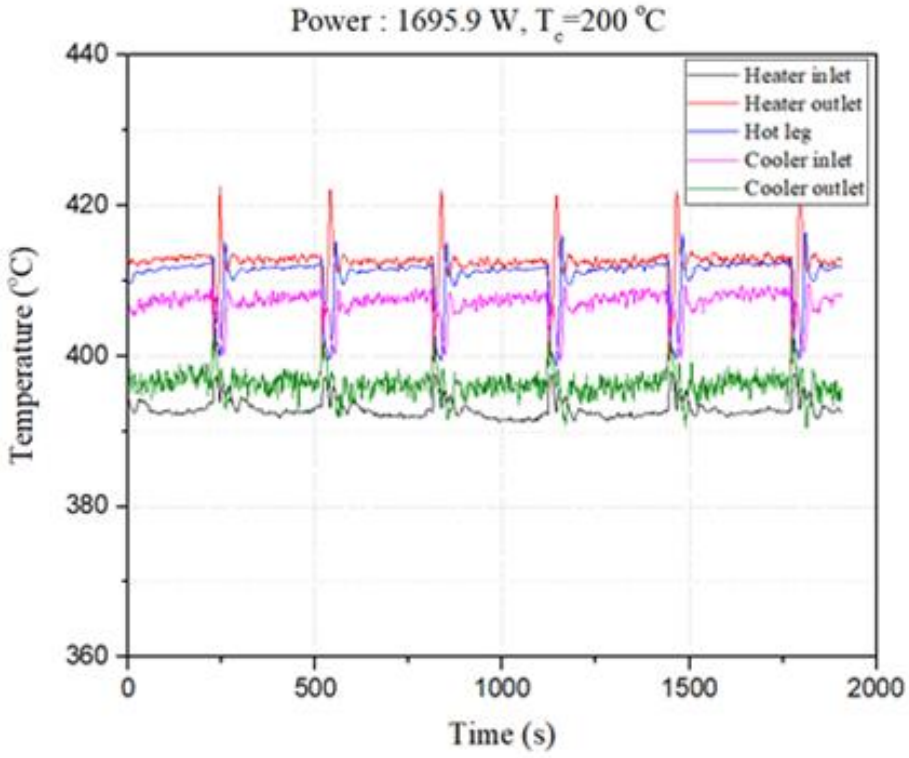

(c)

Fig. 4.2. (a) Temperature histories at heat input of 485.8W (b) Temperature histories at heat input of 1247.5W (c) Temperature histories at heat input of 1695.9W

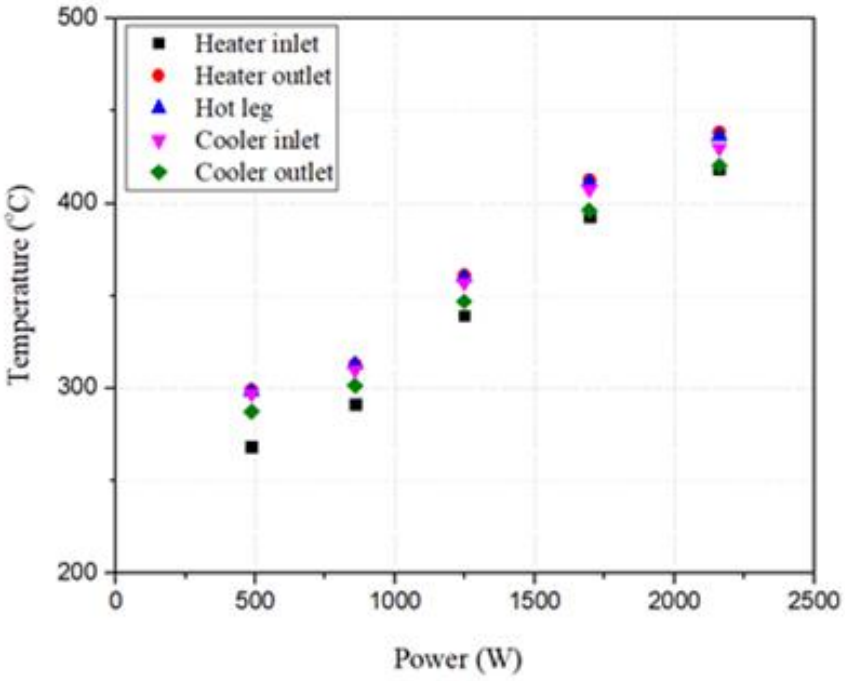

Fig. 4.3. Temperatures of HITEC at different points with respect to power input

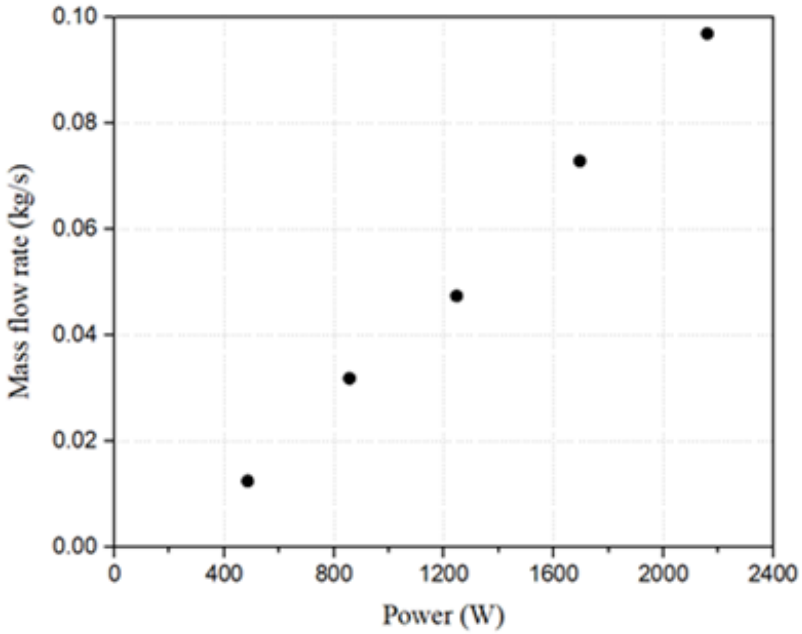

Fig. 4.4. Natural mass flow rate of HITEC with respect to power input

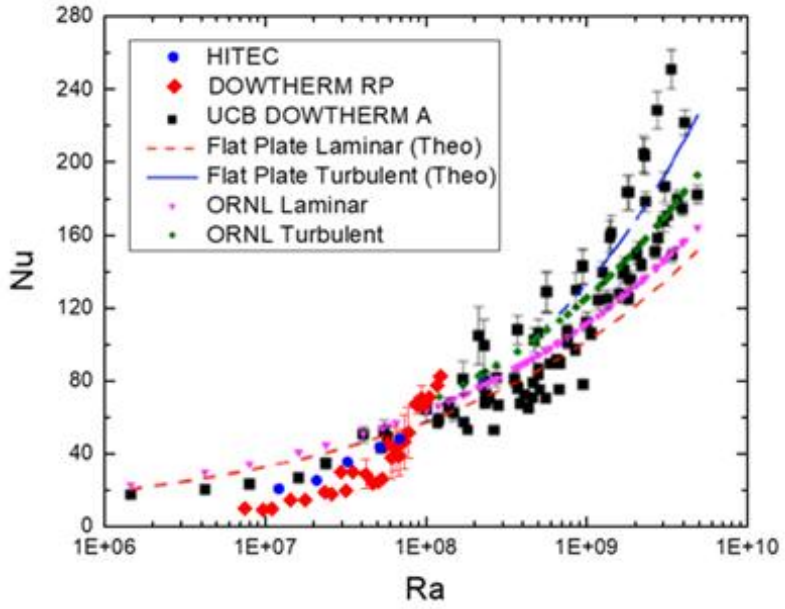

Fig. 4.5. Comparison of natural heat transfer of HITEC with the previous experimental data

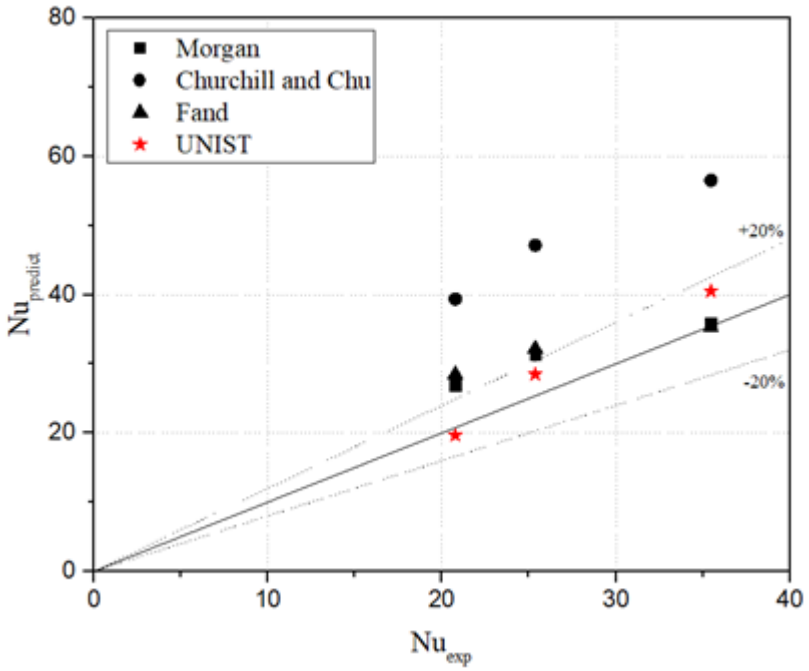

Fig. 4.6. Comparison of correlations for the present experimental data

Chapter 5. CONCLUSIONS AND RECOMMENDATIONS

5.1 Conclusion

Molten salts are promising heat transfer for advanced energy transport system like advanced nuclear system. The fundamental study on the single-phase heat transfer of molten salt becomes important, so the present paper focuses on the study on single-phase heat transfer behavior of molten salt, which is characterized by its high-Prandtl number, in both natural and forced circulation system with numerical and experimental approaches.

The feasibility of high-Pr fluid to passive heat transport system was tested by employing adjoint-based sensitivity analysis method. The adjoint system for natural circulation inside a closed circulation system were developed with more efficient computational effort. The general sensitivity analyses were performed with different design parameters which were categorized into fluid property, geometric parameter, heater and cooler conditions, pressure drop parameters, and Nusselt correlation. The effects of implementation of temperature-dependent fluid property, the orientations of heat exchanger, and operating temperature range, on the entire system sensitivity were analyzed. It is found that the variation of fluid properties with respect to the temperature gives great effect on the reliability of heat transfer performance in the system. In addition, the orientation of heat exchanger determined directly heat transfer performance, which could reduce the reliability of stable natural circulation.

To understand the advantages in using high-Pr fluids for passive heat transport system, the sensitivities of Nusselt number were compared with different fluids. System sensitivities were largely reduced when the fluids were replaced with high-Pr fluids. That is, the passive heat transport system using high-Pr fluids worked more stable and reliable in the aspect of heat transfer performance. Sensitivity analysis with respect to empirical constants in existing correlation for different fluids showed that the sensitivities of Nusselt number with respect to exponent constants associated with Prandtl number depended on the fluids. As a result, the use of high-Pr fluid to the passive heat transport system made it difficult to predict reliable Nusselt number due to the failure of prediction with existing correlation.

The feasibility of high-Pr fluid to the passive heat transport system was successfully tested showing the most reliable heat transfer performance, while the reliable prediction of heat transfer performance required to clarify the distinct heat transfer behavior of high-Pr fluid that the existing correlations didn’t take account of.

Then the experimental study on heat transfer behaviors of high-Prandtl number fluid was conducted to figure out the distinct heat transfer behavior of high-Pr fluid. Experimental investigation of the forced convective heat transfer phenomena of high-Pr oil and the natural convective heat transfer behavior of high-Pr salt was performed. It is suggested that the distinct heat transfer feature of high Prandtl number fluid is attributed to the existence of local natural convection in radial direction, which is induced by

the weak thermal diffusivity and resulting large radial temperature difference of high Prandtl number fluid. The theoretical discussion on the local natural convection of high-Prandtl number oil verifies its existence in the heat transfer between fluid and heated wall. Based on the discussion, new correlation was introduced by employing simple additive terms of previous Nusselt-Grashof relationship. The proposed correlation well agrees with experimental data from the present work as well as the previous work, which demonstrates the effect of local natural convection on the convective heat transfer performance of high Prandtl number fluid. For the verification, the further experimental works using molten heat transfer salt was designed and the preliminary test on molten salt natural circulation was performed. The proposed Nu-Gr correlation well predicted the heat transfer of HITEC in validated range by reducing the importance of constant and enhancing the importance of Grashof number to take account of local natural convection effect in high-Pr fluid flow. The further experimental campaign will be the extension of proposed concept and prediction of heat transfer performance to the broad range of flow regime and optimization of high-Pr fluid system based on the prediction.

5.2 Recommendations

Molten salts are promising heat transfer media for various heat transport systems, especially for liquid fuel circulation system and passive safety system of nuclear reactors. However, still the fundamental knowledge on the single-phase heat transfer of molten salt is insufficient to design heat transport system and predict its performance. The present study provides effective and validated technique to design and optimize passive heat transport system using molten salts. In addition, the numerical analysis method gives the way to reduce uncertainties in predicting heat transfer performance of passive heat transport system using molten salt. The established experimental facilities provide the chance to perform further experimental campaign using practical molten salts for both forced and passive systems. Finally, the proposal of idea about heat transfer of high-Pr fluid can give physical basis to understand thermal-hydraulic characteristics of molten salts.

References

1. Bettis ES, Schroeder RW, Cristy GA, Savage HW, Affel RG, Hemphill LF. The Aircraft Reactor Experiment—Design and Construction. *Nucl Sci Eng*. 1957;2(6):804-825. doi:10.13182/NSE57-A35495.
2. Alexander LG. Molten-salt fast reactors. In: *Proceedings of Breeding Large Fast Reactors*. ANL-6792; 1963. doi:10.1073/pnas.0703993104.
3. Taube M. Fast Reactors Using Molten Chloride Salts as Fuel. 1978.
4. Ottewitte EH. Configuration of a molten chloride fast reactor on a thorium fuel cycle to current nuclear fuel cycle concerns. 1982.
5. Ottewitte EH. Cursory First Look at the Molten Chloride Fast Reactor as an Alternative to the Conventional BATR Concept. 1992;(April):67.
6. Whatley ME, McNeese LE, Carter WL, Ferris LM, Nicholson EL. Engineering Development of the MSBR Fuel Recycle. *Nucl Appl Technol*. 1970;8(2):170-178. doi:10.13182/NT70-A28623.
7. Furukawa K, Lecocq A, Kato Y, Mitachi K. Thorium molten-salt nuclear energy synergetics. *J Nucl Sci Technol*. 1990;27(12):1157-1178. doi:10.1080/18811248.1990.9731310.
8. Vergnes J, Lecarpentier D. The AMSTER concept (actinides molten salt transmutER). *Nucl Eng Des*. 2002;216(1-3):43-67. doi:10.1016/S0029-5493(02)00026-2.
9. Mathieu L, Heuer D, Brissot R, et al. The thorium molten salt reactor: Moving on from the MSBR. *Prog Nucl Energy*. 2006;48(7):664-679. doi:10.1016/j.pnucene.2006.07.005.
10. Mathieu L, Heuer D, Merle-Lucotte E, et al. Possible Configurations for the Thorium Molten Salt Reactor and Advantages of the Fast Nonmoderated Version. *Nucl Sci Eng*. 2009;161(1):78-89. doi:10.13182/NSE07-49.
11. Ignatiev V, Feynberg O, Gnidoi I, et al. Progress in Development of Li , Be , Na / F Molten Salt Actinide Recycler & Transmuter Concept. *Proc ICAPP '07*. 2007.
12. Holcomb DE, Flanagan GF, Patton BW, Gehin JC, Howard RL, Harrison TJ. *Fast Spectrum Molten Salt Reactor Options*.; 2011.
13. Holcomb D. U . S . MSR Development Program & Supportive Tasks. In: *2 Nd SAMOFAR Meeting*. Karlsruhe, Germany; 2016.
14. Scott I. Stable salt fast reactor. In: *Molten Salt Reactors and Thorium Energy*. ; 2017:571-580. doi:10.1016/B978-0-08-101126-3.00021-X.
15. Grimes WR. Molten-Salt Reactor Chemistry. *Nucl Appl Technol*. 1970;8(2):137-155. doi:10.13182/NT70-A28621.
16. Ingersoll DT, Forsberg C, Ott LJ, et al. *Status of Preconceptual Design of the Advanced High-Temperature Reactor (AHTR)*.; 2004. doi:ORNL/TM-2004/104.

17. Williams DF. *Assessment of Candidate Molten Salt Coolants for the Advanced Highi-Temperature Reactor (AHTR).*; 2006. doi:ORNL/TM-2006/69.
18. NREL. Concentrating Solar Power Projects. https://www.nrel.gov/csp/solarpaces/by_technology.cfm. Published 2011.
19. EASTMAN. Therminol VP-1 Vapor Phase/Liquid Phase Heat Transfer Fluid. https://www.therminol.com/products/Therminol-VP1. Published 1999.
20. Dow Chemical Company. Dowtherm A - Heat Transfer Fluid, Product Technical Data. 1997.
21. LANXESS. DIPHYL - Heat Transfer Fluids. http://advancedindustrialintermediates.com/en/products-applications/applications-aii-brands/diphylr/. Published 2009.
22. Kuravi S, Trahan J, Goswami DY, Rahman MM, Stefanakos EK. Thermal energy storage technologies and systems for concentrating solar power plants. *Prog Energy Combust Sci*. 2013;39(4):285-319. doi:10.1016/j.pecs.2013.02.001.
23. Peng Q, Yang X, Ding J, Wei X, Yang J. Design of new molten salt thermal energy storage material for solar thermal power plant. *Appl Energy*. 2013;112:682-689. doi:10.1016/j.apenergy.2012.10.048.
24. Peng Q, Ding J, Wei X, Yang J, Yang X. The preparation and properties of multi-component molten salts. *Appl Energy*. 2010;87(9):2812-2817. doi:10.1016/j.apenergy.2009.06.022.
25. Boerema N, Morrison G, Taylor R, Rosengarten G. Liquid sodium versus Hitec as a heat transfer fluid in solar thermal central receiver systems. *Sol Energy*. 2012;86(9):2293-2305. doi:10.1016/j.solener.2012.05.001.
26. Pacio J, Wetzel T. Assessment of liquid metal technology status and research paths for their use as efficient heat transfer fluids in solar central receiver systems. *Sol Energy*. 2013;93:11-22. doi:10.1016/J.SOLENER.2013.03.025.
27. Cordaro JG, Rubin NC, Bradshaw RW. Multicomponent Molten Salt Mixtures Based on Nitrate/Nitrite Anions. *J Sol Energy Eng*. 2011;133(1):011014. doi:10.1115/1.4003418.
28. Vignarooban K, Xu X, Wang K, et al. Vapor pressure and corrosivity of ternary metal-chloride molten-salt based heat transfer fluids for use in concentrating solar power systems. *Appl Energy*. 2015;159:206-213. doi:10.1016/j.apenergy.2015.08.131.
29. Sieder EN, Tate GE. Heat Transfer and Pressure Drop of Liquids in Tubes. *Ind Eng Chem*. 1936;28(12):1429-1435. doi:10.1021/ie50324a027.
30. Eckert ERG, Diaguila AJ, Curren AN. *Experiments on Mixed-Free-and-Forced-Convective Heat Transfer Connected with Turbulent Flow through a Short Tube*. NACA TN-2974, National Advisory Committee for Aeronautics; 1953.
31. Hoffman HW, Cohen SI. *Fused Salt Heat Transfer - Part III: Forced-Convection Heat Transfer in Circular Tubes Containing the Salt Mixture NaNO2-NaNO3-KNO3*. USAEC

Report ORNL-2433, Oak Ridge National Laboratory; 1960.

32. McAdams WH. Heat Transmission. *SPE*. 1954;SPE 00096(4):427-435. http://www.onepetro.org/mslib/servlet/onepetropreview?id=00000096&soc=SPE.
33. Gnielinski V. New Equations for Heat and Mass Transfer in Turbulent Pipe and Channel Flow. *Int Chem Eng*. 1976;16(2):359-368.
34. Morgan VT. The Overall Convective Heat Transfer from Smooth Circular Cylinders. *Adv Heat Transf*. 1975;11(C):199-264. doi:10.1016/S0065-2717(08)70075-3.
35. Churchill SW, Chu HHS. Correlating equations for laminar and turbulent free convection from a horizontal cylinder. *Int J Heat Mass Transf*. 1975;18(9):1049-1053. doi:10.1016/0017-9310(75)90222-7.
36. Fand RM, Brucker J. A correlation for heat transfer by natural convection from horizontal cylinders that accounts for viscous dissipation. *Int J Heat Mass Transf*. 1983;26(5):709-716. doi:10.1016/0017-9310(83)90021-2.
37. Kim Y Il, Lee YB, Lee CB, Chang J, Choi C. Design concept of advanced sodium-cooled fast reactor and related R & D in Korea. *Sci Technol Nucl Install*. 2013;2013. doi:10.1155/2013/290362.
38. Seo S Bin, Kim IG, Bang IC. Risk-reduction of passive decay heat removal system by using gallium-water for UCFR and SMR. *Int J Energy Res*. 2017;41(2):207-219. doi:10.1002/er.3593.
39. Wu G, Li Y, Wang M, Chen Y, Wang L. Design and performance analysis of passive residual heat removal system for a lead-cooled fast reactor. *Prog Nucl Energy*. 2018;103(December 2017):236-242. doi:10.1016/j.pnucene.2017.11.018.
40. Farmer MT, Sienicki JJ. Analysis of transient coolant void formation during a guillotine-type hx tube rupture event in the star-lm system employing a supercritical CO 2 brayton cycle. In: *Proceedings of the International Conference on Nuclear Engineering (ICONE12)*. Vol 1. ; 2004:359-367.
41. Reyes JN, Groome J, Woods BG, et al. Testing of the multi-application small light water reactor (MASLWR) passive safety systems. *Nucl Eng Des*. 2007;237(18):1999-2005. doi:10.1016/j.nucengdes.2007.01.014.
42. Kim YS, Bae SW, Cho S, Kang KH, Park HS. Application of direct passive residual heat removal system to the SMART reactor. *Ann Nucl Energy*. 2016;89:56-62. doi:10.1016/j.anucene.2015.11.025.
43. Robertson RC. *Conceptual Design Study of a Single-Fluid Molten-Salt Breeder Reactor*. Oak Ridge National Laboratory, Tennessee; 1971.
44. Ju H, Suk Y, Shin A, Duk N. Review of SFR Design Safety using Preliminary Regulatory PSA Model. 2013:24-25.

45. Butt HN, Ilyas M, Ahmad M, Aydogan F. Assessment of passive safety system of a Small Modular Reactor (SMR). *Ann Nucl Energy*. 2016;98:191-199. doi:10.1016/j.anucene.2016.07.018.
46. Cho N, Kim IS, Lee C-J. Development of PSA Audit Guideline and Regulatory PSA Model for SMART. In: *Workship on PSA for New and Advanced Reactors*. Paris, France; 2011:225-232.
47. Cristhian G. Design and transient analysis of passive safety cooling systems for advanced nuclear reactors. 2011.
48. Ruiz DE, Cammi A, Luzzi L. Dynamic stability of natural circulation loops for single phase fluids with internal heat generation. *Chem Eng Sci*. 2015;126:573-583. doi:10.1016/j.ces.2014.12.050.
49. Avigni P, Wysocki AJ, Yoder GL. Liquid Salt Test Loop modeling using TRACE. *Ann Nucl Energy*. 2017;106:170-184. doi:10.1016/j.anucene.2017.04.003.
50. Kudariyawar JY, Srivatsav AK, Vaidya AM, Maheshwari NK, Satyamurthy P. Computational and experimental investigation of steady state and transient characteristics of molten salt natural circulation loop. *Appl Therm Eng*. 2016;99:560-571. doi:10.1016/j.applthermaleng.2015.12.114.
51. Srivastava AK, Kudariyawar JY, Borgohain A, Jana SS, Maheshwari NK, Vijayan PK. Experimental and theoretical studies on the natural circulation behavior of molten salt loop. *Appl Therm Eng*. 2016;98:513-521. doi:10.1016/j.applthermaleng.2015.12.065.
52. Jiao X, Shao S, Wang K, Yang Q, He Z, Chen K. Functional reliability analysis of a molten salt natural circulation system. *Nucl Eng Des*. 2018;332(March 2018):127-136. doi:10.1016/j.nucengdes.2018.03.024.
53. Lions J-L (Jacques-L. Optimal control of systems governed by partial differential equations. *J Opt Theory Appl*. 1971;99:396. doi:10.1007/978-3-642-65024-6.
54. Ulbrich S. Adjoint-based derivative computations for the optimal control of discontinuous solutions of hyperbolic conservation laws. *Syst Control Lett*. 2003;48(3-4):313-328. doi:10.1016/S0167-6911(02)00275-X.
55. Carnarius A, Thiele F, Özkaya E, Gauger N. Adjoint approaches for optimal flow control. *AIAA Pap*. 2010;(July):1-15. doi:doi:10.2514/6.2010-5088.
56. Kontoleontos EA, Papoutsis-Kiachagias EM, Zymaris AS, Papadimitriou DI, Giannakoglou KC. Adjoint-based constrained topology optimization for viscous flows, including heat transfer. *Eng Optim*. 2013;45(8):941-961. doi:10.1080/0305215X.2012.717074.
57. Luo J, Zhou C, Liu F. Multipoint Design Optimization of a Transonic Compressor Blade by Using an Adjoint Method. *J Turbomach*. 2014;136(2014):051005. doi:10.1115/1.4025164.
58. Zhang P, Lu J, Song L, Feng Z. Study on continuous adjoint optimization with turbulence

models for aerodynamic performance and heat transfer in turbomachinery cascades. *Int J Heat Mass Transf*. 2017;104:1069-1082. doi:10.1016/j.ijheatmasstransfer.2016.08.103.

59. Son S, Lee JI. Application of adjoint sensitivity analysis method to supercritical CO2power cycle optimization. *Energy*. 2018;147:1153-1164. doi:10.1016/j.energy.2018.01.117.
60. Shin Y, Seo S Bin, Kim IG, Bang IC. Natural circulation with DOWTHERM RP and its MARS code implementation for molten salt-cooled reactors. *Int J Energy Res*. 2016;40:1122-1133. doi:DOI: 10.1002/er.3512.
61. Shin Y, Seo S Bin, Bang IC. Study on flow characteristics of high-Pr heat transfer fluid near the wall in a rectangular natural circulation loop. *Int J Heat Mass Transf*. 2018;121:1350-1363. doi:10.1016/j.ijheatmasstransfer.2018.01.064.
62. Stripling HF. Adjoint-based uncertainty quantification and sensitivty analysis for reactor depletion calculations. 2013.
63. Stripling HF, Anitescu M, Adams ML. A generalized adjoint framework for sensitivity and global error estimation in time-dependent nuclear reactor simulations. *Ann Nucl Energy*. 2013;52:47-58. doi:10.1016/j.anucene.2012.08.019.
64. Humbird KD, McClarren RG. Adjoint-based sensitivity analysis for high-energy density radiative transfer using flux-limited diffusion. *High Energy Density Phys*. 2017;22:12-16. doi:10.1016/j.hedp.2016.12.002.
65. Cao Y, Li S, Petzold L, Serban R. Adjoint Sensitivity Analysis for Differential-Algebraic Equations: The Adjoint DAE System and Its Numerical Solution. *SIAM J Sci Comput*. 2003;24(3):1076-1089. doi:10.1137/S1064827501380630.
66. Fink JK. *Thermodynamic and Transport Properties of Sodium Liquid and Vapor*.; 1995. doi:10.2172/94649.
67. Korson L, Drost-Hansen W, Millero FJ. Viscosity of water at various temperatures. *J Phys Chem*. 1969;73(1):34-39. doi:10.1021/j100721a006.
68. Coastal Chemical Company. *HITEC ® Heat Transfer Salt*.; 2009. doi:http://www.skyscrubber.com/MSR%20-%20HITEC%20Heat%20Transfer%20Salt.pdf.
69. White FM. Fluid Mechanics. *Book*. 2009;17(3):864. doi:10.1111/j.1549-8719.2009.00016.x.Mechanobiology.
70. Incropera FP, Bergman TL, Lavine AS, DeWitt DP. *Fundamentals of Heat and Mass Transfer*.; 2011. doi:10.1073/pnas.0703993104.
71. Samanta S, Guha A. A similarity theory for natural convection from a horizontal plate for prescribed heat flux or wall temperature. *Int J Heat Mass Transf*. 2012;55(13-14):3857-3868. doi:10.1016/j.ijheatmasstransfer.2012.02.031.
72. Zhang T, Jia L, Wang Z. Validation of Navier-Stokes equations for slip flow analysis within transition region. *Int J Heat Mass Transf*. 2008;51(25-26):6323-6327.

doi:10.1016/j.ijheatmasstransfer.2008.04.049.

73. Wang ZC, Tang DW, Hu XG. Similarity solutions for flows and heat transfer in microchannels between two parallel plates. *Int J Heat Mass Transf*. 2011;54(11-12):2349-2354. doi:10.1016/j.ijheatmasstransfer.2011.02.027.
74. Glicksman LR, Hyre MR, Farrell PA. Dynamic similarity in fluidization. *Int J Multiph Flow*. 1994;20(SUPPL. 1):331-386. doi:10.1016/0301-9322(94)90077-9.
75. Teplitskiy YS. Similarity of transport processes in fluidized beds. *Int J Heat Mass Transf*. 1999;42(20):3887-3899. doi:10.1016/S0017-9310(99)00044-7.
76. Tricoli V. Heat transfer in turbulent pipe flow revisited: Similarity law for heat and momentum transport in low-Prandtl-number fluids. *Int J Heat Mass Transf*. 1999;42(8):1535-1540. doi:10.1016/S0017-9310(98)00258-0.
77. Lin HT, Lin LK. Similarity solutions for laminar forced convection heat transfer from wedges to fluids of any Prandtl number. *Int J Heat Mass Transf*. 1987;30(6):1111-1118. doi:10.1016/0017-9310(87)90041-X.
78. Bardet PM, Peterson PF. Options for scaled experiments for high temperature liquid salt and helium fluid mechanics and convective heat transfer. *Nucl Technol*. 2008;163:344-357.
79. Shin Y, Seo S Bin, Bang IC. Study on flow characteristics of high-Pr heat transfer fluid near the wall in a rectangular natural circulation loop. *Int J Heat Mass Transf*. 2018;121:1350-1363. doi:10.1016/j.ijheatmasstransfer.2018.01.064.
80. Rouch H, Geoffroy O, Rubiolo P, et al. Preliminary thermal-hydraulic core design of the Molten Salt Fast Reactor (MSFR). *Ann Nucl Energy*. 2014;64:449-456. doi:10.1016/j.anucene.2013.09.012.
81. Ignatiev V, Feynberg O, Gnidoi I, et al. Progress in Development of Li , Be , Na / F Molten Salt Actinide Recycler & Transmuter Concept. In: *Proceedings of ICAPP '07*. Nice, France, May 13-18; 2007.
82. Nelson PA, Butler DK, Chasanov MG, Meneghetti D. Fuel Properties and Nuclear Performance of Fast Reactors Fueled with Molten Chlorides. *Nucl Appl*. 1967;3(September):540-547.
83. Cantor S, Cooke W, Dworkin S, Robbins D, Thoma E, Watson M. *Physical Properties of Molten-Salt Reactor Fuel, Coolant and Flush Salts*. Vol ORNL-TM-23.; 1968.
84. Cantor S. *Density and Viscosity of Several Molten Fluoride Mixtures*. Vol ORNL-TM-43.; 1973.
85. Dow Chemical Company. Dowtherm RP - Heat Transfer Fluid, Product Technical Data. 1997.
86. Kline SJ, McClintock FA. Describing uncertainties in single-sample experiments. *Mech Eng*. 1953;75(1):3-8. doi:10.1016/j.chaos.2005.11.046.
87. Lienhard IV JH, Lienhard V JH. *A HEAT TRANSFER TEXTBOOK, Fourth Edition.*; 2012.

doi:978-04864793161.

88. Hilpert R. Wärmeabgabe von geheizten Drähten und Rohren im Luftstrom. *Forsch auf dem Gebiet des Ingenieurwesens A*. 1933;4(5):215-224. doi:10.1007/BF02719754.
89. Igarashi T. Local heat transfer from a square prism to an airstream. *Int J Heat Mass Transf*. 1986;29(5):777-784. doi:10.1016/0017-9310(86)90129-8.
90. Ahmed GR, Yovanovich MM. Experimental Study of Forced Convection From Isothermal Circular and Square Cylinders and Toroids. *J Heat Transfer*. 1997;119(1):70-79. http://dx.doi.org/10.1115/1.2824102.
91. Yoo S-Y, Park J-H, Chung C-H, Chung M-K. An Experimental Study on Heat/Mass Transfer From a Rectangular Cylinder. *J Heat Transfer*. 2003;125(6):1163-1169. http://dx.doi.org/10.1115/1.1603780.
92. Shin Y. Study on Natural Circulation Heat Transfer and Flow Characteristics of High-Pr Oil Simulant of Molten Salts. 2017.
93. Hoffman HW, Lones J. *Fused Salt Heat Transfer, Part II: Forced Convection Heat Transfer in Circular Tubes Containing NaF-KF-LiF Eutectic*. Vol ORNL-1777.; 1955. doi:10.1017/CBO9781107415324.004.
94. Silverman MD, Huntley WR, Robertson HE. *Heat Transfer Measurements in a Forced Convection Loop with Two Molten-Fluoride Salts: LiF-BeF2-ThF2-UF4 and Eutectic NaBF4-NaF*. Vol ORNL/TM-53.; 1976.
95. Yu-ting W, Bin L, Chong-fang M, Hang G. Convective heat transfer in the laminar-turbulent transition region with molten salt in a circular tube. *Exp Therm Fluid Sci*. 2009;33(7):1128-1132. doi:10.1016/j.expthermflusci.2009.07.001.
96. Chen C, Wu YT, Wang ST, Ma CF. Experimental investigation on enhanced heat transfer in transversally corrugated tube with molten salt. *Exp Therm Fluid Sci*. 2013;47:108-116. doi:10.1016/j.expthermflusci.2013.01.006.
97. Lu J, Sheng X, Ding J, Yang J. Transition and turbulent convective heat transfer of molten salt in spirally grooved tube. *Exp Therm Fluid Sci*. 2013;47:180-185. doi:10.1016/j.expthermflusci.2013.01.014.
98. Lu J, Shen X, Ding J, Peng Q, Wen Y. Convective heat transfer of high temperature molten salt in transversely grooved tube. *Appl Therm Eng*. 2013;61(2):157-162. doi:10.1016/j.applthermaleng.2013.07.037.
99. Shen X, Lu J, Ding J, Yang J. Convective heat transfer of molten salt in circular tube with nonuniform heat flux. *Exp Therm Fluid Sci*. 2014;55:6-11. doi:10.1016/j.expthermflusci.2014.02.015.
100. Chen X, Wang C, Wu Y, Liu B, Ma C. Characteristics of the mixed convection heat transfer of molten salts in horizontal square tubes. *Sol Energy*. 2017;147:248-256.

doi:10.1016/j.solener.2017.03.031.

101. Peterson PF, Scarlat RO, Zweibaum N, Laufer M, Bickel J. *Integral and Separate Effects Tests for Thermal Hydraulics Code Validation for Liquid-Salt Cooled Nuclear Reactors*. Vol Project No.; 2012.
102. Zweibaum N, Huddar L, Hughes JT, et al. Role and Status of Scaled Experiments in the Development of Fluoride-Salt-Cooled, High-Temperature Reactors. *Int Congr Adv Nucl Power Plants*. 2015:434-445.
103. Kang G-U, Chung B-J, Kim H-J. Natural convection heat transfer on a vertical cylinder submerged in fluids having high Prandtl number. *Int J Heat Mass Transf*. 2014;79:4-11. doi:10.1016/j.ijheatmasstransfer.2014.07.077.

Acknowledgement (감사의 글)

처음 부산을 떠나 새로 지어지는 학교에 입학할 때는 제가 대학원까지 마무리하며 감사의 글을 쓰고 있을 줄은 생각하지 못했습니다. 아직 실감이 나지는 않지만, 길다면 길고 짧다면 짧은 시간 동안 저와 함께 해주신 많은 분들께 감사의 인사를 드리고자 합니다.

먼저 항상 저에게서 눈을 떼지 않으시고 사랑과 은혜로 감싸주시는 하나님께 이 모든 영광을 돌립니다. 이 모든 것이 저에게 뜻하신 바를 이루고자 하심을 믿으며, 그에 항상 감사드립니다.

제가 힘들 때나 기쁠 때나 항상 옆에서 묵묵히 기도해주시고 응원해주신 부모님께 감사드립니다. 당신께 받은 은혜 평생토록 사랑으로 보답하도록 하겠습니다. 사랑하고 감사합니다.

저에겐 또다른 부모님이신 교수님께 감사의 인사를 드립니다. 학부생 때부터 언제나 한결같이 연구에 열정적이신 그 모습은 저의 평생의 롤모델입니다. 학위 과정 중에 우여곡절이 많았지만 끝까지 지지해주시고 이끌어주셔서 정말 감사드립니다.

저의 학위 과정을 함께한 연구실 선 후배님들에게 감사의 인사를 드립니다.
진정한 얼리버드로 저에게 부지런함이 무엇인지 보여주신 승원이형, 묵묵하게 자신이 맡은 일을 처리하는 책임감을 보여주신 성만이형, 항상 새로운 것을 생각하고 시도하는 창의성을 보여주신 성대형, 저에게 필요한 신실함과 믿음을 보여주신 사라누나, 티내지 않으면서도 다 챙겨주는 츤데레의 정석을 보여준 한이형 을 만난 덕분에 제가 한 단계 더 성장하고 인생에 필요한 많은 것들을 배울 수 있었습니다. 정말 감사합니다.
입학 동기지만 항상 한 발 앞서 선배같이 이끌어주고, 나의 문제를 항상 함께 고민해주었던 경모
연구실 생활에 항상 웃음이 가득하게 만들어준, 인생을 즐기며 사는 방법을 가르쳐준 성보
연구적인 문제들뿐만 아니라 많은 인생 고민들까지 함께 나누었던 나의 커피메이트 인국
후배지만 배울 것이 참 많은, 항상 생각하고 연구하는 연구자의 모범을 보여준 영신이
어떤 일이라도 지지해주고 나에게 힘이 되어주던, 함께 맥주 마시는게 좋았던 효
나와 같이 연구를 시작하고 함께 실험하고 고민하면서 같이 고생한, 우리 동네 옆집 유경이
할 거도 많은데 못난 형들 챙긴다고 항상 고생하는, 밤샘 동지 민호
내가 학교에 없을 때도 항상 묵묵히 뒤에서 일처리한다고 고생한, 벤치클리어링 한얼이
이젠 그냥 대학원생 같은, 항상 싹싹하게 챙겨주는 지용이까지
모두가 있어서 나의 연구실 생활이 행복하고 즐거웠습니다. 정말 감사합니다.

책으로만 공부한 샌님에게 현장을 가르쳐 주시고 많은 실험 경험들을 채워주신, 저의 학위 과정 내내 절대 빠뜨릴 수 없는 이종수 사장님께도 감사의 인사를 드립니다.

마지막으로 나의 학교 생활을 함께하고 언제나 나에게 힘이 되어준 친구들에게 감사의 인사를 전하며, 끝이 아닌 새로운 출발을 위해서 다시 뛸 준비를 하러 가도록 하겠습니다. 감사합니다.